Development and Optimisation of Fast Energy Yield Calculations (FEnYCs) of Photovoltaic Modules

By

Jyotirmoy Roy

Doctoral Thesis

Submitted in partial fulfilment of the requirements

for the award of

Doctor of Philosophy of Loughborough University

December 2013

Dedication

This thesis is dedicated to my little daughter Surjaa Roy and to my parents.

Abstract

Development and optimisation of a robust energy yield prediction methodology is the ultimate aim of this research.

Outdoor performance of the PV module is determined by the influences of a variety of interlinked factors related to the environment and device technologies. There are two basic measurement data sets required for any energy yield prediction model. Firstly, characterisation of specific PV module technology under different operating conditions and secondly site specific meteorological data. Based on these two datasets a calculation procedure is required in any specific location energy yield estimation.

This research established a matrix based multi-dimensional measurement set points for module characterisation which is independent of PV technologies. This novel approach has been established by demonstrating an extended correlation of different environmental factors (irradiance, temperature and spectral irradiance) and their influences on the commercial PV device technologies. Utilisation of the site specific meteorological data is the common approach applied in this yield prediction method. A series of modelling approach, including a tri-linear interpolation method is then applied for energy yield calculation.

A novel Monte Carlo simulation is demonstrated for uncertainty analysis of irradiance (pyranometer CM 11) & temperature (PT 1000) measurements and ultimately the yield prediction of c-Si and CIGS modules. The degree of uncertainties of irradiance is varies from ±2% to ±6.2% depending on the level of monthly irradiation. The temperature measurement uncertainty is calculated in the range of ±0.18°C to ±0.46%°C in different months of the year. The calculated uncertainty of the energy yield prediction of c-Si and CIGS module are ±2.78% and ±15.45%.

This research validated different irradiance translation models to identify the best matched model for UK climate for horizontal to in-plane irradiance. Ultimately, the validation results of the proposed Fast Energy Yield Calculation (FEnYCs), shows a good agreement against measured values i.e. 5.48%, 6.97% and 3.1% for c-Si, a-Si and CIGS module respectively.

Acknowledgements

I would like to thank Dr. Ralph Gottschalg for offering an EPSRC PhD funding for this research and the continuous support though out the journey of this thesis. Without this partial funding this work would never have been possible. Very special thanks to Dr. Thomas Betts for his constant support, suggestions and motivational discussions from the beginning of this work including at the write up stage – many thanks Tom.

I would like to express my gratitude of CREST members especially Dr. Sheryl William, Dr. Pongpan Vorasayan, Dr. Martin Bliss, Dr. Jiang Zhu, Dr. Ketut Astawa, Dr. Matthias Strobel and Dr. Christos Monokrousses.

A special thanks goes to my brother Dr. Amitava Roy, who directed me in this scope of solar energy research and his continual support and motivation in all years of my life.

A very special thanks to my wife Somali Roy for her loving support, motivation though out these years.

Finally, I would like to thank my parents and my brother who have been nothing but supportive throughout this degree.

Contents

List of Figures

List of Tables

List of Publications and Presentations Arising Through This Work

JOURNAL & CONFERENCE PUBLICATIONS

- **Roy, J**., Betts, T.R., Gottschalg, R., "Accuracy of the Energy Yield Prediction of Photovoltaic Modules" *JAPANESE JOURNAL OF APPLIED PHYSICS*, 51(10), ISSN: 0021-4922., Japan, 2012.
- **Roy, J**., Betts, T.R., Gottschalg, R., "Accuracy of the Energy Yield Prediction of Photovoltaic Modules" Proceedings of PVSEC 21, Japan, December 2011.
- **Roy, J**., Betts, T.R., Gottschalg, R., "Validation of the Energy Yield Prediction of Photovoltaic Modules" Proceedings of the 7th Photovoltaic Science Application and Technology Conference and Exhibition, UK, March 2011.
- Bliss, M., **Roy, J**., Betts, T.R., Gottschalg, R., "Indoor Measurement of GTE-Matrix for Energy Rating" Proceedings of the 6th Photovoltaic Science Application and Technology Conference and Exhibition, Southampton, UK, March 2010.
- **Roy, J**., Bliss, M., Betts, T.R., Gottschalg, R., "Effect of I-V Translations of Irradiance-Temperature on the Energy Yield prediction of PV module and spectral changes over Irradiance and temperature" Proceedings of the 6th Photovoltaic Science Application and Technology Conference and Exhibition, Southampton, UK, March 2010.
- **Roy, J.**, Qiu, Y., Betts, T.R., Gottschalg, R., "Modelling Uncertainty of Photovoltaic Module Energy Rating" Proceedings of the 5th Photovoltaic Science Application and Technology Conference and Exhibition, Wrexham, UK, April 2009.
- **Roy, J.**, Betts, T.R., Gottschalg, R., Mau, S., Zamini, S., Kenny R.P, Müllejans H, Friesen G , Dittmann S, Beyer H.G , Jagomägi A., "Validation of Proposed Photovoltaic Energy Rating standard and sensitivity to environmental parameters" Proceedings of the 23rd European Photovoltaic Solar Energy Conference, Fiera Valencia, Spain, September 2008.

- Zhu, J, **Roy, J.**, Bründlinger, R., Betts, T.R., Gottschalg, R., "Effect of timing and voltage dependence on inverter sizing" Proceedings of the 23rd European Photovoltaic Solar Energy Conference, Fiera Valencia, Spain, September 2008.
- **Roy, J.**, Betts, T.R., Gottschalg, R., "Evaluation of proposed photovoltaic energy rating standard: validation against outdoor measurements". Proceedings of the 4th Photovoltaic Science Application and Technology Conference and Exhibition, Bath, UK, April 2008.
- Mau, S., Zamini, S., Bergmair, B., Ruppert, E., Williams, S.R., **Roy, J**., Betts, T.R., Gottschalg, R.,' Müllejans, H., "Quantifying environmental effects for different device technologies based on proposed energy rating standard", Proceedings of the 22nd European Photovoltaic Solar Energy Conference, Fiera Milano, September 2007.

PRESENTATIONS

- **Roy, J.**, Betts, T.R., Gottschalg, R., Mau, S., Zamini, S., Kenny R.P, Müllejans H, Friesen G , Dittmann S, Beyer H.G , Jagomägi A., "Validation of Proposed Photovoltaic Energy Rating standard and sensitivity to environmental parameters" Talk at Sub-project 4 of EU "Performance" project in JRC, EU Commission, ISPRA, Italy, October 2008.
- **Roy, J.**, Betts, T.R., Gottschalg, R., "IEC 61853 – Energy rating standard" PI-Berlin, Germany, 2008.
- Bliss, M., **J. Roy**, Betts, T.R., Gottschalg, R.,"Advanced Energy Prediction System for Photovoltaic Devices" poster at UKERC Energy Summer School 2009, Brighton, UK, July 2009.
- **Roy, J.**, Qiu, Y., Betts, T.R., Gottschalg, R., "Investigation of Measurement and Modelling Uncertainties that Affect the Energy Prediction Accuracy" Talk at Sub-project 4 of EU FP6 project, "Performance" in CEA, Cadarache, France, September 2009.

- **Roy, J.** , "Reliable Photovoltaic Performance Predictor" Talk at UK-India Young Scientist Networking Conference, British Council, Kolkata, India, December 2009.
- **Roy, J.** , "Photovoltaic Performance" Talk at "Getting Ready for Renewable Energy –GND" Europe India Initiative, International Conference, Pune, India, December 2009.
- **Roy, J**., Betts, T.R., Gottschalg, R., "Energy Yield: The Reliable Performance Predictor of Photovoltaic Devices" poster at Midland Energy Graduate School (MEGS) Annual Conference, Loughborough, UK, 2010.

1 Introduction

Currently, comparison between different solar module technologies is primarily based on the power rating under Standard Test Conditions (STC) [i.e. irradiance at 1000 W/m^2, normal angle of incidence, standard spectrum with AM1.5G distribution and 25ºC module temperature] [1-2]. The price of PV modules is principally dictated by the rated power and PV modules are sold based on cost/watts peak (W_p) at STC conditions. In reality PV modules or systems rarely operate at the STC conditions, as the parameters of the STC conditions change over the time period. So rated power (W_p) alone does not provide sufficient information to users about the performance of a PV module or system under many different environmental conditions, which largely affect the conversion efficiency.

On the other side, electricity cost dictates in terms of cost/kWh. So it is the energy generation of a PV system over a given timespan that determines revenue. As a result the estimated energy generation is required to make a true cost analysis of the system in order to estimate the internal rate of return (IRR) or payback period of any investment. As a result, a shift towards energy yield prediction is becoming necessary for end users and also for the system designers to optimise the system design appropriately as per the climatic conditions of the operational site.

Outdoor performance of the PV modules is determined by the influences of a variety of interlinked factors related to the environment and module technologies, which is explained in Chapter 2. Module performance largely depends on the effects of irradiance, temperature, spectral variation and the angle of incidence variation. In general, energy generation of all PV technologies increases with increasing irradiance. But the performance variation against temperature for different PV technologies is different. With increasing temperature, performance of thin film technologies decrease at lower rate compared with crystalline silicon (c-Si) modules. Also the spectral response of PV modules varies with different material technologies. Common requirements for energy prediction of PV module are described in Figure 1.

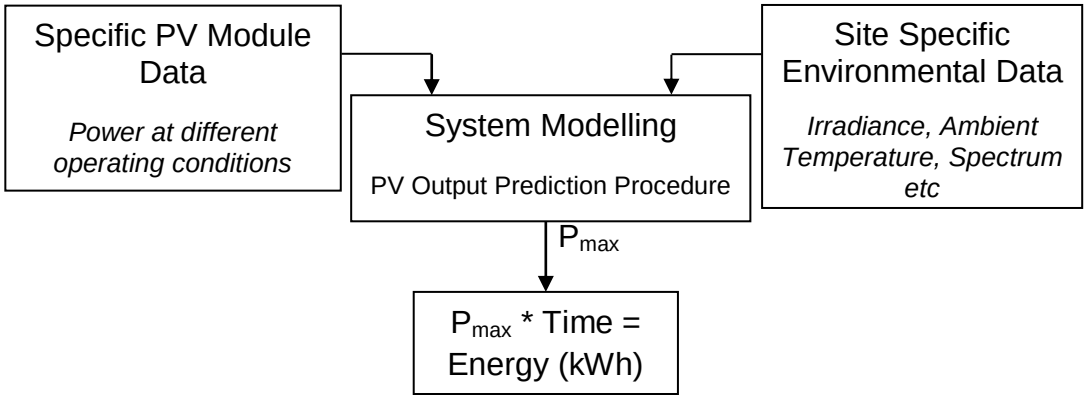

Figure 1: Components of energy prediction method

Chapter 3 explains the number of current energy prediction methods available by other research groups in various institutions [3-9]. The limiting factors in the existing prediction methods are illustrated here; a number of methods only taken into account the effects of global irradiance and temperature without considering spectral and angular dependency and also limited to c-Si technologies. Considering the growth of thin film PV modules in the market, it is essential to look at the performance of thin film module at different spectrum, as thin film modules are spectrally sensitive compare to the c-Si technology.

Existing energy prediction methods are based on either outdoor or indoor measurements to characterise PV modules to generate module input data for prediction model. Both indoor and outdoor module characterisation process has limitations. It is difficult to achieve high accuracy from the indoor based module characterisation measurement methods. This is due to the limitation in the availability of indoor measurement system which can generate compatible outdoor operating conditions that a PV module can see in real operations. Module characterisation can also be done in outdoor operating conditions. In outdoor based energy prediction methods, long term exposure of PV devices is required to get the performance data of PV module at wide range of climatic condition for a specific site. This can provide higher accuracy but this process is very time consuming, as it requires long term exposure (at least a year) of PV modules to measure the performance of that PV module at wide range of climatic condition for a specific site.

So the major problem with the existing energy prediction methods is lack of fast and accurate prediction method for emerging new module technologies in the PV market.

Energy yield prediction method can be called Energy Rating method if the procedure follows the standardised method which includes standardised meteorological datasets and standardised PV module measurements. The international standard body, IEC - International Electrotechnical Commission - is working on a standard for energy rating of different PV technologies counting different climatic conditions through the specification of environmental data for a number of reference days (IEC 61853) [14-17]. The aim of this proposed test standard is to assess PV module performance in terms of both peak power (W_p) and energy production (kWh) and to characterize the response parameters of the module. Details of this proposed standard is described in Chapter 3.

First phase of this research is validated the proposed IEC 61853 energy rating method, considering the measured module characterisation parameters including wide range of environmental aspects such as different components of irradiance (direct and diffuse irradiance) with angular variation, temperature as a function of irradiance, ambient temperature and wind speed, effects of spectral irradiance from the long term outdoor measurements. This method can separate out the performance of different PV technologies currently available in the marketplace, as the response of different PV modules varies with the variable environmental conditions. The spectral response and temperature effect also varies with different PV technologies and these effects are addressed by this IEC method.

Chapter 4 explains the modelling the IEC energy rating algorithm and the uncertainty analysis of the environmental parameter measurement. This includes the modelling and validation of the irradiance and temperature translation methods and identified the best suited irradiance translation model for the UK climate. This chapter also analysed the uncertainty analysis of the irradiance and temperature measurements as environmental input data for prediction model. A robust uncertainty analysis model is established which is then validated in the UK climate which can also be utilised in other location. Finally the uncertainties of the energy yield prediction of different PV modules are explained, which can significantly facilitate the financial evaluation more accurately of any investment on PV systems.

The ultimate aim of this study is to develop and optimise a cost effective robust methodology for Fast Energy Yield Calculations – FEnYCs (pronounced ‘phoenix’) for Photovoltaic Modules of different technologies, considering the influence of all relevant environmental factors generally experienced outdoors. The development of the FEnYCs method is illustrated in Chapter 5 by analysing the range of different operating environmental conditions in the UK climate.

The objective of the FEnYCs method is to address the limitation of the module characterisation by developing a time saving and cost effective accurate methodology for energy yield prediction. Specifically, the challenge is to minimize the required experimental dataset from months of outdoor measurements to at most a few hours in the laboratory, while maintaining high accuracy by generating compatible outdoor weather conditions. Minimising the experimental time can also minimise the measurement cost significantly. This will represent a significant improvement on current indoor-based methodologies and help the prediction process become cost effective.

The novelty of this project is to establish the FEnYCs methodology by developing a multi-dimensional matrix as a function of different weather conditions for characterisation of PV modules. This method will allow characterising any module technology available in the marketplace. Multi-dimensional power matrix generates wide range of irradiance and temperature with varying spectrum. Uncertainties in the energy rating method including measurements and modelling uncertainties one of the major objectives of this research work, explained in chapter 5.

Validation of FEnYCs methodology against the real outdoor measurement is been performed in this thesis and illustrated in the Chapter 5. Three commercial PV module types are installed and measured over annual period of time at CREST Outdoor Measurement System (COMS). An uncertainties flow of the FEnYCs methodology is demonstrated including previously estimated environmental parameters uncertainty and modelling uncertainty.

In conclusion, the ultimate aim of this research is to develop a new assessment method for fast energy yield prediction which should be independent of the PV module technologies. This has been established by making a multi-dimensional performance matrix of specific performance parameters of PV modules. This thesis

optimises the number of measurement points of each parameter in the multi-dimensional performance matrix for module characterisation indoor, which is compatible with real outdoor operation. A research to establish an accurate and time saving robust energy yield prediction method for PV modules under variable environmental conditions is demonstrated in this thesis.

2 Environnemental Influences on PV Module Performance.

2.1 Introduction

The performance of overall PV systems depends on various factors such as performance of the PV modules, inverter (for on-grid system), battery (for off-grid system), mounting mechanism, wiring etc. This research focuses on the study of module performance only, which may then be fed in to a system-level model.

This chapter describes the fundamentals of solar PV module behaviour. It explains different electrical parameters of a solar PV module and the influence of variable environmental factors on the performance characteristics of different PV devices. Proper understanding of the PV module behaviour against variable environmental conditions is essential for energy yield prediction of PV devices.

Firstly, the chapter explains the principal PV module characteristic parameters i.e. short-circuit current (I_{sc}), open-circuit voltage (V_{oc}), maximum power (P_{max}), fill factor (FF), conversion efficiency (η) and parasitic resistances (R_S, R_{SH}) [18-19]. This is followed by a description of the changes in the current-voltage (I-V) characteristic and the above parameters at non-STC conditions of irradiance and temperature.

The influencing environmental parameters i.e. irradiance, temperature, spectrum and angle of incidence on the performance of different PV modules are also explained later in this chapter. The chapter concludes with critical findings and how these are applicable to the rest of the work of this thesis.

2.2 PV Module Performance Parameters

The performance of PV modules here is assessed with respect to the I-V characteristics of the module. First the electrical parameters (I_{sc}, V_{oc}, P_{max} etc) within

the I-V characteristics are defined below and then their changes with changing environmental parameters are explained, under which the PV module operates in real operation.

A two diode model of a solar cell is shown in Figure 2. The electrical parameters of the I-V curve of a crystalline silicon PV module are shown in Figure 3, which includes also the power-voltage curve.

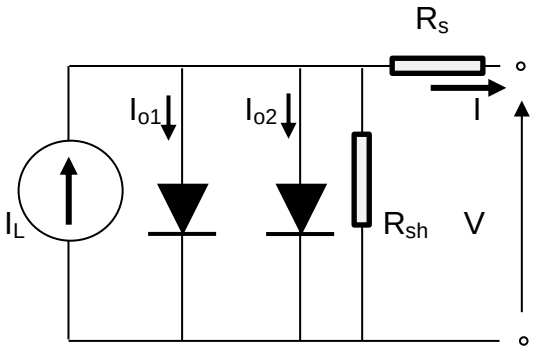

Figure 2: Two diode model of solar cell

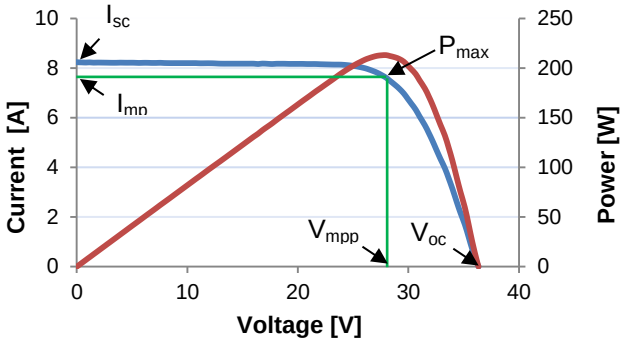

Figure 3: I-V and power characteristics of a PV module

Current output under illumination/sunlight from the two diode model of a solar cell (Figure 2) is given by equation (1**)** [18].

$$I = I_L - \frac{V + IR_S}{R_{SH}} - I_{01}\left(e^{\frac{V+IR_s}{n_1 V_T}} - 1\right) - I_{02}\left(e^{\frac{V+IR_S}{n_2 V_T}} - 1\right) \quad (1)$$

Where I_L = light generated current (A)

I_{01} = the diffusion diode current (A)

I_{02} = the recombination diode current (A)

n1 & n2 = diode ideality factor

R_s = series resistance

R_{sh} = shunt resistance

Short-circuit Current (I_{sc}): The short-circuit current is the current output of a photovoltaic cell or module under illumination when the voltage is zero (Figure 3) [19]. For an ideal solar cell at most moderate resistive loss mechanisms, the short-circuit current (I_{SC}) and the light-generated current (I_L) are identical. Therefore, the short-circuit current is the largest current which may be drawn from the solar cell or module.

Open Circuit voltage (V_{oc}): This is the maximum voltage across a photovoltaic cell or module when no current is flowing.

Maximum Power (P_{max}): A solar cell or module operates over a wide range of voltage (V) and current (I) under different environmental conditions. The maximum power point (mpp) is the point occurs at the knee (Figure 3) of the I-V curve at a particular load for which the module can deliver maximum electrical power (equation (2)). At maximum power, the voltage and current are called voltage at maximum power point (V_{mpp}) and current at maximum power point (I_{mpp}), respectively. At short circuit and open circuit conditions the output power is zero.

$$P_{\max} = V_{mpp} * I_{mpp} \tag{2}$$

Fill Factor: The fill factor (FF) is defined as the ratio of maximum power ($P_{max}=I_{mpp}*V_{mpp}$) to the product of the short-circuit current (I_{sc}) and the open-circuit voltage (V_{oc}) (Figure 4). The Fill Factor is another indicator sometimes used for evaluating the performance of PV modules in real operating conditions [20].

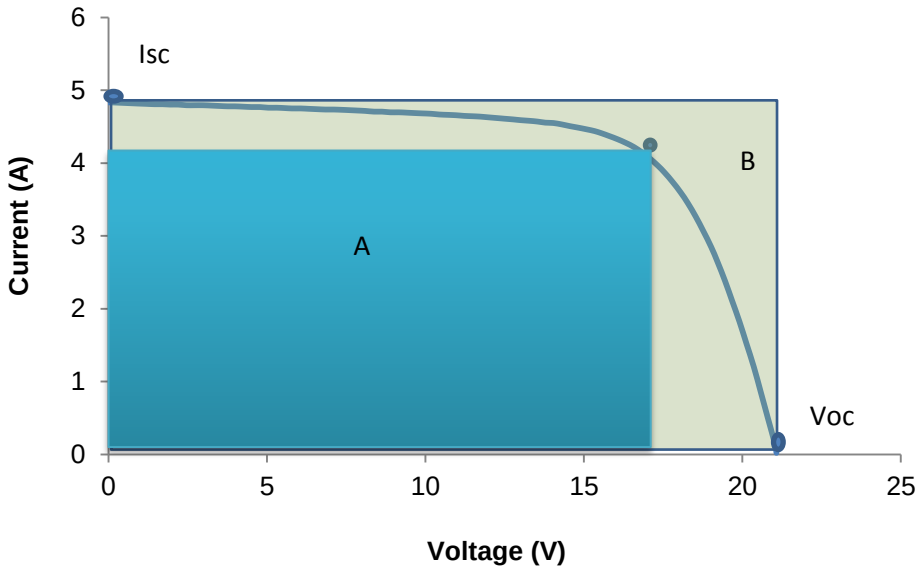

Figure 4: I-V curve and Fill Factor of PV module.

$$FillFactor\ (FF) = \frac{(V_{\max} * I_{\max})}{(V_{oc} * I_{sc})} = \frac{P_{\max}}{(V_{oc} * I_{sc})} = \frac{Area''A''}{Area''B''} \qquad (3)$$

Conversion Efficiency: Efficiency is the most commonly used parameter to describe device quality and for comparison between different solar cells or modules. The efficiency of a PV device is defined as the ratio of the maximum power (P_{max}) to the product of irradiance (G) and surface area (A_c) of the device.

$$\text{Conversion efficiency } (\eta) = \frac{P_{\max}}{(G * A_c)} = \frac{FF * V_{oc} * I_{SC}}{G * A_c} \qquad (4)$$

Parasitic Resistances: The performance of a PV device is reduced by loss mechanisms represented as internal resistances. These are classified as series (R_S) and shunt (R_{SH}) resistance (Figure 5). In an ideal device, R_{SH} would be infinite to avoid the path for current to leak and R_S would be zero to prevent any voltage drop between the junction and device terminals [19, 21].

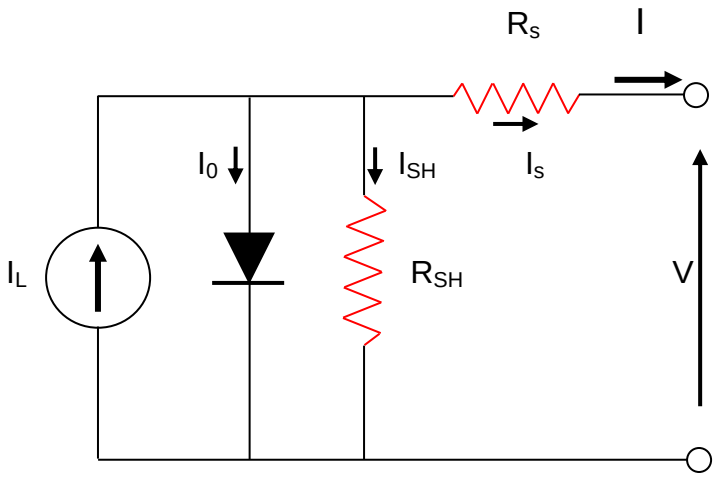

Figure 5: Parasitic series and shunt resistances in a solar cell circuit.

With the presence of series (R_S) and shunt (R_{SH}) resistances in the PV device the equation for current output is modified from (1) to (5).

$$I = I_L - I_0 * \exp\left[\frac{q(V + IR_S)}{nkT}\right] - \frac{V + IR_S}{R_{SH}} \quad (5)$$

Series resistance basically comes from resistance in the semiconductor layer, contact resistance between metallic contacts with silicon and imperfect connections at the top and rear contacts of the module (Figure 6) [21]. Series resistance has no effect on V_{OC} but near the maximum power point with relatively high current flow, the I-V curve is strongly affected which affects the maximum power (P_{max}) and ultimately the energy yield values over the time period.

Shunt resistance represents impurities near junctions which cause leakage of current near the edges of PV cells [21]. Low shunt resistance causes power losses in solar module by providing an alternate current path for the light-generated current which decreases the current flow to the output terminals of the PV device. The effect of shunt resistance is significant particularly at low irradiance levels, as the leakage current becomes significant relative to the small light-generated current (Figure 7). Both series and shunt resistance reduce the power at maximum power point (P_{max}) of the I-V curve [21].

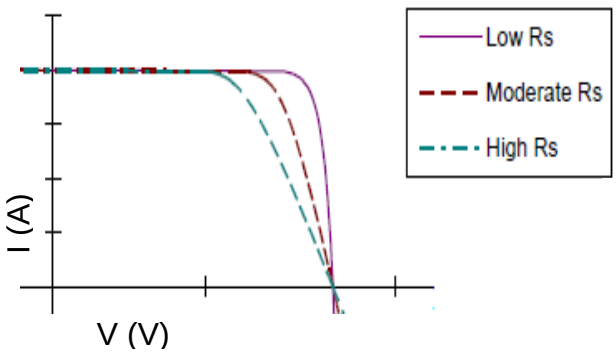

Figure 6: Effect of series resistance

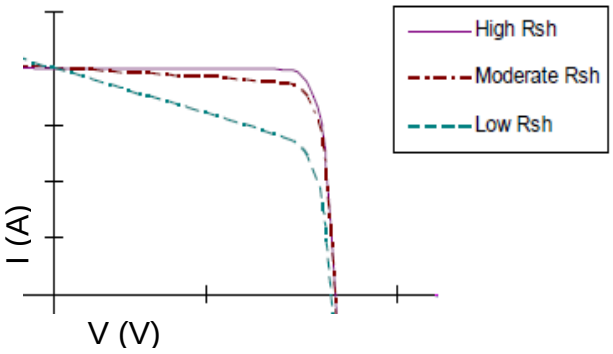

Figure 7: Effect of shunt resistance

2.3 Environmental Effects on PV Module Performance

All the above PV performance parameters vary with different environmental conditions, especially to variable irradiance and temperature in different locations. An increase in the irradiance increases the light-generated current (I_L) of the PV module and thus increases the total current, which leads to logarithmic increase of the voltage as per equation (2). As a result, both the power output and efficiency increase.

Varying the total irradiance on the PV modules affects all PV parameters, including the short-circuit current, open-circuit voltage, FF, efficiency and the impact of series and shunt resistances. Higher irradiance influences all the above parameters in the positive direction. I_{sc} increases linearly against irradiance and V_{OC} increases logarithmically with increased sunlight as per the equation (6) [19].

$$V_{oc} = \frac{kT}{q} \ln\left(\frac{I_{sc}}{I_o} + 1\right) \tag{6}$$

An increase in temperature decreases the band gap, the gap between valance band and conduction band of the semiconductor material, which increases the dark current. The reduced band gap also increases the light-generated current which increases I_{sc} modestly but the increasing dark current reduces voltage faster than photocurrent increases, hence decreases the output power of the module (Figure 8).

Effects of irradiance and temperature on the I-V characteristics of PV devices are plotted in Figure 8 and Figure 9 [22].

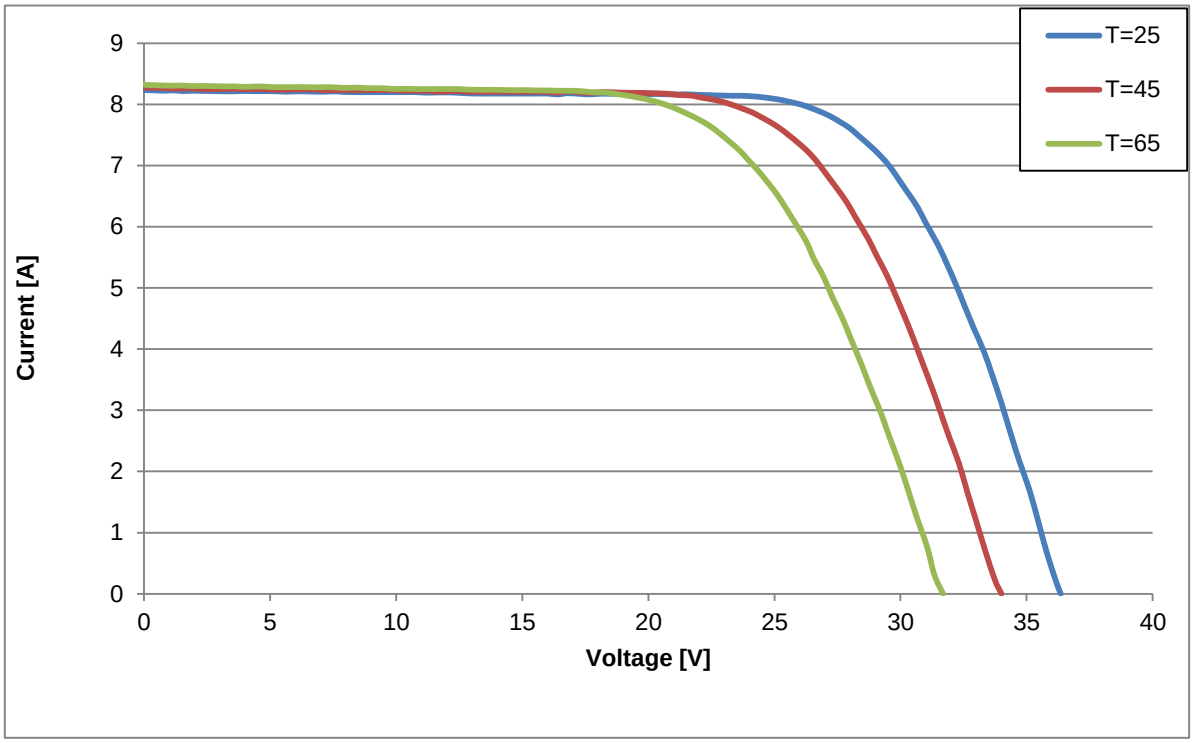

Figure 8: Effect of temperature on the I-V characteristics of a PV module

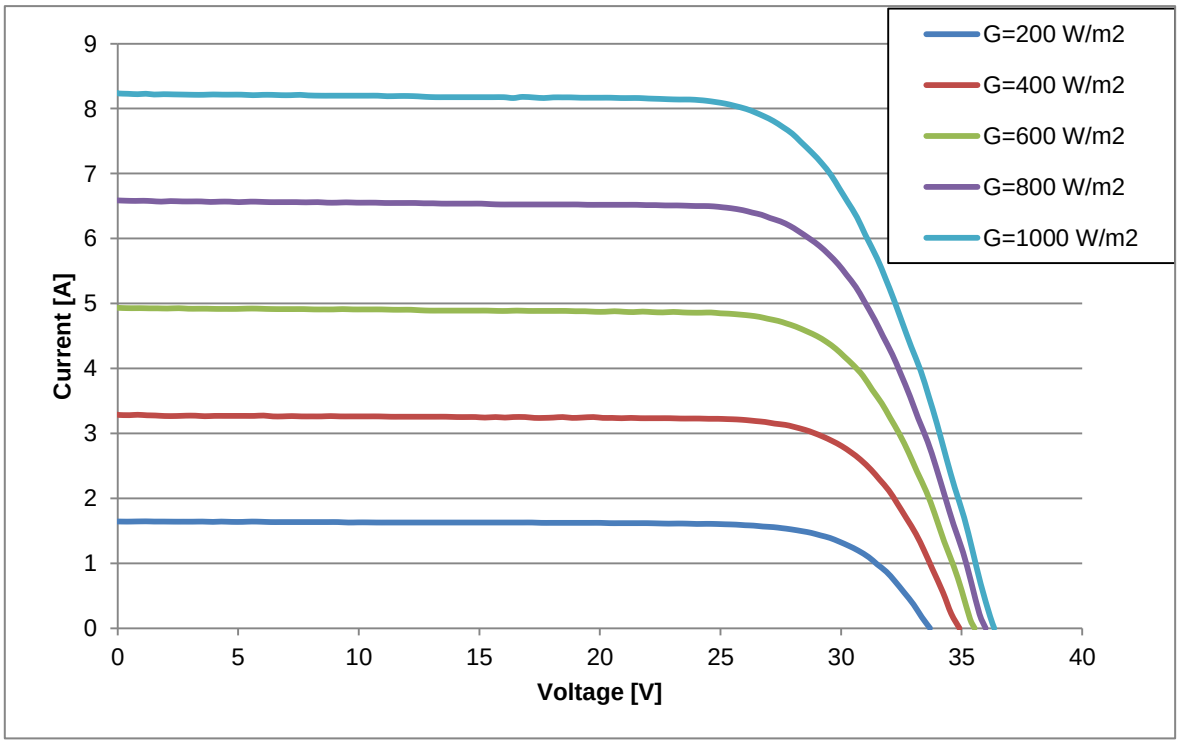

Figure 9: Effect of irradiance on the I-V characteristics of a PV module.

Sensitivity to environmental drivers varies with different material technologies commercially available in the marketplace such as crystalline silicon (c-Si), amorphous silicon (a-Si), Copper Indium Gallium Selenide (CIGS), etc, which explains below.

2.3.1 Irradiance Effects

Irradiance is one of the most influencing environmental parameters that affect the performance of any PV module technologies. Total solar irradiance is composed of direct and diffuse components of sunlight [18]. Direct irradiance is defined as the solar radiation received on the PV module from the sun's disk directly and diffuse irradiance is defined as the solar radiation received from sun after scattering by the atmosphere, from the remainder of the sky dome. Direct irradiance is the major fraction of total solar radiation in outdoor clear sky conditions. Increasing cloud cover increases the ratio of diffuse to total irradiance in any location. The effects of total irradiance on different PV module technologies (c-Si, a-Si and CIGS) are described here. The change of power generation at different irradiance levels of three module technologies is shown in Figure 10. The maximum power (P_{max}) of all three modules at different irradiance values have been normalised to their respective P_{max} at STC (equation (7)).

$$Normalised\ Power\ = \frac{P_{\max @ \text{ different Irradiance}}}{P_{\max @ STC}} \tag{7}$$

The power generation of all three technologies shows a similar trend against irradiance.

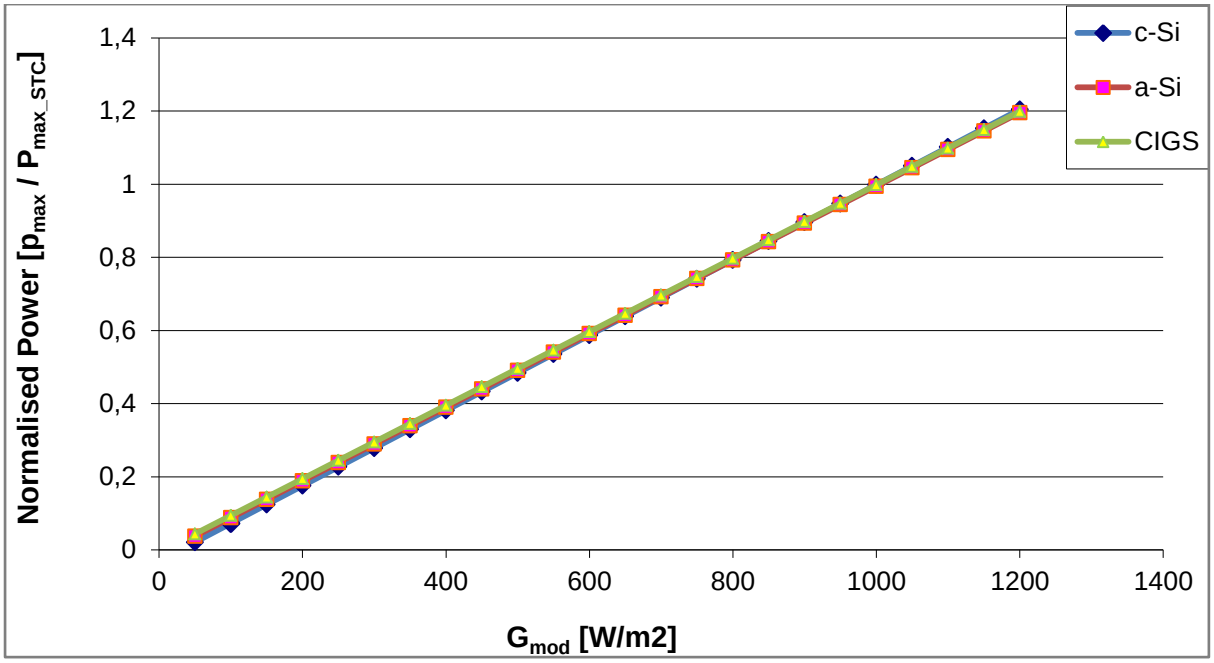

Figure 10: Normalised power of c-Si, a-Si and CIGS modules as a function of irradiance.

Figure 10 indicates that the power of all three modules examined within the scope of this work shown a linear in nature against irradiance. But it should also be noted that this linearity characteristics are mostly occurs at higher irradiance level. The non-linear nature of power of all the above modules at lower irradiance is not quite visible in the bigger range of irradiance scale in Figure 10. These non-linear characteristics are explained in the later chapter.

2.3.2 Temperature Effects

Another influencing environmental parameter that has an influence on the performance of PV module is site specific ambient temperature (T_{amb}). The module temperature (T_{mod}) can be estimated as a function of incident solar irradiance on the module as well as ambient air temperature, thermal properties of module encapsulation and the thermal effects of the mounting structure, also wind speed.

A temperature coefficient describes the relative change of any voltage, current or power with change in temperature. Temperature coefficients are expressed as percentage change per unit of temperature. The temperature coefficients of different

performance parameters are different for different PV modules. The performance of different PV modules has been measured at different temperatures and the results of the normalised power variation are shown in Figure 11.

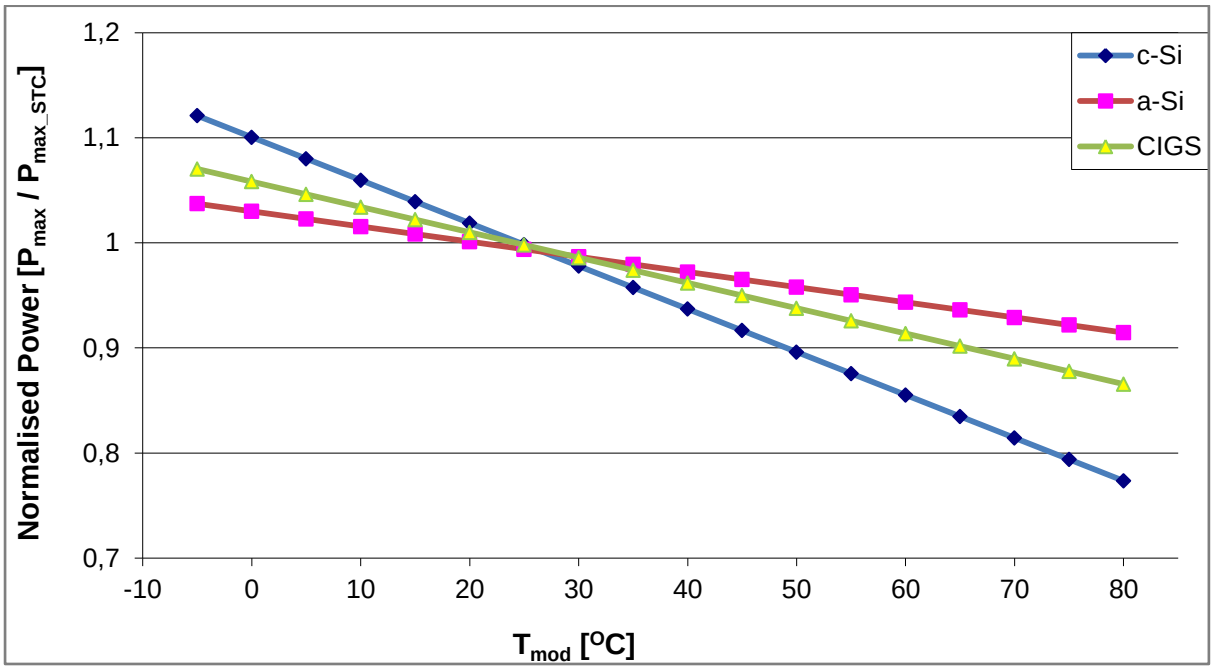

Figure 11: Normalised power of c-Si, a-Si and CIGS modules as a function of module temperature.

It is visible from Figure 11 that the rate of decrease in power for the crystalline silicon (c-Si) module is higher compared to other modules at increasing temperature [23]. The amorphous silicon (a-Si) module exhibits the lowest relative temperature coefficient [24-28] of the PV modules analysed in this thesis. The procedures to determine the temperature coefficients are described in the standard IEC 60891:1987 [29], IEC 61215 & IEC 61646.

K. Nishioka et al. [30] describes the strong effect of temperature on the conversion efficiency when the module temperature is higher. They claim that a 0.1%/°C improvement in the temperature coefficients can increase the annual energy of PV module near 1%. A large temperature coefficient will result in a decrease of the annual output energy of PV system on a larger scale compared to lower temperature coefficients.

2.3.3 Spectral Effects

Performance of PV modules at STC is reported with respect to an air mass 1.5 (AM 1.5) standard spectrum which explains in IEC60904-3. Air mass refers to the relative path length of the direct solar beam through the atmosphere. When the sun is at zenith, the path length is 1.0 (AM1.0) as in Figure 12. AM 1.0 does not necessarily mean that it will occur at solar noon because the sun is usually not overhead at solar noon in most seasons and locations [31]. Increasing the angle of the sun from zenith, the air mass increases as per equation (8). The air mass value is a calculated geometrical quantity influenced only by location, date and time. It is the prime influencer for the direct irradiance spectrum.

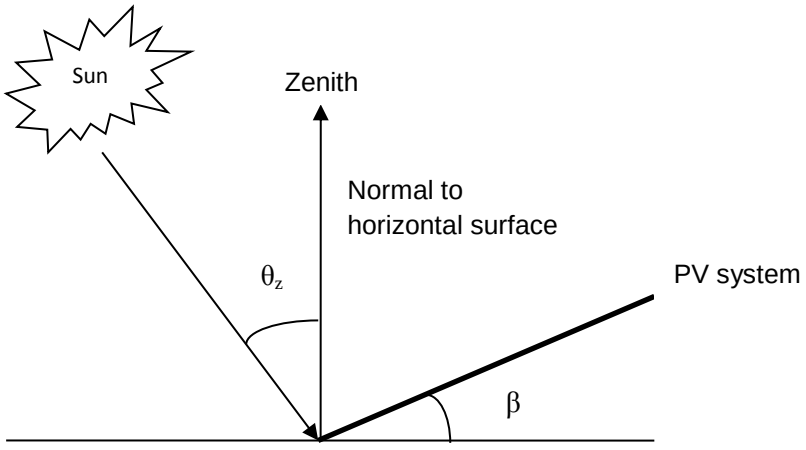

Figure 12 : Solar zenith angle (θ_z) and tilt angle of PV module (β)

$$AM = 1/\cos\theta_Z \tag{8}$$

Where θ_Z is the solar zenith angle as shown in Figure 12.

The effect of spectral variations in the irradiance is becoming significant, considering the availability and the commercial success of new generation PV module technologies; this is because the spectral responses of different devices are different, leading to a variety of sensitivity for different technologies. The spectral variation of solar irradiance can have a significant influence on the current generation of some device technologies in real operating conditions [32].

Short-circuit current generation of a device in outdoor operation is a product of variable spectral irradiance and spectral response of the device, as shown in equation (9). Figure 13 illustrates the spectral response of three different devices with the spectral irradiance at AM 1.5 standard spectrum.

$$I_{SC} = \int_a^b E(\lambda) * SR(\lambda) d\lambda \tag{9}$$

$$G = \int_a^b E(\lambda) \boldsymbol{d}\lambda \tag{10}$$

Where E is spectral irradiance (W/m^2/nm), SR is spectral response (A/W), G is irradiance (W/m^2) and for terrestrial applications the integration limits a & b are 300nm and 1400nm respectively.

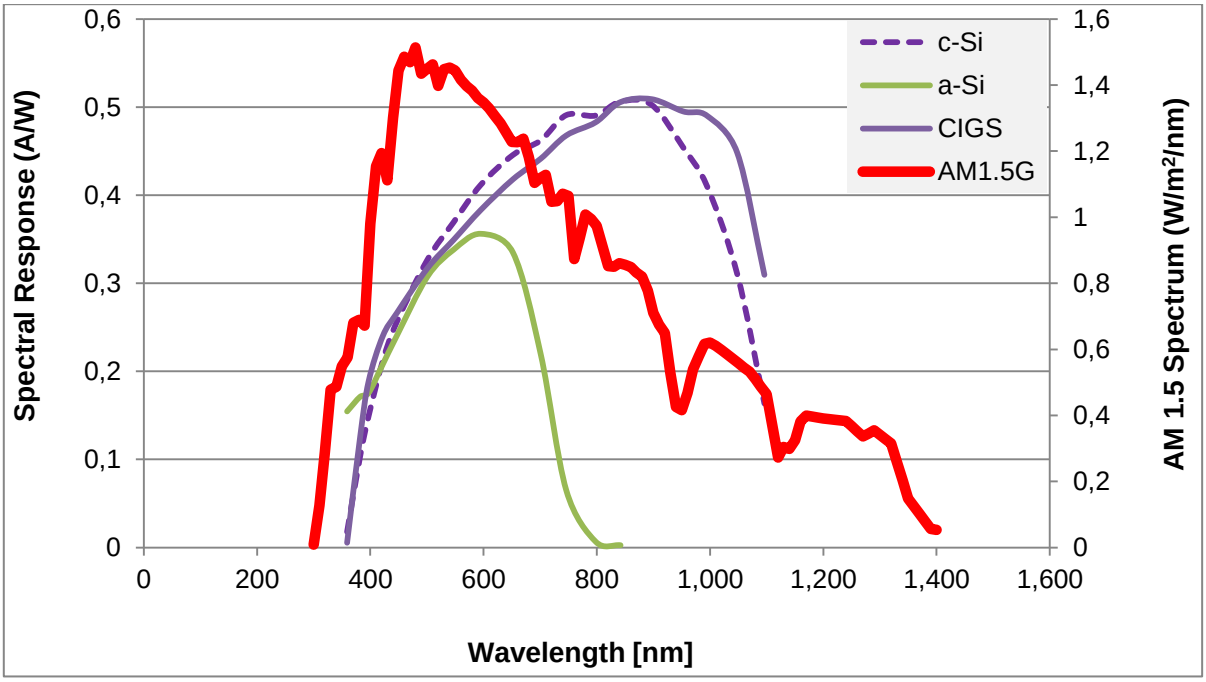

Figure 13: Spectral response of c-Si, a-Si and CIGS module and the spectral irradiance of the AM 1.5 standard spectrum.

The spectrally sensitive band of the c-Si module is approximately 300nm to 1150nm and the upper wavelength limit is slightly higher for the CIGS module. For other thin film devices, Cadmium Telluride (CdTe) lies between 350nm to 900nm and the upper wavelength limit for a-Si is limited to 780nm. Above difference in spectral sensitivity of different PV technologies are due to their different band gap properties.

Sensitivity of power at different AM spectrum is analysed for all three PV modules. In Figure 14 is it shown that the highest performance of the a-Si module occurs at low air mass conditions, which means around noon time. But c-Si shows best performance in early morning and late afternoon when the air mass value is higher (Figure 14). If the spectral response at shorter wavelengths (blue response) is low and the longer wavelengths (red response) is high, then generation of short-circuit current (I_{sc}) (as per the equation (9)) is higher at medium air mass. Generation of current (I_{sc}) for the a-Si module decreases with increasing air mass because of the narrow spectral response band - 350nm to 780nm (Figure 13). Generation of I_{sc} changes with the changing solar spectrum during the day and year as the spectrum changes with the distance that light has to travel through the atmosphere.

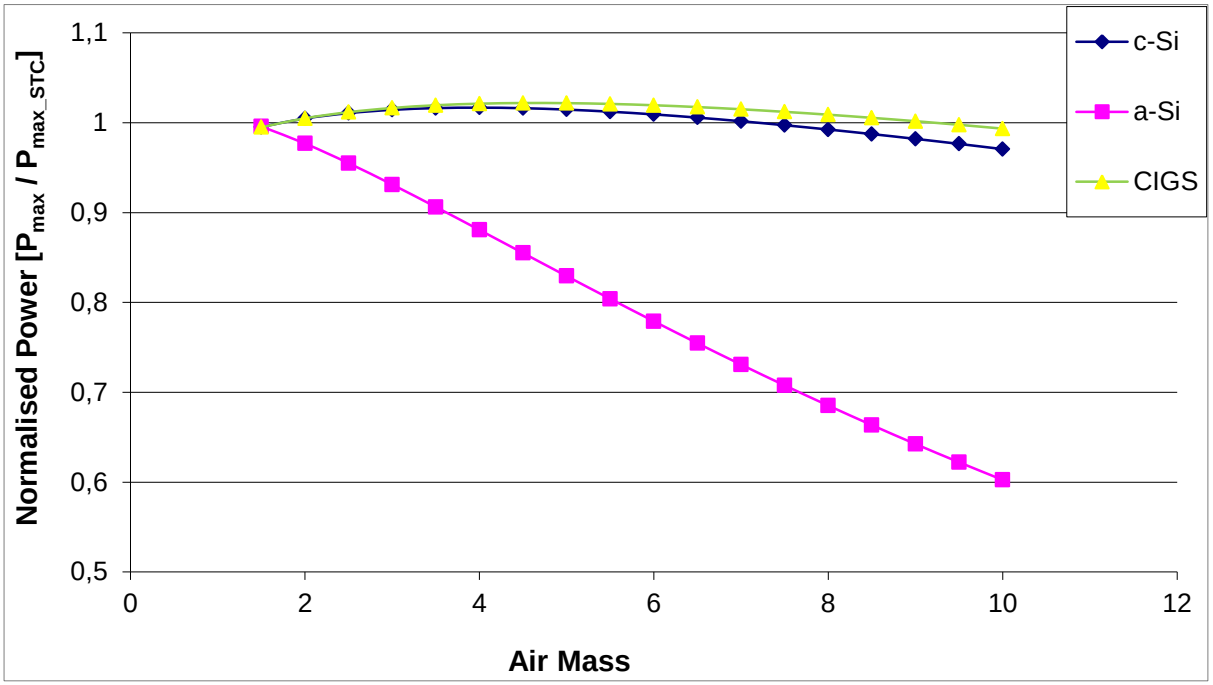

Figure 14: Normalised power of c-Si, a-Si and CIGS modules as a function of air mass.

Spectral distribution is the secondary driver (after irradiance and temperature) for maximisation of current generation. Multi-junction solar cells are promising to maximum utilisation of solar irradiance at different spectra, hence maximisation of PV system energy output. Minemoto et al [33] describes the effects of spectral irradiance distribution in outdoor performance of amorphous Si//thin-film crystalline Si (a-Si//μc-Si) stacked PV devices. The top surface of the module consists of a hydrogenated a-Si solar cell and bottom surface of μc-Si solar cell with a monolithic series-connected tandem structure.

These multi-junction cells have advantages over conventional crystalline silicon modules, because of an improvement in spectral response at different wavelength ranges and better utilisation of the solar spectrum. The top cell (a-Si) absorbs shorter wavelength light and the bottom cell (μc-Si) absorbs longer ones, as a result increase the overall voltage because of the two series connected cells.

Few energy prediction methods not included the spectral correction of irradiance at AM 1.5 spectrum. The impact of spectral variation on the annual energy yield of PV modules are important in order to achieve better estimation accuracy, especially for thin film PV devices.

2.3.4 Angle of Incidence Effects

Angle of incidence of sunlight is one of the parameters of the standard test conditions. It has an important influence on the power output of the PV devices and hence the energy yield. This angle is defined as the angle between the normal to the module plane and the sun, as seen in Figure 15.

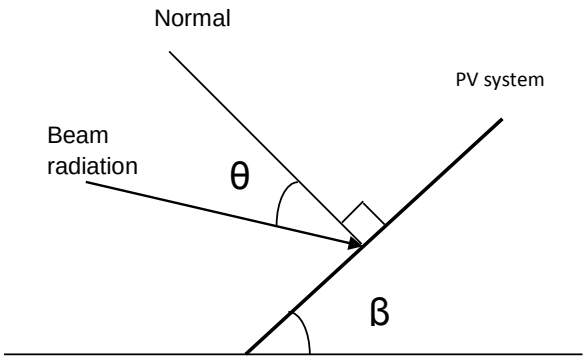

Figure 15: Angle of incidence (θ) and tilt angle (β) of the module

The conventional method to calculate angle of incidence is given in the equation (11).

$$\theta = Cos^{-1}\left[Cos\theta_Z * Cos\beta + Sin\theta_Z * Sin\beta * Cos(\gamma_S - \gamma)\right] \quad (11)$$

Where θ = angle of incidence

θ_z = zenith angle

β = tilt angle

γ_S = solar azimuth angle: angle between due south and the position of the Sun

γ = azimuth angle of module

Optical losses, reflection and transmission, occur due to the variation of the incident light angle on the PV module.

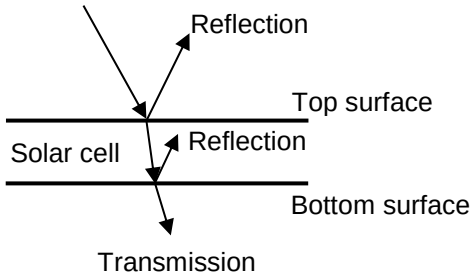

Figure 16: Optical losses in a PV module

Optical losses can be minimised by using an anti-reflection coating (ARC) on the top surface and reflector on the back surface. Texturing the front surface of the glass can also reduce the reflection losses. Transmission of solar radiation through to the solar cell is affected by the incidence angle; Figure 17 shows the tracing of a ray through the solar cell.

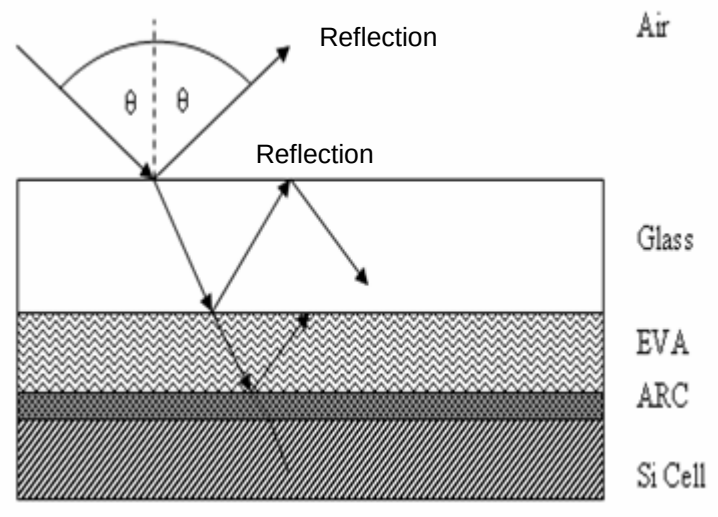

Figure 17: Tracing of ray incident on a typical module encapsulation [34].

Due to the optical properties of the top glass cover, high angles of incidence usually lead to more reflection losses on the surface of the module than low angles do, so variable AOI also affects the annual output of the PV module.

2.4 Distribution of Realistic Environmental Conditions and Their Impact on the Distribution of Energy

To date, all manufacturers describe the performance of their PV modules under STC conditions [i.e. irradiance at 1000 W/m^2, normal angle of incidence, standard spectrum with AM1.5G distribution and 25ºC module temperature]. But the operational performance is largely explained by the local weather conditions in the specific operating location.

The annual distributions of the realistic environmental parameters in maritime climate are illustrated in this chapter. The annual irradiance, temperature, angle of incidence and air mass data has been taken from the CREST outdoor monitoring system. Distributions of annual environmental data and the energy distribution against those parameters in Loughborough are shown in Figure 18 to Figure 25.

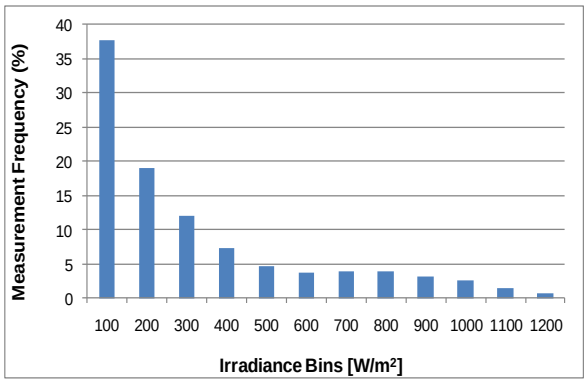

Figure 18: Distributions of irradiance measurement

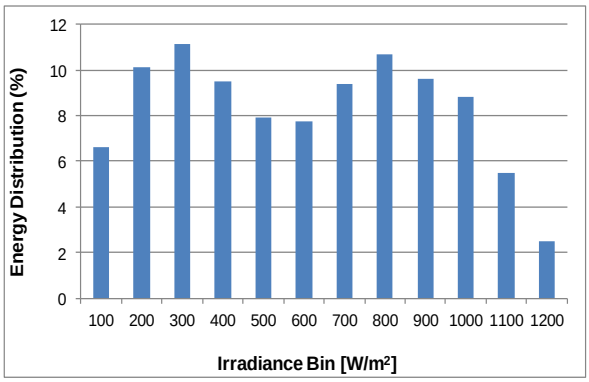

Figure 19: Distributions of energy of a c-Si module against irradiance

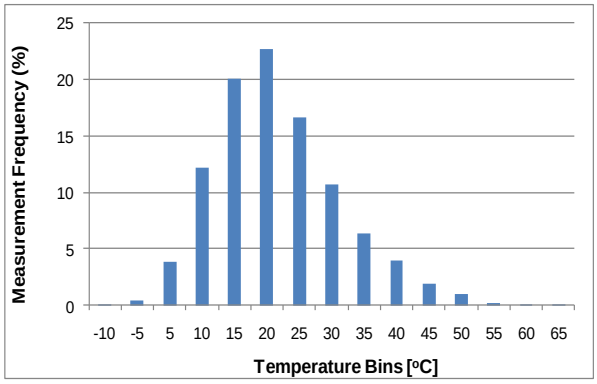

Figure 20: Distributions of temperature measurement

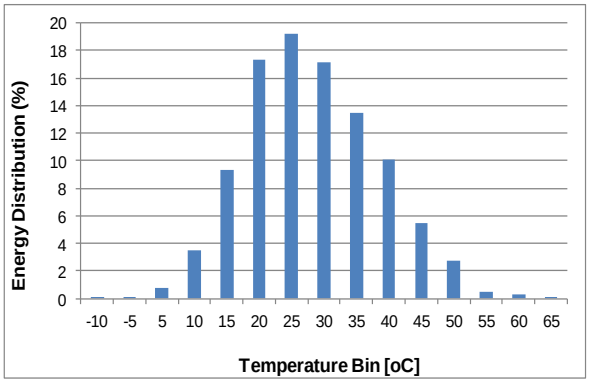

Figure 21: Distributions of energy of a c-Si module against temperature

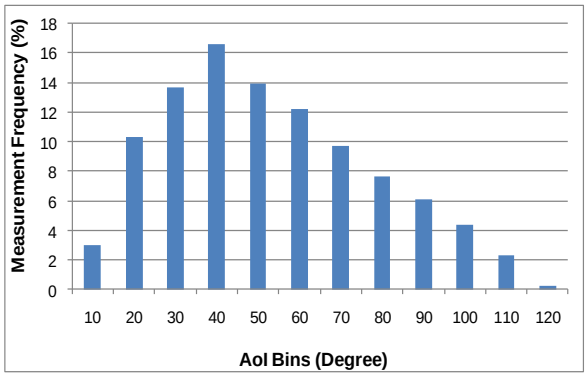

Figure 22: Distributions of angle of incidence measurement

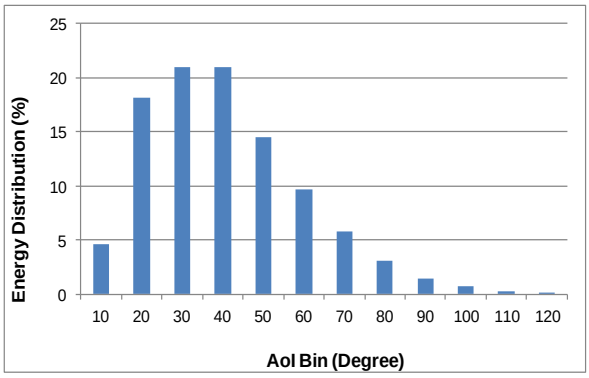

Figure 23: Distributions of energy of a c-Si module against angle of incidence

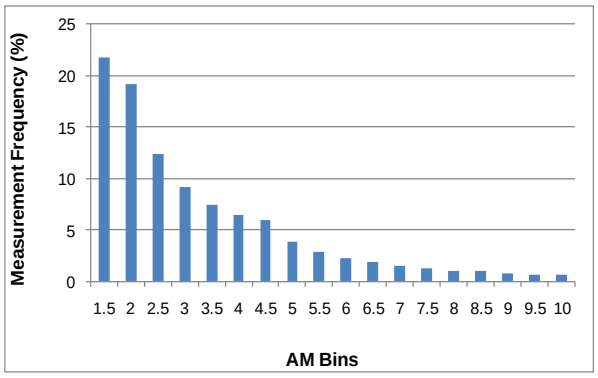

Figure 24: Distributions of air mass measurement

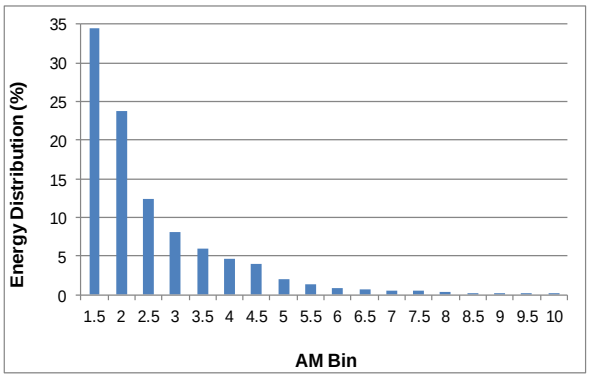

Figure 25: Distributions of energy of a c-Si module against air mass

Annual measured data of the above four environmental parameters are binned. The chosen bin sizes for irradiance, temperature, angle of incidence and air mass are 100 W/m^2, 5°C, 10° and 0.5, respectively. This gives the distributions of each parameter at Loughborough and demonstrates what a PV module will encounter in real operation. It is clearly visible from Figure 18 to Figure 24 that the availability of STC conditions is very rare in real operation at Loughborough. Annual STC irradiance and temperature availability at Loughborough are 2.57% and 16.59%, respectively. The availability of all four STC parameters at the same time is close to zero. These values are site specific and one can see different figures in different locations. But the availability of a larger proportion of STC conditions in any location is near to impossible. As a result, there is a requirement of a reliable performance indicator at realistic operating conditions, which should count the influence of different environmental conditions on the PV modules. The effects of different weather conditions on different PV module technologies are illustrated below.

2.5 Conclusions

This chapter illustrated the electrical performance parameters of PV devices and the distributions of the available environmental parameters at Loughborough, UK. A comparison of the realistic operating conditions for PV modules referenced against STC parameters was presented. The contributions of non-STC conditions towards

annual energy production are identified. Each irradiance bin (at 100W/m2 bin width) represents up to 11% contribution towards annual energy generation in Loughborough, UK. STC temperature and Standard spectrum contributes just under 20% and 35% of the annual energy generation respectively. Whereas Normal incidence angle contribution for the non-tracking PV system is negligible. It should also be noted that the above values is site dependent. Availability of non-STC conditions leads to the need of an energy based estimation method for better understanding of PV performance in real operation.

In UK climate at Loughborough, about 30% of total electrical energy is generated at irradiances below 300W/m^2. This leads to the need for an energy yield prediction methodology with good low-light characterisation and modelling considerations, specially commercial PV market in the UK is very promising and the irradiance profile in the UK and in Germany is not very dissimilar, which is the biggest solar PV market so far.

This chapter also analyses the sensitivity of the environmental parameters for different PV module types. Better understanding of the performance variation of different PV module technologies in relation to the variable environmental conditions, help establishing a required robust energy yield prediction method. Technology inter-comparison against temperature shown that the power loss of c-Si module is 1-2% /degree centigrade compare to a-Si device. Also a required robust energy yield prediction methodology should include the technology independent spectral irradiance factor, as a-Si module shows better performance at 1.5AM and c-Si module shows its best AM response spectrum is at 4AM.

Existing energy yield prediction methods are introduced in the next chapter in order to compare the current methods and a proposed robust yield prediction method. An accurate prediction method not only assists to estimate financial return of investment more accurately, it also generates confidence within the whole PV community.

3 Energy Yield Prediction Methodologies and Modelling for Energy Rating

3.1 Introduction

Accurate energy yield prediction is an essential requirement for the Photovoltaic (PV) community. This should include better understanding of the behaviour of different PV module performance parameters against different climatic conditions and good quality weather data.

PV modules are typically rated at Standard Test Conditions (STC[†]) [35-36]. This STC rating is basically a rating of power output of module which does not provide relevant information about the performance of different PV modules in different weather conditions. STC rating provides only a snapshot of performance under a favourable (laboratory based) but rarely-seen-in-practice set of conditions. When looking at long term energy output, it is not helpful since the power output and the efficiency varies depending on the conditions.

It is also necessary to mention that the scope of this thesis analyses the DC energy prediction of the system without including AC part of the system.

These days, large scale PV systems are being commissioning in different locations supported by financial organizations and they are interested to know their payback period or internal rate of return (IRR) of their investment more accurately. In this context, cost per kWh production of PV systems has become the most important factor for the PV community. Hence, the prediction of energy yield of a proposed PV system is directly relevant to the income generation.

[†] Irradiance 1000 W/m^2, Module Temperature 25 °C, Angle of Incidence 0°, Spectrum AM1.5G

Prediction of energy yield and the energy rating is two different measures of a system. Energy yield prediction is a site specific quantify, whereas energy rating can be defined as the prediction of energy by means of a standardised methodology in relation to a standardised weather dataset.

To describe the energy yield prediction of PV modules, it is necessary to introduce the different elements involved in the process. An energy prediction method includes:

- PV module characterisation data as module input
- Meteorological datasets as site input
- Energy prediction methodology.

Research on energy yield prediction is an on-going topic within the PV research communities and there are several energy prediction methods available by different research groups [37-49] and those methods are similar to a certain extent. But presently, there is no standard available which describes an energy yield prediction method in a standardised way with a standardised weather dataset – energy rating. International standardisation body - International Electrotechnical Commission (IEC) has proposed an energy rating method – IEC 61853.

This chapter describes the state-of-the-art in-present energy yield prediction methods and then describe the evaluation effort of the energy rating method as a scope of this thesis to identify the scale of influencing weather parameters on the performance of PV module.

3.2 Existing Energy Yield Prediction Methods

Some of the current energy prediction methods are outlined below. They attempt to account for the varying outdoor operating conditions that PV systems encounter in operation. As explained above that any energy yield prediction would require two sets of input data and a calculation method.

To get the PV module characterisation data as a module input into the prediction model, one of two methods is generally applied.

- Firstly, some prediction model considers the module efficiency (η) as a function of irradiance (G) and module temperature at 25^{o}C, i.e. η (25^{o}C, G). This method also requires the temperature coefficients at the specified irradiance.
- The second method is a matrix method, where modules are characterise in terms of power (P_{max}) or efficiency as a function of wide range of irradiance (G) and temperature (T), i.e. P (G, T) or η (G, T).

The method developed by CEA (Caderache, France) is called *Meteorological, Optical and Thermal Histories for Energy Rating in Photovoltaics* (MOTHERPV*)* [38]. This method gives the prediction of the performance ratio (PR) - the ratio of actual energy yield to the theoretical generation based on the power rating and incident solar irradiation - for sites with a good knowledge of the frequency distribution of the incoming energy (as a function of irradiance) and the module temperature. This prediction method requires a short measurement campaign at a given site with number of irradiance and temperature levels. The irradiance value is calculated by dividing the short circuit current of the module by its short circuit current at STC. Then the non-linearity coefficient of power (η_{rel}) of a module as a function of the irradiance is calculated using equation (12).

$$\eta_{rel} = P(G, T_{Mod}) / P_{STC} * G \qquad (12)$$

Where,

P (G, T_{Mod}) is the power at the module when the G is irradiance and T_{Mod} is module temperature.

P_{STC} is the power at the module at Standard Test Conditions

G is the target irradiance

Then the relative module efficiency is calculated as a function of irradiance and measured module temperature using equation (13).

$$\eta(G) = \eta(G_{ref}) * [1 + \alpha * (G) * \{T_{\mathrm{mod}}(G) - T_{\mathrm{mod}\,ref}(G)\}] \quad (13)$$

Where η (G_{ref}) is the conversion efficiency of the module at reference irradiance G_{ref} and reference module temperature $T_{mod\ ref}$. η (G) is the targeted efficiency at targeted G and T_{mod}. α is the irradiance-dependent temperature coefficient of the module efficiency.

This method considered the effects of irradiance, temperature and Air Mass (AM) spectrum on the performance of a PV module. But it is difficult to achieve a wide range of PV operating conditions within the short measurement time period in other location.

The energy prediction methodology developed by ECN, Netherlands [37, 38] is called *Yield Simulator* which is similar to the MOTHERPV method. Yield Simulator measures the efficiency as a function of ambient temperature and in-plane irradiance considering direct and diffuse components of irradiance. The temperature coefficients of the module are calculated as a function of irradiance within the range 250 W/m^2 to 1000 W/m^2 at intervals of 250 W/m^2.

Bucher el. at. developed a method, called *Realistic Reporting Conditions (RRC)* [41]. This method uses indoor measurements of module characteristics and hourly tabulated weather data to calculate the hourly efficiency of a PV module. Williams el at. developed the *Site Specific Conditions* (SSC) model based on the RRC method to predict the energy yield of different PV modules [37]. The flow diagram of the RRC method is shown in Figure 26. The required inputs for module characterisation data are irradiance, module temperature and spectral response of the individual module. Thus the I-V characteristics and temperature coefficients of a module are obtained.

This model described the effect of the site-specific meteorological parameters - the global irradiance (G), its spectral distribution (E (λ)) and the cell temperature (T) - on the deviation of the module efficiency (η) from the STC efficiency (η_{STC}).

They are defined as follows:

G-effect:	$rG = \eta_G/\eta_{STC}$	influence of G on η
T-effect:	$rT= \eta_{G,T} / \eta_G$	influence of T on η
E(λ)-effect:	$rE = \eta_{G,E} / \eta_G$	influence of E(λ) on η
RRC-effect:	$rRRC = \eta_{RRC}/ \eta_{STC}$	influence of G, T and E (λ) on η

Realistic module efficiency is then estimated using hourly tabulated weather conditions.

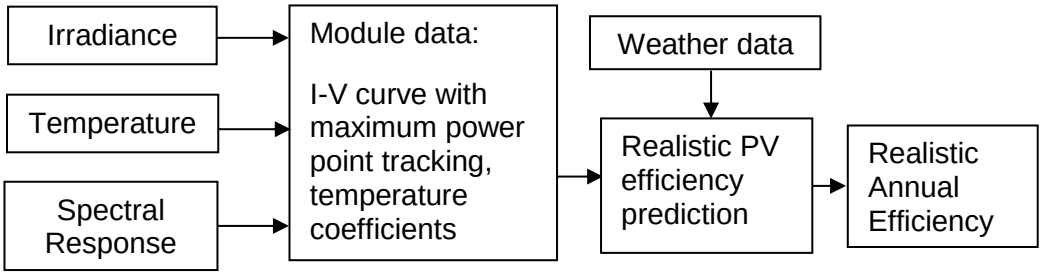

Figure 26: Flow diagram of RRC energy prediction method

Indoor module characterisation method of the RRC model offers wide range of irradiance, temperature and spectrum data in a controlled environment within a short period of time. But mismatch of the representation of the outdoor data in the indoor measurement data point cannot be ignored, which can increase the error in the yield prediction.

ESTI-JRC, ISPRA developed [43] another energy prediction method. For PV module input data this method employs a power matrix as a function of irradiance and ambient temperature, P (G, T_{amb}). Another matrix of weather data as a function of total irradiance and ambient temperature, N (G, Ta) for a site is also used in this method. Correlating these two matrices the energy yield is then estimated. This method characterises the module indoors under a wide range of irradiance and temperature and transforms the indoor measured power matrix in respect of module temperature into ambient temperature. The ESTI-JRC energy yield prediction method is illustrated in Figure 27.

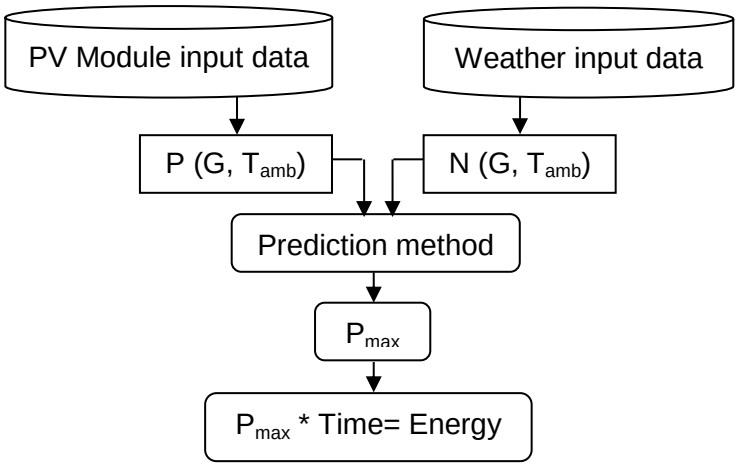

Figure 27: Flow chart of ESTI-JRC energy yield prediction method

The ESTI-JRC matrix method is validated based on irradiance and temperature only, without taking into account the effects of different Air Mass (AM) spectrum, or angles of incidence (AoI). This makes the prediction model simplified but the possible error can come from other environmental parameters. Especially, irradiance spectrum at different Air mass is a key environmental parameter when one considers spectrally sensitive thin film modules.

Another performance model developed by SUPSI, Switzerland is called the *Matrix method* [49] and is similar the ESTI-JRC method. In this Matrix method, modules are characterised in order to generate a power matrix as a function of in-plane irradiance (G) and back of module temperature (T_{mod}), P (G, T_{mod}) and correlates with irradiance and the ambient temperature (T_{amb}) of the specific location. To make a link between module data and environmental data, the measured module power matrix is converted from P (G, T_{mod}) to P (G, T_{amb}) using equation (14).

$$T_{\mathrm{mod}} = (NOCT - 20^{0}) * G / 800 + T_{amb} \qquad (14)$$

NOCT is the nominal operating cell temperature which is defined based on the mounting structure of the module, irradiance at 800 W/m^2 and 20°C ambient temperature.

Energy predictions methods are explained above have limitations in different ways. Some models only considered irradiance and temperature effects without considering the spectral and angular affects, which potentially increase the level of

prediction error. Also, some methods are limited to a particular module technology. Outdoor based module characterisation methods generally required a long time exposure of PV modules to cover a reasonable amount of data for energy predictions, which is a time consuming effort (at least a year). But it gives better accuracy in the prediction as this method considers all influencing weather parameters in the module characterisation method.

Indoor based module characterisation methods generally limited to irradiance and temperature and this is largely due to the limitation of the availability of the measurement equipment. But this method can allow getting module characterisation data in a wide range of irradiance and temperature conditions; hence an energy yield prediction could be quicker. Strength and limitations of the above methods are tabulated below:

Method	Strengths	Limitations
MOTHERPV and YIELD SIMULATOR	• Outdoors fast module characterisation • Spectral effects included	• Short measurement period will not be representative to cover full range of weather conditions in other location
RRC and SSC	• Indoors fast module characterisation • Spectral mismatch correction included	• Potential error from spectral mismatch corrections
MATRIX METHOD	• Simple indoors fast module characterisation • Spectral effects not included	• Spectral mismatch error

Table 1: Strength and limitations of the existing energy yield prediction methods

To address some of these issues, the International Electrotechnical Commission (IEC) has proposed an energy rating standard for PV modules, which considers all major parameters that affect the performance of PV modules. A detailed description of the modelling efforts of the proposed standard is explained and the evaluation in the next sections.

3.3 IEC Energy Rating Standard

The aim of this proposed energy rating standard is to establish a reliable and accurate energy rating method for evaluating the performance of different PV technologies in real operating conditions. This standard aims to address the

following issues, which is similar to the requirement of other energy yield predictions described above:

- Establish a direction for mapping the module performance over a wide range of temperature and irradiance conditions.
- Establish the test method to find out spectral response of different modules at variable spectrum,
- Effects of incidence angle of the irradiance,
- Estimate the module operating temperature as a function of ambient temperature, irradiance and wind speed,
- Establish a prediction model that should apply to any module technology under different climatic conditions worldwide.

Information on this proposed standard is published elsewhere [50]. This chapter describes the modelling aspects and the issue arises during evaluation. The IEC energy rating standard is modelled and first time validated during the course of this work. The execution of a detailed evaluation and the validation of this proposed standard include the impact analysis of different environmental parameters - including spectral effect - on the energy generation of PV module technologies. Dependency of energy production on spectral response of different PV module technologies is included in this standard. The validation results and uncertainty analysis are revealed in chapter 4.

The proposed standard - IEC 61853, is divided in different parts, are described below.

Part 1 [51] indicates the requirement for evaluating PV module performance in terms of power rating over a wide range of irradiance and module temperature. This gives a full set of characterization data at different irradiance and module temperature in a matrix form. **Part 2** [52] explains the measurement and analytical approach used to incorporate the effects of angle of incidence (AOI), spectral response and the estimation of module operating temperature from more usually available weather data. **Part 3** [53] consists of the calculation of energy rating procedures based on measured and modelled values of parts 1 and 2 by implementing some reference weather data profiles which are yet to be finalised (and were previously to be

described in so-called part 4 [54] of the proposed draft standard). Detailed description of the individual parts is given below.

3.3.1 **Part 1: Measurement Method**

This part explains the measurement requirement for the evaluation of the effects of irradiance and temperature on PV module power output. This is carried out by taking I-V measurements at a number of different irradiances at AM1.5G spectrum and different module temperatures. The experimental procedure can be performed using the following ways to create the performance matrix as shown in Table 2 and these measurements can be performed in an indoor or outdoor based measurement system.

I. Dependency of the parameters, I_{sc}, V_{oc}, I_{max}, V_{max} and P_{max} at a range of irradiance (100 to1100 W/m^2) and at a range of module temperature (15^{0}C to 75^{0}C) at fixed module temperature.

Temperature (°C)	Irradiance (W/m^2) 1100	1000	800	600	400	200	100
15	NA	•	•	•	•	•	•
25	•	•	•	•	•	•	•
50	•	•	•	•	•	•	NA
75	•	•	•	•	NA	NA	NA

Table 2: Performance matrix of PV module as a function of irradiance at AM1.5G and temperature

Temperature coefficients of I_{sc}, V_{oc}, I_{max}, V_{max} and P_{max} can be extracted from the matrix as functions of irradiance. Spectral and angular measurements are undertaken in part 2. The above module characterisation measurements are done indoors in a controlled environment under a short measurement campaign.

3.3.2 **Part 2: Measurement Method**

Part 2 describes the measurements of spectral response, angle of incidence (AoI) and module operating temperature.

The angle of incidence dictates the fraction of direct beam irradiance available for the conversion of electrical energy of the PV module. The test method of AoI response characterisation is based on measuring the I_{sc} of the test module over a range of incidence angles. The method prescribed to change the angle between module normal and light incidence (on the module) from -80^o to +80^o at 10° intervals both for azimuth and tilt direction [52]. For each AoI, at least three readings of short-circuit current and module temperature are taken, at different irradiances. The relative light transmission is calculated using equation (15):

$$\tau(\theta) = {I_{SC}}/{Cos\theta * I_{SC}(0)} \quad (15)$$

Where θ is the angle of incidence angle with respect to the module normal.

Module operating temperature: In real operating conditions, the temperature of a PV module (T_{mod}) is primarily a function of the ambient air temperature (T_{amb}), total solar irradiance (G) and the wind speed on the active surface of the module. The temperature difference, (T_{mod} - T_{amb}), largely depends on ambient temperature. The pyranometer, irradiance measurement sensor, or PV reference device is recommended to be mounted in the same plane as the test module to measure the total irradiance. The wind speed measuring instrument is required to be installed at 0.7m above the top of the test module and at 1.2m to the east or west of the module. An ambient air temperature sensor also needs to be installed near the wind sensor in a shaded enclosure with good ventilation. Module temperature can be taken by averaging the values of four back contact temperature sensors. A data set is then prepared in the form of T_{amb}, T_{mod}, wind speed and G and that are grouped based on different wind speed ranges as follows,

Wind speed group	wind speed range
1	<1 m/s
2	<1 m/s to <2 m/s
3	<2 m/s to <3 m/s
4	<3 m/s to <5 m/s

5	<5 m/s to <7 m/s
6	<7 m/s to <9 m/s

Table 3: IEC 61853 wind speed range

Plotting the difference between module and ambient temperature (T_{mod} - T_{amb}) against G at various wind speed groups, the thermal coefficients ‘a’ and ‘b’ can be estimated. The module operating temperature can be calculated then using equation (16).

$$T_{\mathrm{mod}} = T_{amb} + b * G + a \tag{16}$$

3.3.3 **Part 3: Energy Rating Calculations**

This section describes the modelling part of energy prediction algorithm. The energy rating calculation procedure is illustrated in Figure 28. The left column demonstrates the input parameters measured in part 1 and part 2 as module input data. The right column describes the environmental input parameters, while the centre column lays out the calculation methodology. The primary input parameters that influence the energy rating calculation are outlined below; those have been described above in part 1 and part 2.

- Relative light transmittance into the module
- Thermal coefficients ‘a’ and ‘b’ describing module operating temperature
- Spectral response of the module
- Matrix of P_{max} vs. irradiance (at AM 1.5G) and module temperature

The input weather data for energy rating calculation includes the direct and diffuse irradiance with respect to module incidence angle to get the available irradiation into the module. The incident spectrum, wind speed and ambient temperature are the other environmental parameters considered in this model. The detailed overview of the proposed energy rating procedure is outlined in Figure 28.

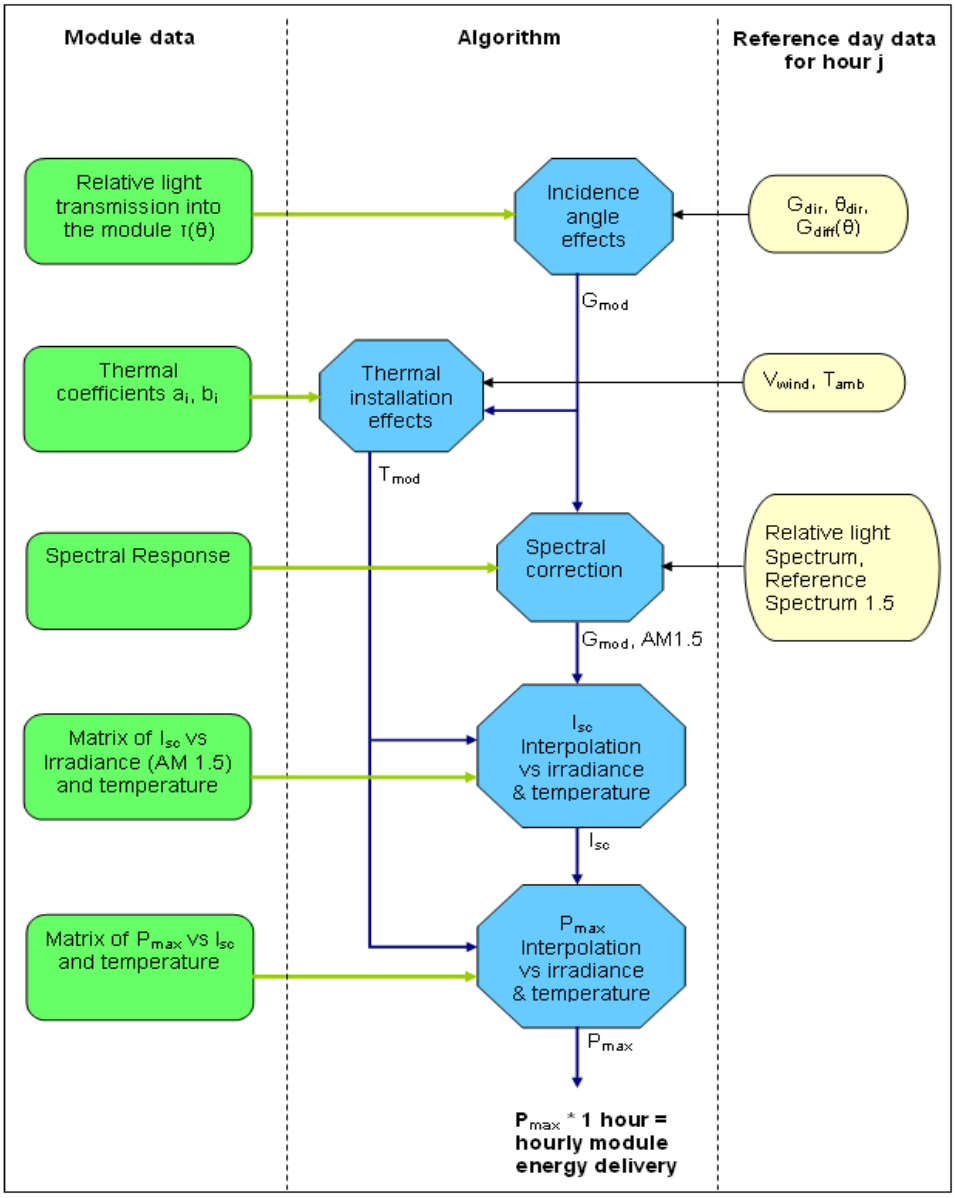

Figure 28: Overview of Energy Rating Procedure.

3.3.4 **Reference Dataset**

The original IEC draft standard presented six reference days [54] to cover extreme combinations of ambient temperature and irradiance to estimate the energy yield of the module. It is also worth mentioning that at the current state of this standard, identification of another dataset is ongoing. But at the time of this study, the old dataset (that has six reference days) are tabulated with irradiance, ambient temperature, wind speed, angle of incidence and spectral distribution over each day, with the cases labelled as:

- HIHT (High irradiance, high temperature)
- HILT (High irradiance, low temperature)
- MIMT (Medium irradiance, medium temperature)
- MIHT (Medium irradiance, high temperature)
- LILT (Low irradiance, low temperature)
- NICE (Normal Irradiance, cool environment)

The above reference days are distinguished in Figure 29 for a typical crystalline silicon device with different module temperatures (T_{mod}) and incident irradiance on the module (G_{mod}). T_{mod} is calculated according to the IEC algorithm, considering the effects of irradiance and wind speed with the given ambient temperature. G_{mod} is calculated considering the given beam and diffuse irradiance components of the different reference days and the transmittance values with the different angle of incidence (AOI), measured for the module. Reference day conditions are tabulated at hourly intervals in the figure below, each point is one of these entries. For HIHT, there are two different irradiance values are calculated at 50°C T_{mod}, which raise an quality issue of the available reference days.

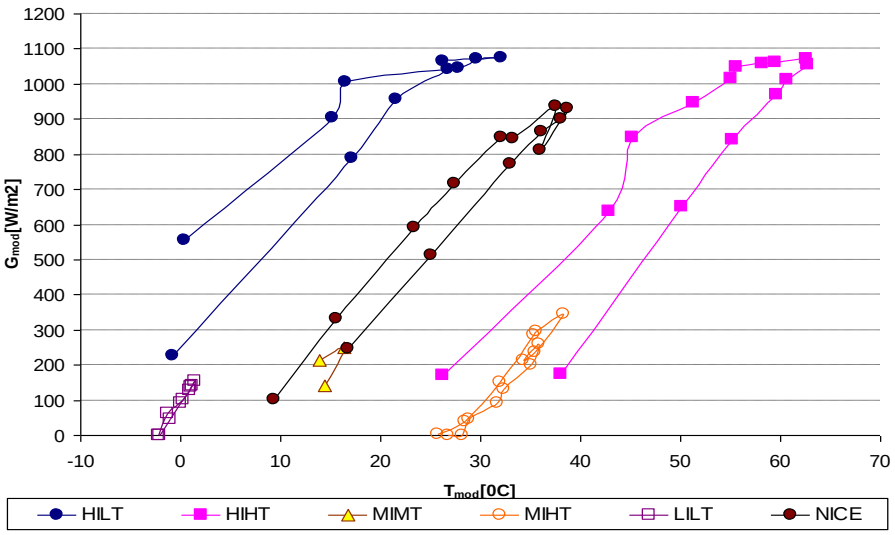

Figure 29: Characteristics of a c-Si module on each of the six standard reference days with different irradiance and temperature levels.

Sun spectra of six reference days are analysed and very different incidence spectrum variations are noticed as shown in Figure 30.

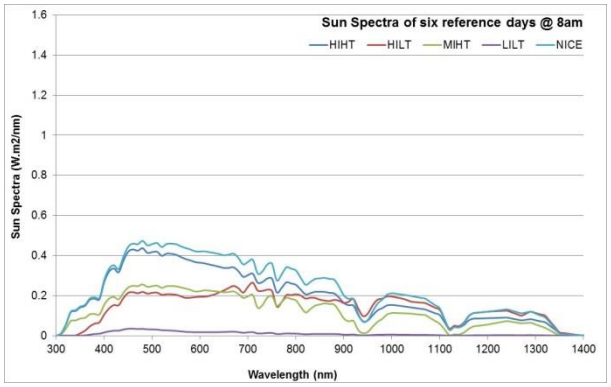

Figure 30-a: Spectral irradiance of six reference days at 8am

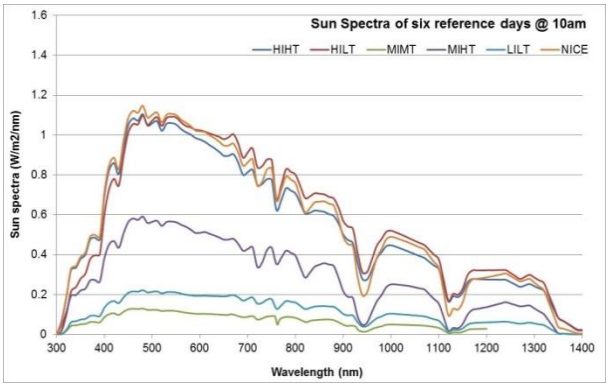

Figure 30-b: Spectral irradiance of six reference days at 10am

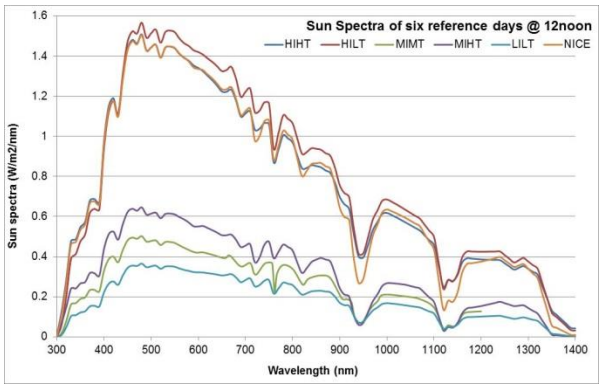

Figure 30-c: Spectral irradiance of six reference days at 12Noon

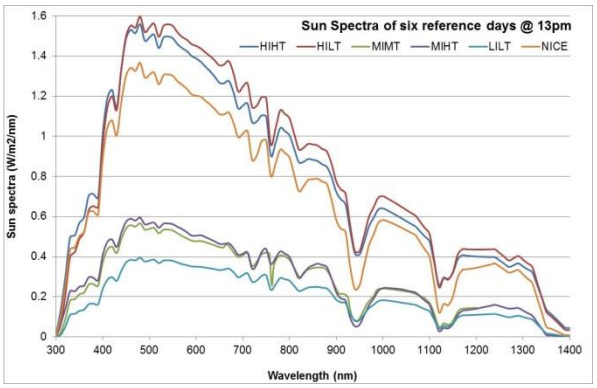

Figure 30-d: Spectral irradiance of six reference days at 13pm

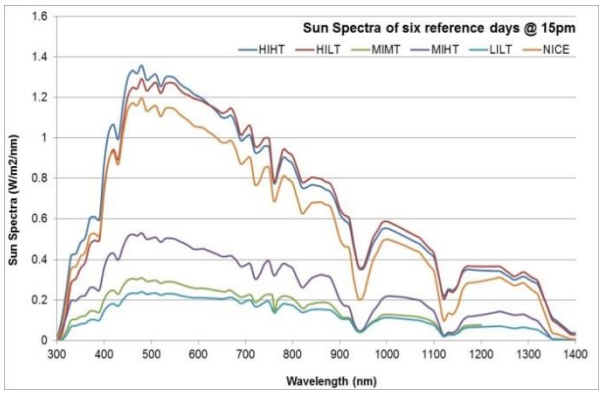

Figure 30-e: Spectral irradiance of six reference days at 15pm

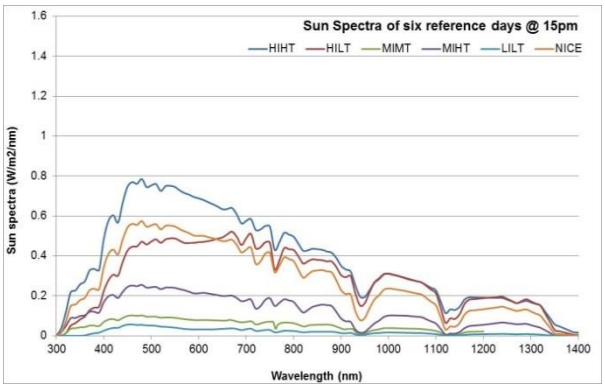

Figure 30-f: Spectral irradiance of six reference days at 17pm

Figure 30 (a-f): Spectral irradiance of six reference days.

It should be noted that there is no data available at 8am and all spectra irradiance data are available up to 1200nm for MIMT. Above graphs shows a difference in spectral irradiance for both high irradiance days.

3.4 Modelling of IEC Energy Rating

Weather data as an input into the energy rating model, were available from the proposed draft standard, including the following environmental conditions of the time period (standard days: time of the day, season, and year),

- Irradiance reaching the module
- Spectral irradiance
- Ambient temperature and wind speed

The following input module characterisation data were measured at AIT Vienna, Austria and JRC, ISPRA, Italy,

- Relative light transmission into the module
- Spectral response of the module
- Matrix of P_{max} vs irradiance at AM1.5G and module temperature (Figure 4).

Three PV modules are investigated as shown in Table 4, small crystalline silicon (c-Si), amorphous silicon (a-Si) and copper indium gallium selenide (CIGS) modules described in [55].

PV Module	Area [m^2]	I_{sc} [A]	V_{oc} [V]	P_{max} [W]
c-Si	0.144	0.66	21.41	10.42
a-Si	0.123	0.28	39.6	6.07
CIGS	0.067	0.39	23.67	5.2

Table 4: Set 1 module parameters at STC

Modelling of input weather data: To get total irradiance penetrating into the solar module, direct and diffuse irradiance is combined in relation with module angle of incidence (AOI). Then the spectral correction is applied in terms of the spectral response of the module and the spectrum of the irradiance. Module operating temperature is estimated as a function of irradiance and ambient temperature considering the module thermal coefficients in different wind speed groups.

3.4.1 **Irradiance Modelling**

Transmittance values of the modules are measured at 10° Angle of incidence (AOI) intervals (0°, 10°, 20°, ……85°) and at 90°AOI the transmittance value have been calculated by linear extrapolation from the measurement points at 80° and 85° AOI. The diffuse fraction of the solar irradiance is also measured at 10^o steps, which is interpolated to 1^o AOI step. Module transmittance is then estimated to the required angles between measured points by linear interpolation. Diffuse irradiance then calculated by the equation (17).

$$G_{diff,\mathrm{mod}} = \int_{0^0}^{90^0} \tau(\theta) G_{diff}(\theta) \cos(\theta) \tag{17}$$

Where, θ = Angle of incidence with respect to module normal

$G_{diff}(\theta)$= Angular distribution of diffuse light

$\tau(\theta)$ = relative light transmittance into the modules at AOI θ

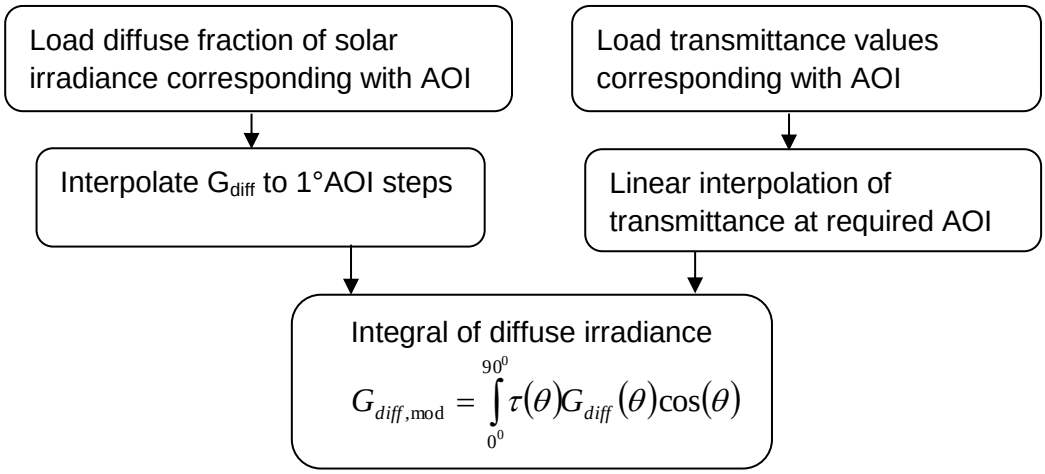

Figure 31: Modelling flow chart of diffuse irradiance calculation

The amount of direct irradiance entering into the module is calculated by the equation below, in which reflection is taken into account.

$$G_{dir,\mathrm{mod}} = \tau(\theta)\cos(\theta) \tag{18}$$

The total irradiance entering into the module is simply the sum after considering the diffuse and direct components,

$$G_{\mathrm{mod}} = G_{dir,\mathrm{mod}} + G_{diff,\mathrm{mod}} \tag{19}$$

3.4.2 **Spectral Correction**

The spectral resolution of the AM1.5G standard spectrum is given in 0.5 nm steps; spectral irradiance in the standard days is given in 10 nm steps. All the spectral response and spectrum data have been interpolated to 1 nm wavelength intervals and the AM1.5G standard spectrum at 1 nm resolution has been used in the procedure for spectral correction. The flow chart given below (Figure 32) explains the steps involved in the spectral response correction.

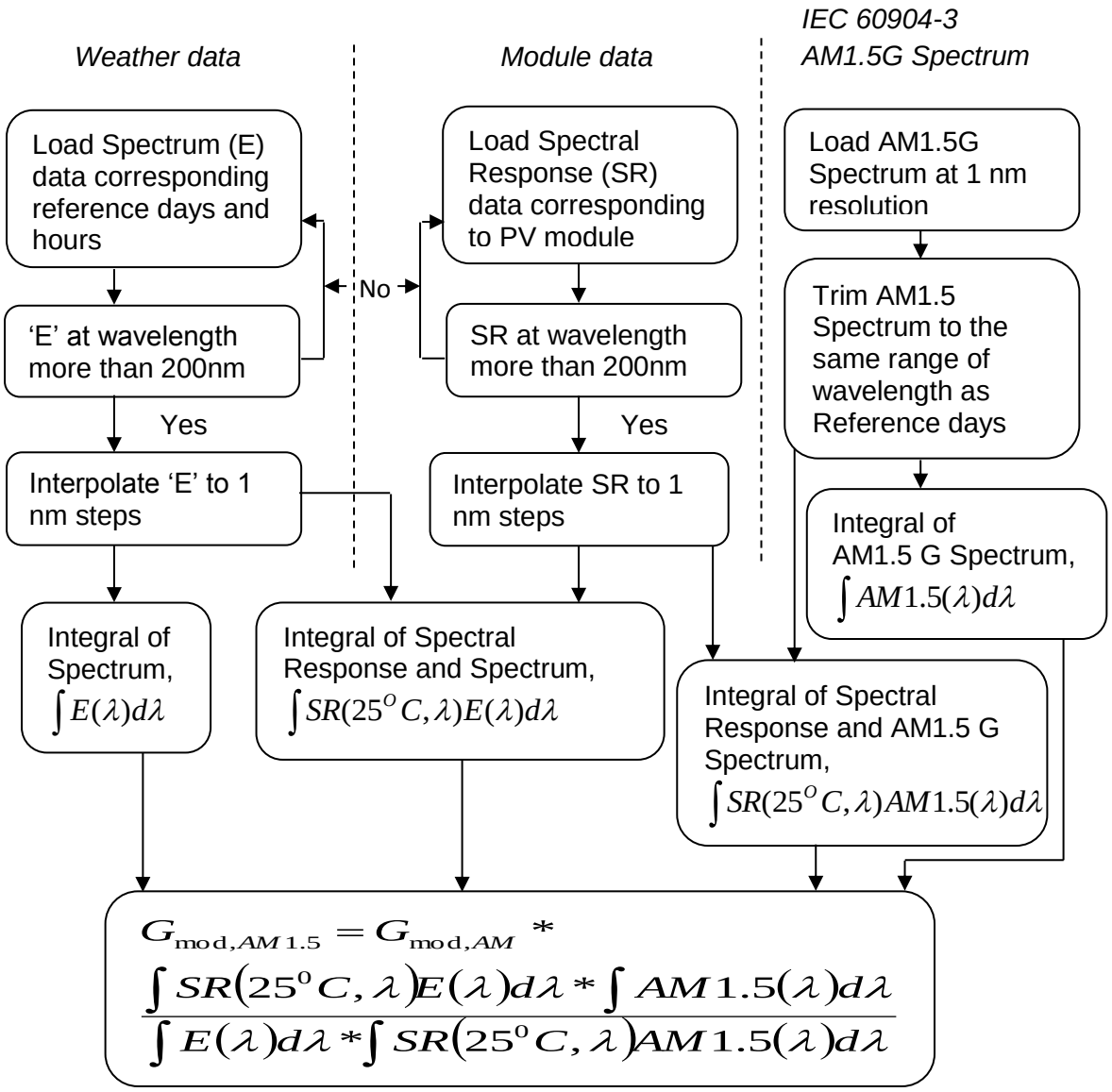

Figure 32: Modelling flow chart of spectral correction of module irradiance

The same wavelength resolution of 1 nm interval for sun's spectrum, spectral response of the module and the standard spectrum at AM1.5G for spectral correction is essential in order to get accurate correction.

3.4.3 **Temperature Modelling**

Module temperature has been estimated as a function of incident irradiance on the module and ambient temperature with thermal coefficients at different wind speed class which is outlined in Figure 33 Thermal coefficients, a and b initially estimated from the slope and intercept of the plot of the difference of module and ambient temperature against irradiance at different wind speed class explained in section 3.3.2.

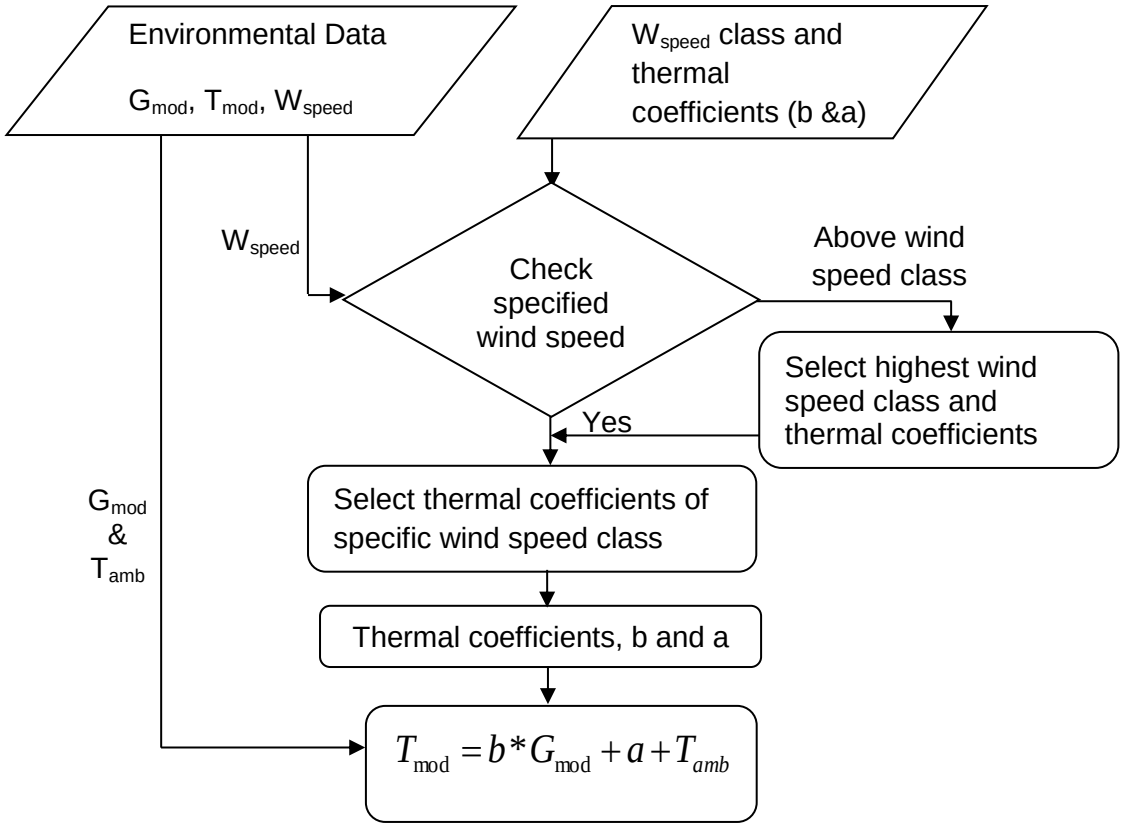

Figure 33: Flow chart of module temperature calculation as a function of irradiance and wind speed.

3.4.4 P_{max} fitting as function of irradiance and temperature

Considering direct and diffuse irradiance, the amount of total irradiance enters into the module ($G_{mod\ AM}$) is spectrally corrected to AM1.5G ($G_{mod\ AM1.5}$) and module temperature (T_{mod}) is estimated as a function of ambient temperature (T_{amb}) and total irradiance ($G_{mod\ AM}$) with thermal coefficients. This has been carried out in order to make the combination of environmental input data ($G_{mod\ AM1.5}$, T_{mod}) and the measured power matrix of module as a function of irradiance at AM 1.5G spectrum ($G_{mod\ AM1.5}$) and module temperature (T_{mod}). Intermediate values of the measured G-T matrix of maximum power (P_{max}) of the modules are calculated by linear fitting approach as explained in Figure 34.

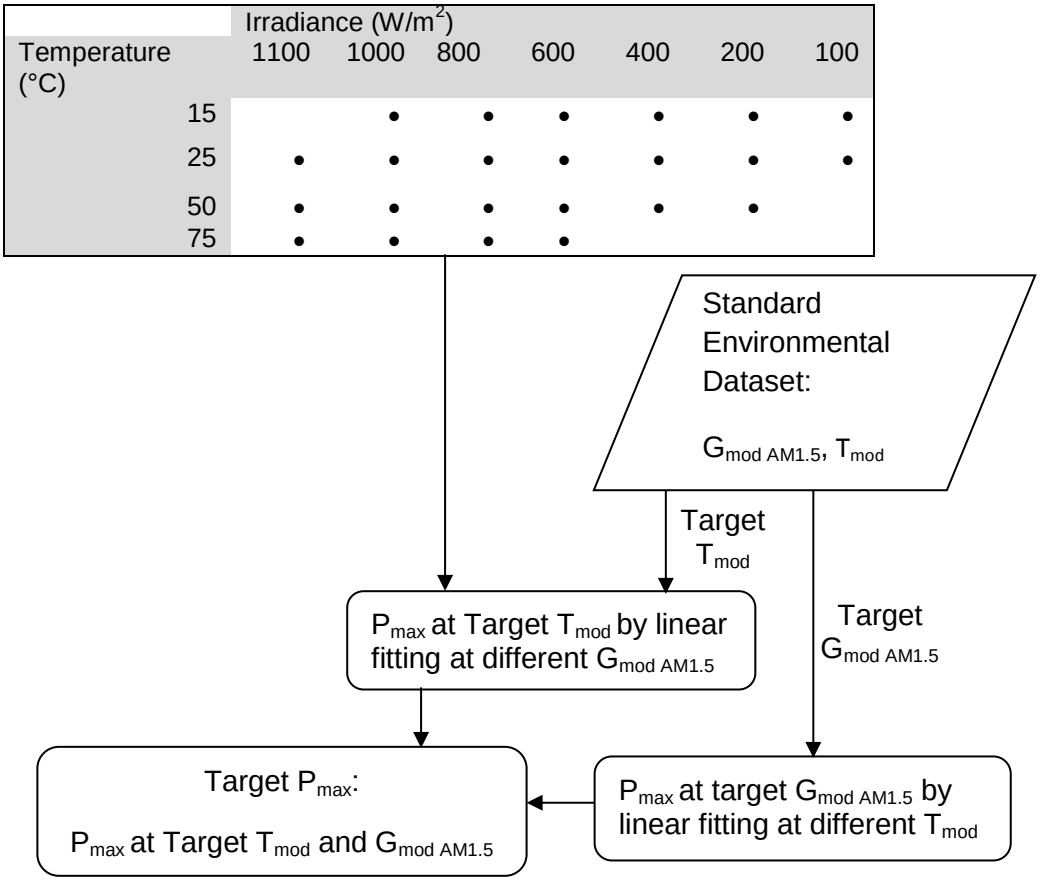

Figure 34: P_{max} fitting as a function of module temperature and module irradiance

The characterised power matrix of the module and the weather data of each reference day (Figure 29) are then analysed in order to estimate the energy output for each day as per the procedure shown in Figure 28.

3.5 Sensitivity analysis

In order to evaluate the importance of the different steps of the above energy rating model an impact analysis against irradiance, temperature, AOI and spectrum is carried out based on daily conversion efficiency and daily energy generation of each reference day using different PV modules outlined in Table 4 (page 40).

Effect of irradiance has been analysed to see the importance of considering the variation of efficiency with irradiance. This sensitivity was carried out based on operating efficiency rather than power, as the main effect would otherwise have been due to the increase of input power. The efficiency of a simulation where each hour had an irradiance of 1000W/m^2 has been carried out and the percentage change compared to the normal irradiance is shown in Figure 35.

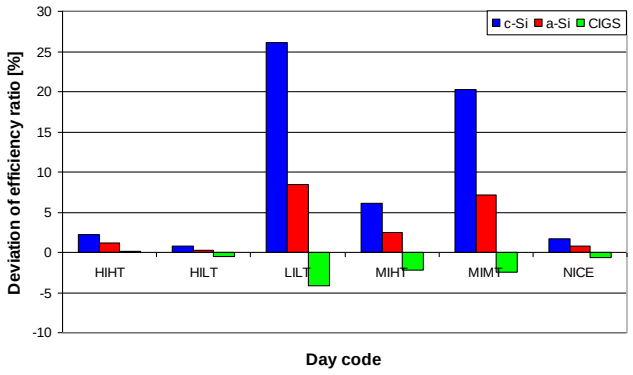

Figure 35**:** Deviation in daily module efficiency between actual and fixed (at STC value) irradiance.

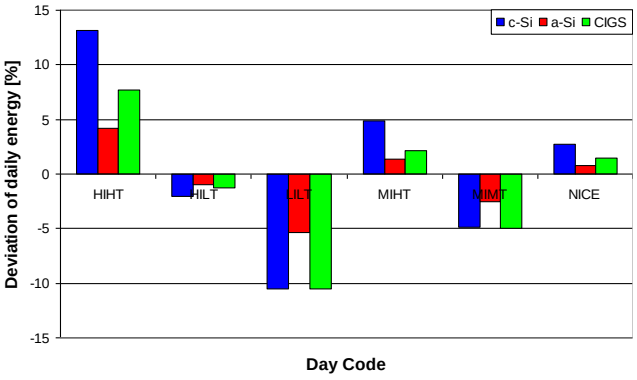

Figure 36: Deviation in daily energy generation between unmodified and modified with fixed (at STC value) temperature.

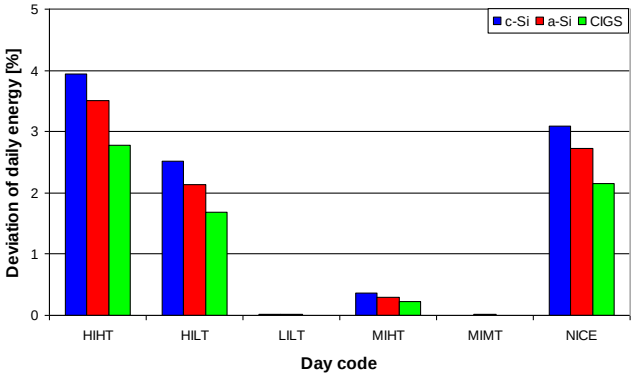

Figure 37: Relative change of daily energy at actual and fixed at normal AOI.

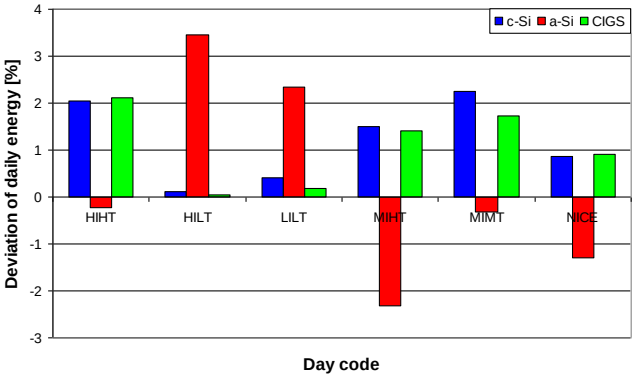

Figure 38: Relative change of daily energy at actual and fixed at spectrum AM 1.5.

Strong deviation has been found for the low irradiance days MIMT and LILT. Specifically the c-Si module is affected, showing an increase of 20-25% if it would be operating at 1000W/m^2 all the time.

The effect of temperature on the energy yield is shown in Figure 36. Here a fixed temperature of 25 degrees was chosen. Again, the c-Si module shows the most significant effect, more than ±10% influence for HIHT and LILT respectively, followed by CIGS and a-Si.

Similarly AOI and spectral influence has been analysed based on relative changes in energy generation for each day which is depicted in Figure 37 and Figure 38 respectively.

Daily spectral effect ranges from 2-3% for all three module technologies. Surprisingly, there is a very significant change between the HIHT and the HILT for the a-Si material, which is due to the different incident spectrum (Figure 30). The angle of incidence is in the range of 2-4%, depending on the material, thus an effect can be represented.

3.6 Conclusions

Two PV module performance metrics – power rating and energy rating – were compared in this chapter. The power rating sets the retail price and so is more linked to a sales point of view, but return on investment is mainly aligned with energy rating. Significant efforts by different research groups on energy yield prediction methods are explained in this chapter, including the evaluation of the proposed IEC standard for energy rating.

This energy rating standard has lack of clarity on the interpolations method and irregular resolution in the given spectral irradiance and spectral response of the modules, which includes the quality of the given spectral data. Similarly, the integration for the diffuse irradiance, where there the interval should be fixed to 1 degree steps. Differences were also observed when applying the G-T-P matrix, were the choices are between choosing the closest measurements or apply an

interpolation for each time step. The complexity of the standard is actually not beneficial for an accurate energy prediction, as it requires data which is actually normally not known (angular distribution of the diffuse irradiance.

The reference days are not particularly representative for an energy rating standard. In the standard days, it is not known how accurate the spectra used in the standard data sets are. Search for a representative standard meteorological dataset for this standard is under way.

The rank of sensitivity of four STC parameters on the performance of PV modules is demonstrated in this chapter. It is identified that the effect of irradiance is the most influencing parameter on the output of the different PV modules in different climatic conditions and the output of the efficiency can varies up to 25% at low irradiance conditions against STC value. The effect of temperature is the second most influencing parameter which can cause a deviation of daily energy yield up to 10% in the high temperature recorded days compare to 25°C. The effects of spectrum and the angle of incidence comes lower in the range compare to irradiance and temperature and the daily energy yield can varies up to 3% against STC parameters depending on the module technology (specially spectrally sensitive thin film modules) and the availability of the different components of irradiance (direct and diffuse).

The existing methods are either technology dependent or they are only considering two main influencing parameters –irradiance & temperature without considering the spectral effects. Reviewing the existing methods and analysis the proposed energy rating standard, it is clear that there is a need of an energy yield calculation procedure which should be technology independent and considering the spectral irradiance factor into account, with the level of uncertainty information available at different stages.

A details analysis of the energy rating methodology is explained in the next chapter and demonstrated the level of accuracy by performing an uncertainty analysis of the yield calculation.

4 Uncertainty in the Performance Modelling of Photovoltaic Modules

4.1 Introduction

This chapter describes the validation and uncertainty analysis of the IEC energy rating procedure. Uncertainties in the energy yield prediction come from both measurements and modelling element in the procedure [56]. Estimation of the energy yield of PV system requires two sets of measured input data (Figure 28 in page 37);

- The PV module characterisation: The current-voltage (I-V) measurements at different irradiance and temperature conditions (Table 2). It may also include spectral response, angular response etc. [57,58]
- The site specific environmental data: Global horizontal irradiance, ambient temperature, spectral irradiance, wind speed etc.

Based on the above measured values, different modelling steps are required in the procedure, comprising [59],

- The translation of global horizontal irradiance into plane of array irradiance,
- Estimation of module temperature,
- Spectral and angular corrections and
- Estimation of maximum power of the PV module over the time period.

Measurement and modelling components of each of the above contribute to the final uncertainty in the energy yield estimation of the PV system. These uncertainty contributions are classified into statistical and systematic errors.

A framework for the uncertainty analysis is established and explained in this chapter. It is then applied to study the measurement uncertainty of the environmental data, mainly concentrated on the irradiance and temperature measurements. The magnitude of uncertainty over the range of irradiance and temperature

measurements is revealed, which gives an indication of the level of uncertainty at different signal strengths of irradiance and temperature measurements.

Different irradiance translation models are analysed and the method best matched for the UK climate is identified. A temperature translation model is also validated against the real measurements. Evaluating different modelling steps, the IEC 61853 energy yield prediction method is validated against the real measurement of annual energy generation of three different PV modules at Loughborough, UK. Uncertainty analysis and the validation of the energy yield estimation indicates the requirement of better measurements and that accurate modelling method identification is necessary for reliable energy yield estimation of a PV system.

4.2 Framework of Uncertainty analysis

The uncertainty in the energy yield estimation directly linked with the quality of the measured environmental data as well as the measured module specific parameters. There is significant published effort made by other researchers towards the various aspects of the PV parameter uncertainty analysis [60-66] and this thesis analyses the uncertainty of the irradiance and temperature measurement.

4.2.1 Types of uncertainty

Uncertainties are classified into two categories in this study: the systematic uncertainty from a fixed bias error and the statistical (random) error from the noise of each parameter [67, 68].

4.2.1.1 Statistical

Statistical uncertainty can be described as the value of a quantity and its random variation when it is observed multiple times. Normal or Gaussian distribution (Figure 39) is a common probability distribution often found when the measured quantities contain a large number of small and independent error contributions.

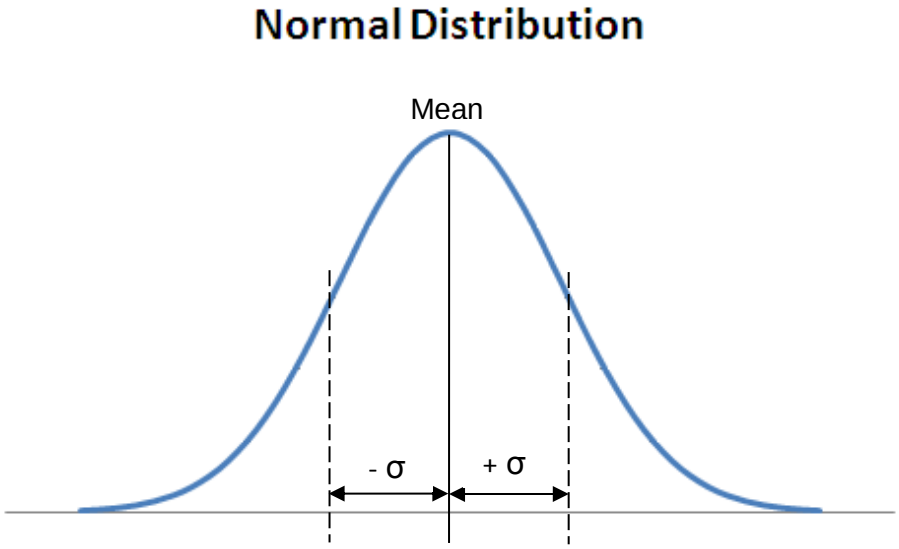

Figure 39: Shape of Normal or Gaussian probability distribution

In Figure 39, the central axis, mean, of the curve corresponds to the expectation of the true value. The two dotted line on the left and right slope are at locations - σ and + σ from central axis, the mean error or standard deviation associated with this distribution curve. The larger the mean error or standard deviation or statistical uncertainty, the broader the curve.

The statistical uncertainty can be calculated by standard deviation (SD) as per the equation (20) [68].

$$\sigma = \sqrt{\frac{\sum_{i=1}^{n}\left(x_i - \bar{x}\right)^2}{n-1}} \tag{20}$$

Where, $\bar{x} = \frac{\sum_{i=1}^{n} x_i}{n}$ and x_i are input parameters. “n” is the total count of simulations.

4.2.1.2 Systematic

Systematic uncertainty can be evaluated based on non-statistical information i.e. from calibration certificates and manufacturers' specifications. This is an offset error which remains with repeated measurements. Systematic uncertainty can determined by comparison to theory or other experiments.

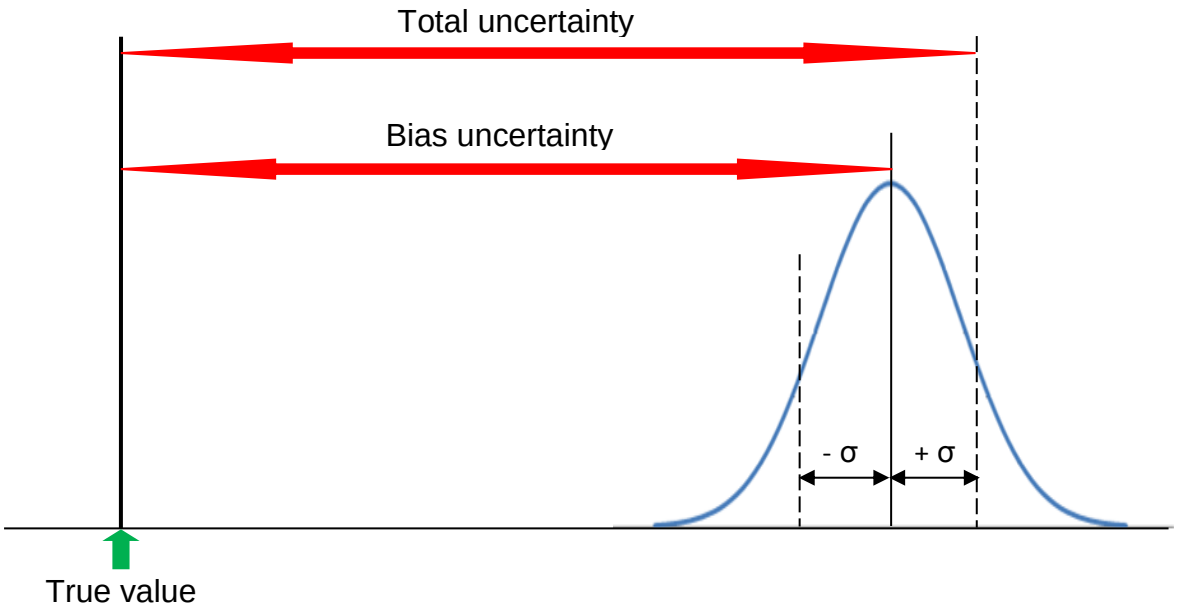

Figure 40: Total uncertainties combining statistical and systematic components.

Overall uncertainty is then determined by combining estimated systematic uncertainty ('B') and statistical uncertainty ('S') as per equation (21) [68].

$$\text{Total Uncertainty} = \sqrt{B^2 + \sigma^2} \tag{21}$$

4.2.2 Monte Carlo Approach

To analyse the uncertainties, a statistical analytical tool - Monte Carlo technique is used in this study. This is done by performing random sampling from the probability distribution of each input parameter and evaluating the model output several times using a different set of randomly selected values from the probability functions. The flow chart of this Monte Carlo method is illustrated in Figure 41 [70]. A normal distribution is used for the probability distribution of each input parameter. The

normal distribution is mostly used distribution in statistics because of the central limit theorem, which states that, under mild conditions, the mean of many random variables independently drawn from the same distribution is distributed approximately normally. Normal distribution defines the mean and a standard deviation to describe the random variation about the mean.

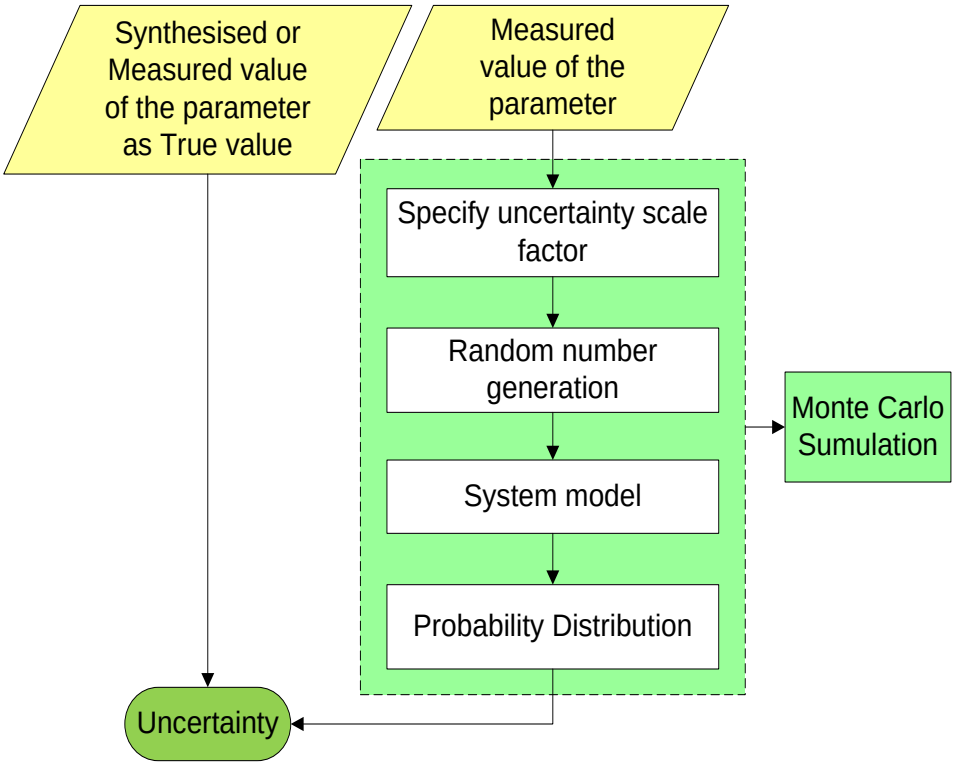

Figure 41: General framework of Monte Carlo simulation approach

4.3 Uncertainty Evaluation of Energy Yield Prediction Method

Any measurement providing input data into the model contributes uncertainty. The level of that uncertainty scale depends on the type of measurement equipment used and the nature of the measurement. One set of inputs for energy yield estimation are measured environmental data, i.e. irradiance, ambient temperature, spectral irradiance, wind speed etc. that influence the performance of the PV system. Irradiance and temperature are the two major parameters (as discussed in Chapter 3) that influence the performance of a system the most. This study concentrated on these two main parameters and their level of measurement uncertainty that comes from the irradiance and ambient temperature measurement devices.

4.3.1 Uncertainties of Environmental Inputs

4.3.1.1 Irradiance Measurement

Irradiance is the primary input parameter that influence the power output of a PV module or system. So, the uncertainty of irradiance measurement largely influences the accuracy of the estimated output for all PV module technologies. The level of irradiance measurement uncertainties varies over a range of irradiance values, hence the level of accuracy of the yield prediction.

There are different irradiance measurement sensors [71, 72] are available in the marketplace offering different levels of measurement uncertainty. The thermopile pyranometer is one of the accurate sensors commonly used for irradiance measurement for commercial and research applications. To-date the irradiance measurement uncertainties are analysed based on the given uncertainty values in the manufacturer datasheet by different researchers [73, 74]. Kratzenberg et al [73] analysed the irradiance measurements uncertainty of a Kipp & Zonen CM 11 thermopile at 800 W/m^2 based on three weeks measured values. This testing period was very short and also didn't consider the low irradiance cases. Strobel et al [74] analysed the uncertainties of irradiance measurements from an annual dataset.

This thesis is aiming to establish a robust model that can analyse the irradiance measurement uncertainty by a CM 11 pyranometer as a case study.

The irradiance uncertainties are categorised into two components:

i. Uncertainties that change over the annual time period of measurement time.

The components of uncertainty (of the CM 11 sensor) utilised in this thesis that change over longer time period are:

Uncertainty cause	CM 11Uncertainty
1. Calibration	±3.4 W/m^2
2. Annual drift	±0.00288 W/m^2
Longer Term Uncertainty	**±3.40288 W/m^2**

Table 5: The uncertainties of CM11 (Kipp & Zonen) pyranometer that change over long timescales.

ii. Uncertainties that change at each timestamp of the measurement.

The components of uncertainty that change from one measurement to other are:

Uncertainty cause	CM 11 Uncertainty
3. Zero-offset due to temperature change (5k/h)	±2 W/m^2
4. Zero-offset due to thermal radiation (200 W/m^2)	±7 W/m^2
5. Tilt error (beam 1000 W/m^2)	±0.25%
6. Spectral sensitivity	±2%
Short Term Uncertainty	**±9 W/m^2 ±2.25%**

Table 6: The uncertainties of CM11 (Kipp & Zonen) pyranometer that changes at each timestamp of the measurement.

There are three analyses available in the CM 11 manual [71] which explain the level of uncertainties of the following uncertainty components depending on the signal strength of irradiance, ambient temperature and zenith (or incident) angle.

Uncertainty cause	CM 11 Uncertainty
7. Non-linearity (0-1000 W/m^2)	Modelled
8. Temperature dependence of sensitivity (-20 to 50°C)	Modelled
9. Directional error (Zenith angle from 0° to 80°)	Modelled

Table 7: The uncertainties of CM11 (Kipp & Zonen) pyranometer that depends on the level of irradiance and temperature sensitivity also on zenith angle.

Extracting the values from the data in the manual (i.e. irradiance sensitivity of non-linearity, temperature sensitivity and directional error at different zenith angle), three models are established which describe the level of uncertainty as the influencing parameter changes.

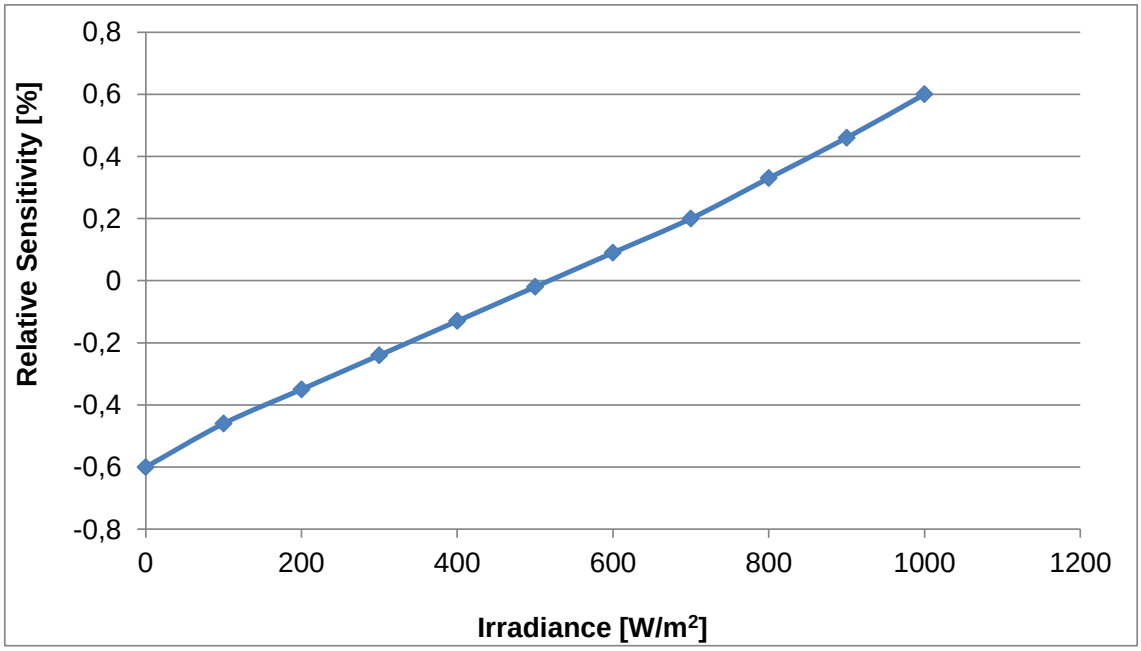

Figure 42: Non-linearity error of Kipp & Zonen CM11 pyranometer.

The non-linearity error, sensitivity variation with irradiance, is equal for any given CM 11 sensor as shown in Figure 42. A linear interpolation method is applied to estimate the non-linearity error against variable irradiance at every timestamp of the measurement. This gives more accurate estimation of the uncertainty scale of non-linearity error against irradiance.

The temperature dependence of the sensitivity is an individual function. For a given CM 11 the uncertainty curve lies somewhere within the upper line (blue line) a lower line (red line) of the Figure 43 from a baseline (green line) reference. A fourth order polynomial interpolation method is applied to estimate the baseline reference at any targeted temperature. Then a Monte Carlo method is utilised for the probability of the distribution of the error based on the standard deviation within upper and lower line of the temperature sensitivity curve of the Figure 43.

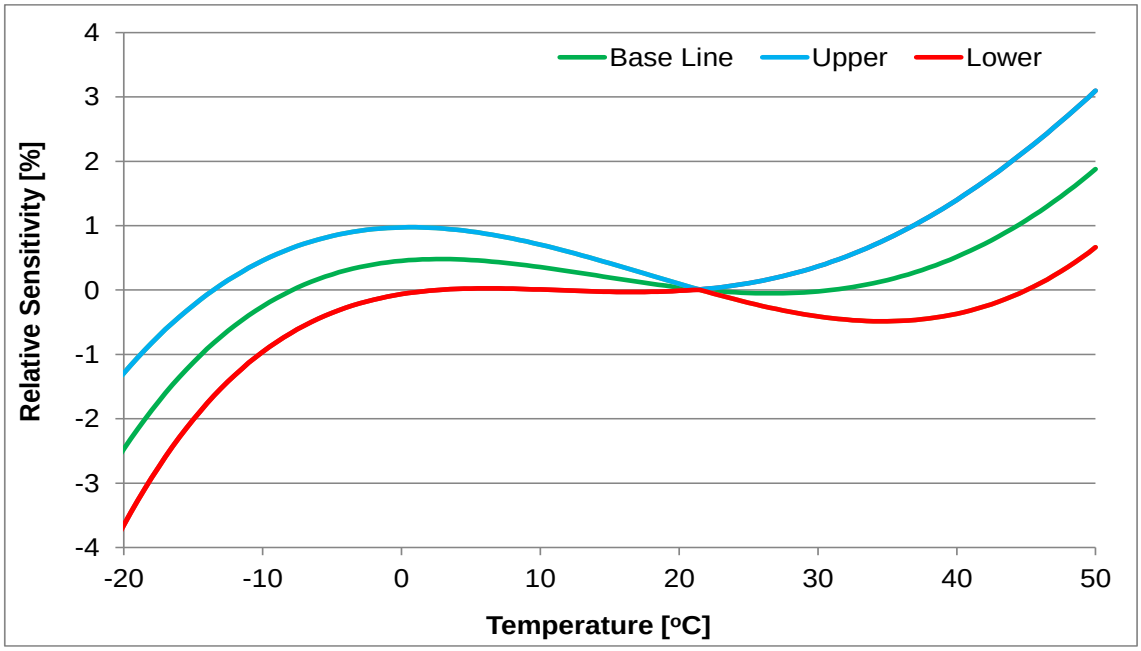

Figure 43: The curve of relative sensitivity variation with instrument temperature of a Kipp & Zonen CM11 pyranometer in the shaded region.

The directional error is the summation of the azimuth and zenith error. Figure 44 shows the maximum relative zenith error in any azimuth direction for the CM 11 sensor.

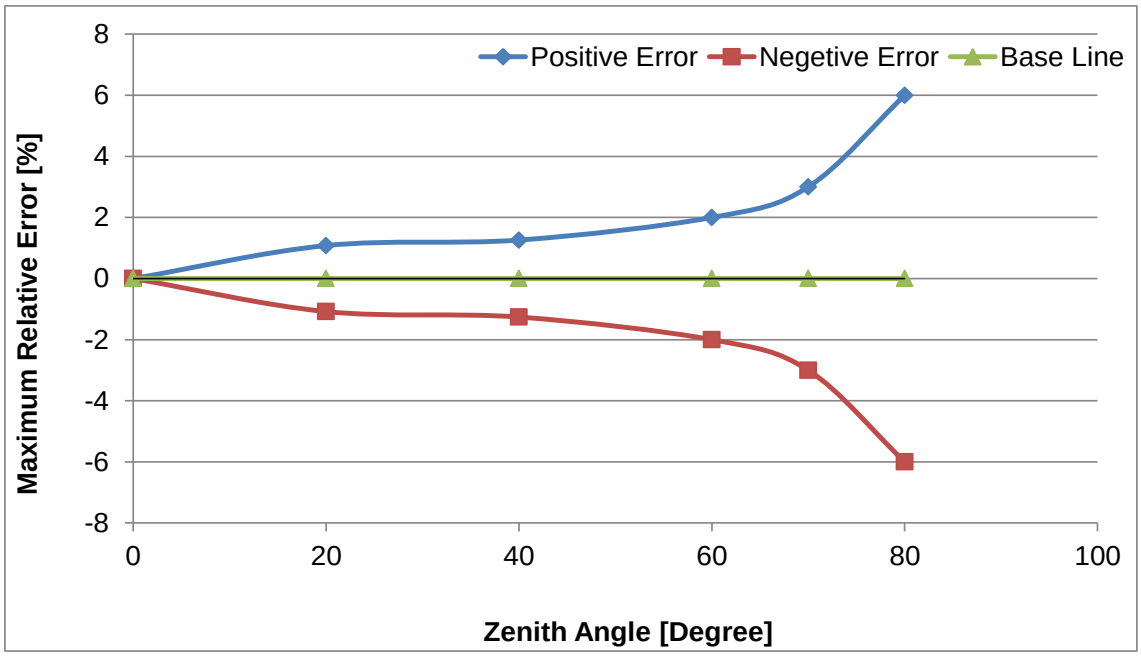

Figure 44: Directional error of Kipp & Zonen CM11 pyranometer

A fourth order polynomial interpolation method is applied to estimate the baseline reference at any targeted zenith angle. Then a Monte Carlo method is utilised for the probability of the distribution of the error based on the standard deviation within upper and lower line of the zenith angle sensitivity curve of the Figure 44.

Based on the above uncertainty components and their scale factors, the annual irradiance measurement uncertainty is evaluated using a Monte Carlo method. The flow chart of the Monte Carlo approach is outlined in Figure 45. All measured irradiance data is taken from the CREST outdoor monitoring system (COMS) at Loughborough University, Loughborough, UK, where irradiance sensors are installed in the horizontal and inclined plane of module installation. Ten second timestamps of the annual data from October 2009 to November 2010 are used for this analysis.

Measured global horizontal irradiance (G_{hor}) data is assumed as the true value in this uncertainty analysis of the irradiance measurement. The same irradiance i.e. G_{hor} is used as the input for Monte Carlo simulation. Here the input parameter for the Monte Carlo simulation is G_{hor} and uncertainty scale factors are listed in Table 5, Table 6 and Table 7. The uncertainty of the G_{hor} measurement from each timestamp is then summed for the whole year in order to obtain the uncertainty in the annual irradiation. Five thousand iterations have been chosen to generate the probability distribution of the annual irradiation, which is shown in Figure 46.

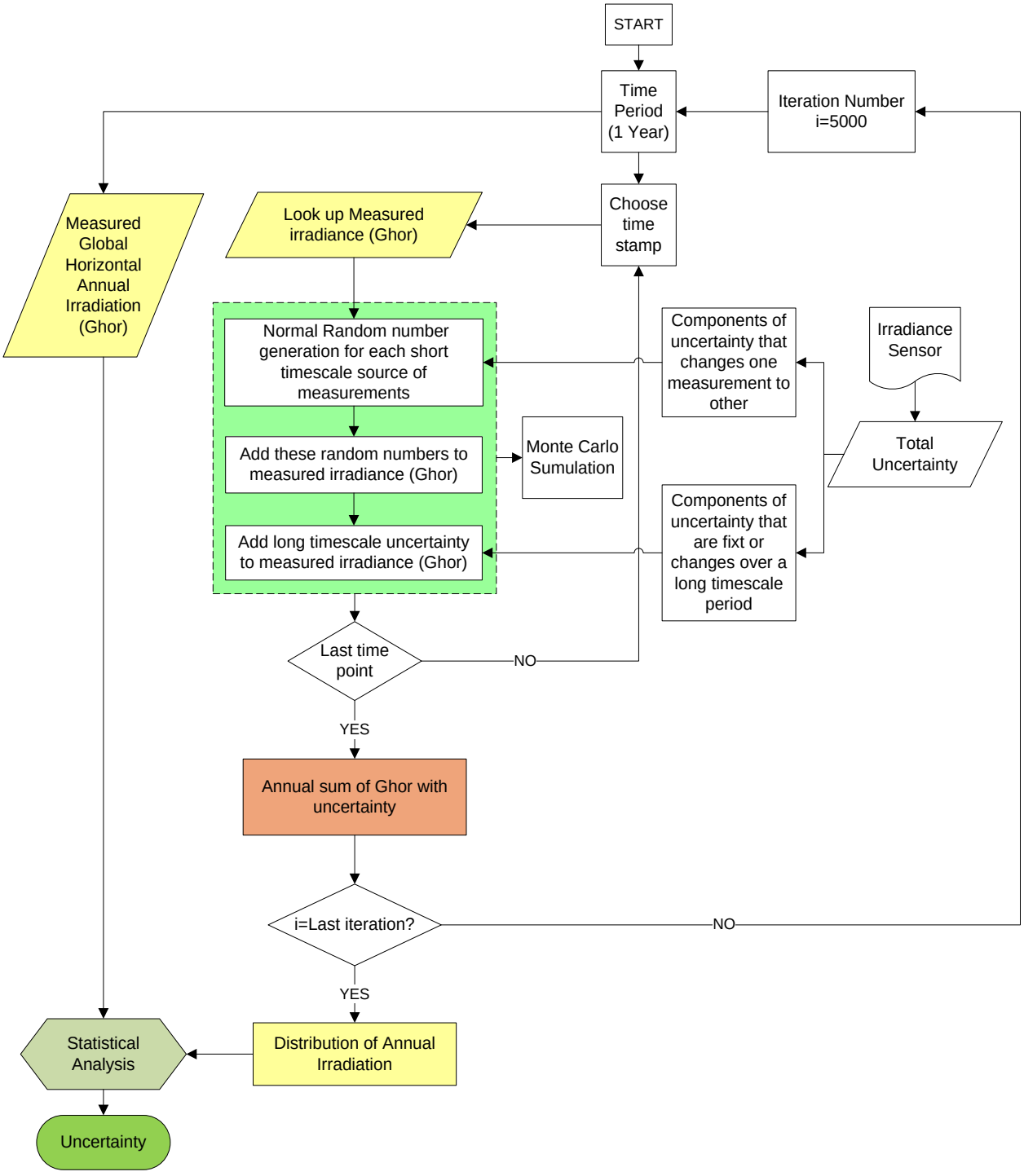

Figure 45: Flow chart of irradiance measurement uncertainty by Monte Carlo approach.

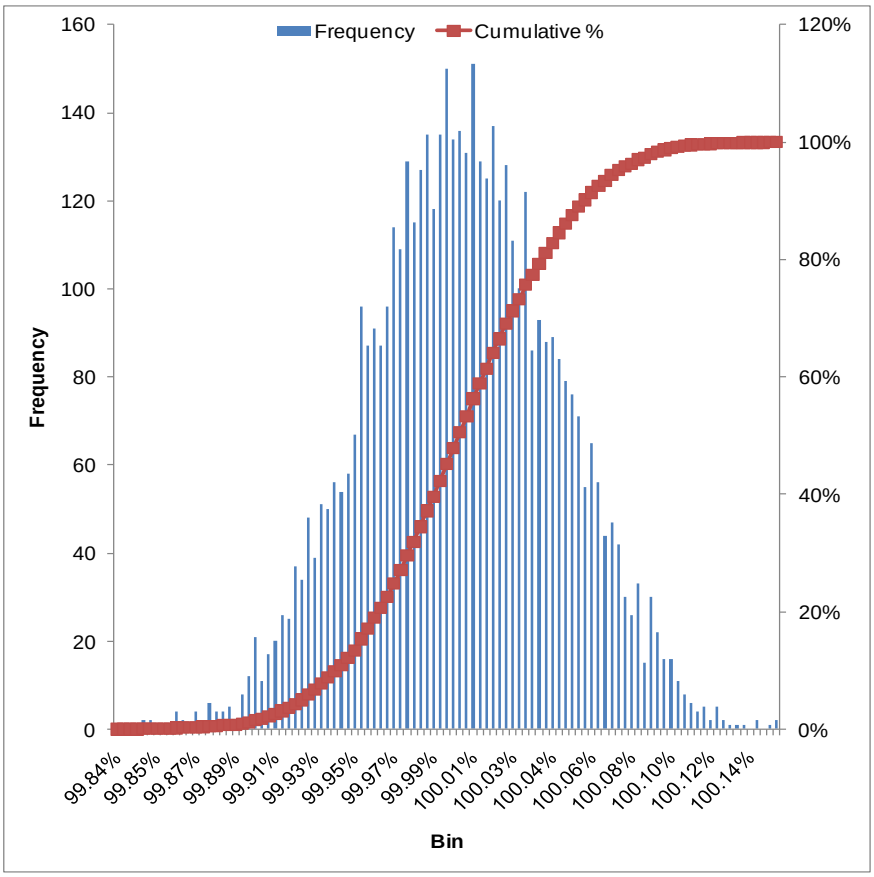

Figure 46: Probability distribution of annual sum of global horizontal irradiation measurement uncertainty by CM 11.

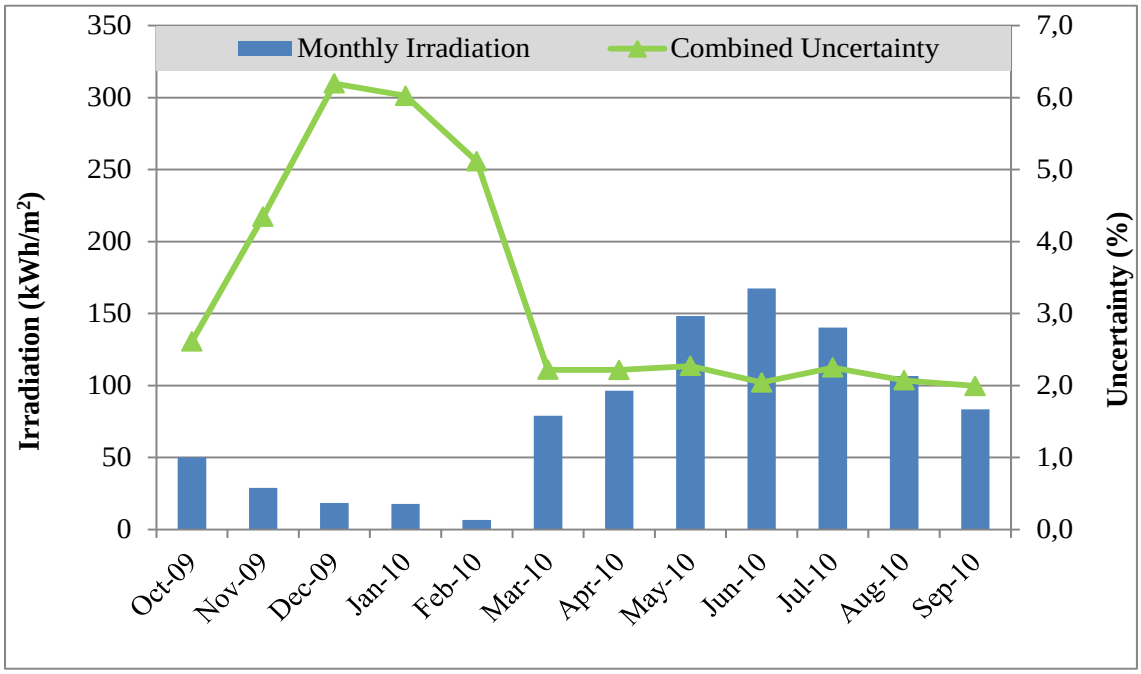

Figure 47: Monthly irradiation (kWh/m^2) and measurement uncertainty in the UK climate.

Using all the above listed uncertainty components, the uncertainty of annual irradiation from measurements with the CM 11 sensor is calculated as ±1.56%. Monthly uncertainty ranges from ±2% to ±6.2% depending on the irradiation in different months of the year (Figure 47). The annual uncertainty is low compare to the monthly uncertainty because of the negative – positive cancel out effect of the five thousand iteration of the simulation. A similar effect is appears in the frequency distribution graph in Figure 46. These values are within the agreement that have been reported elsewhere [73].

4.3.1.2 Temperature Measurement

Temperature is the second most influential parameter after irradiance that determines the power output of a PV module (Figure 35 to Figure 36 in Page 45-46). So, accurate temperature measurement is also critical in order to estimate the energy yield of different PV technologies. As with irradiance, there are a variety of temperature sensors available with different levels of measurement uncertainty. This study takes a Vaisala HMP45C P1000 sensor [75] as a case study, as it is in use for ambient temperature measurements in the CREST outdoor monitoring system. The results are applicable to the sensor that monitors the module temperatures also.

The measurement uncertainty of HMP45C P1000 is taken from the manufacturer datasheet and uses a Monte Carlo method for annual and monthly temperature measurement uncertainty estimation.

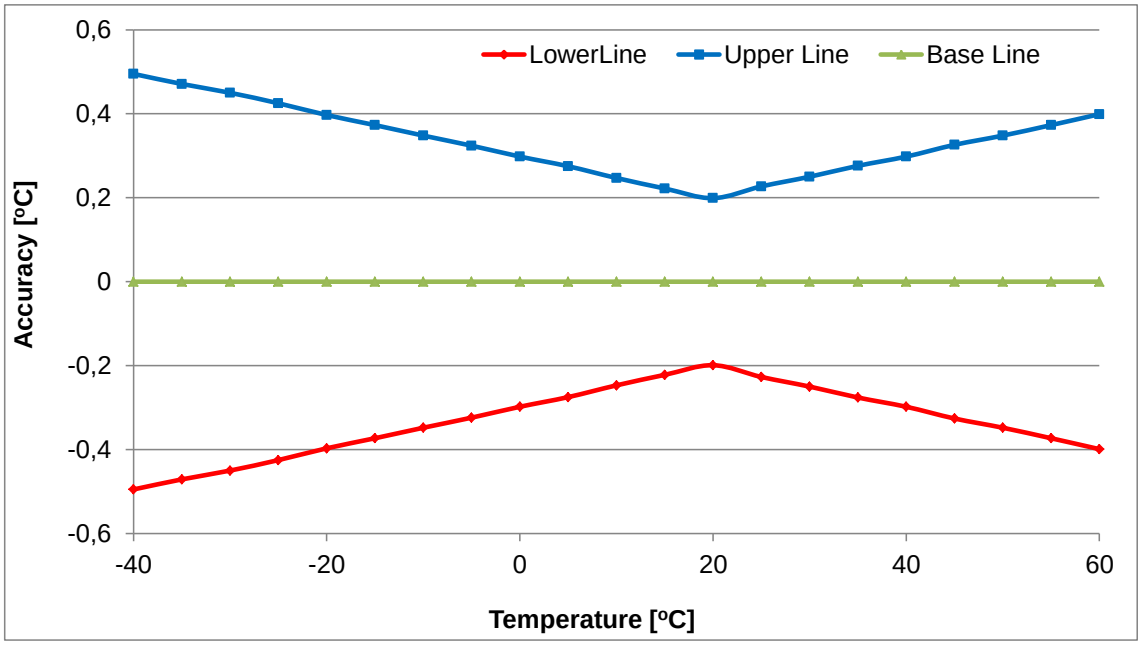

Figure 48: Measurement uncertainty of the HMP45C P1000 sensor.

The flow chart of the Monte Carlo approach is outlined in Figure 49. All measured temperature data is taken from the CREST outdoor monitoring system (COMS). Ten second timestamps of the annual data from October 2009 to November 2010 is used for this analysis.

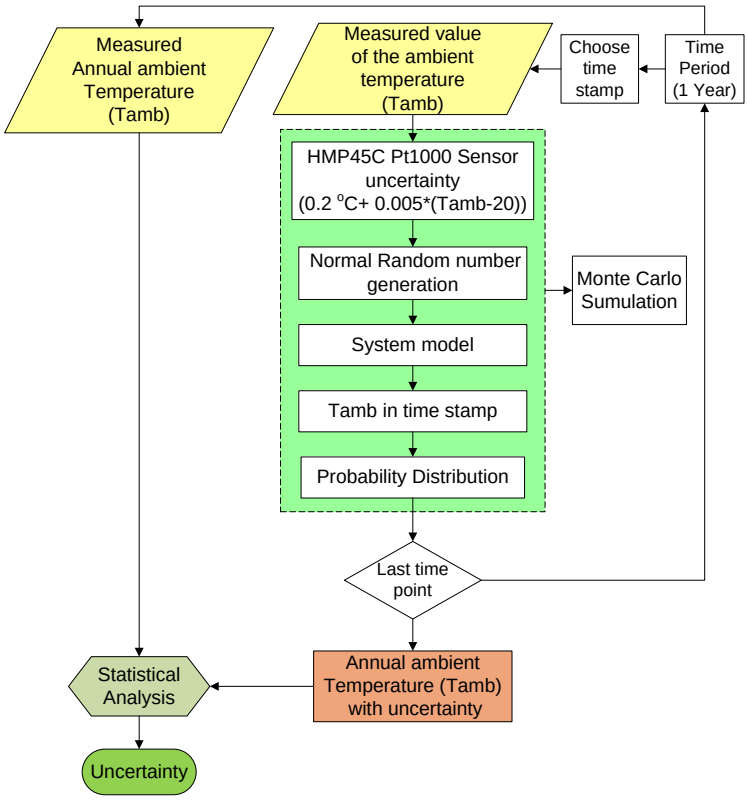

Figure 49: Flow chart of ambient temperature measurement uncertainty by Monte Carlo approach.

Measured ambient temperature (T_{amb}) data are assumed as the true values in this analysis. The uncertainty scale factor of the chosen sensor has been estimated using linear interpolation based on the data shown in Figure 48 and Monte Carlo simulation is used to draw random uncertainty values and estimate annual and monthly average ambient temperature measurement uncertainty. Again, five thousand samples have been chosen to generate random numbers within the given range of uncertainty of T_{amb} at each time stamp for the whole year and the annual sum is estimated for each sample set.

The uncertainty of annual average ambient temperature measurement is calculated as ±0.08°C and the uncertainty of monthly average of ambient temperature is illustrated in Figure 51, which is within agreements that have been reported elsewhere [76]. The probability distribution of Gaussian shape of the annual temperature is shown in Figure 50.

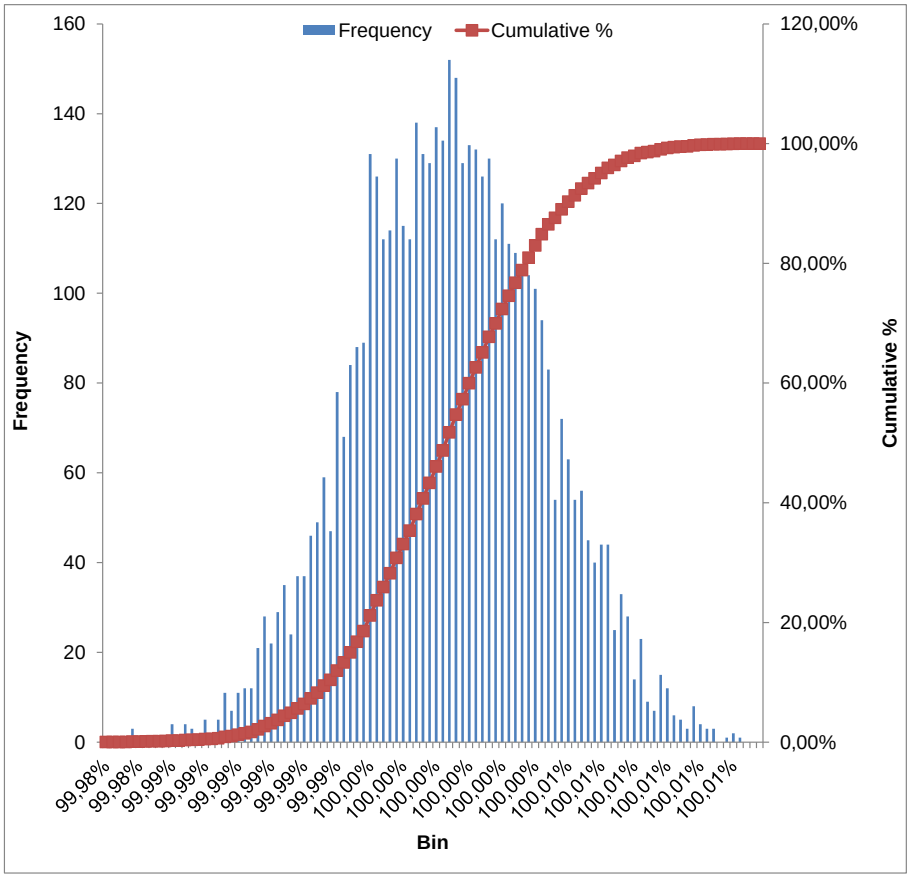

Figure 50: Probability distribution of annual sum of ambient temperature measurement uncertainty.

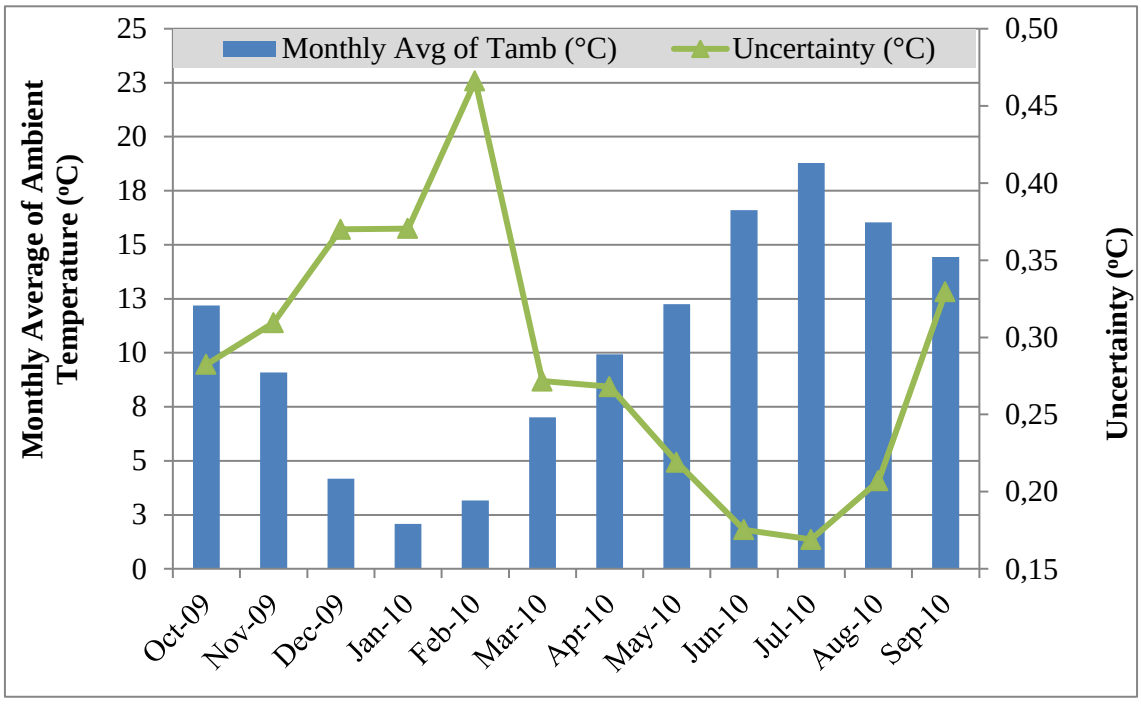

Figure 51: Monthly average ambient temperature and their uncertainties in UK climate.

4.3.2 Energy Yield Uncertainty of PV Modules

Energy yield is then calculated using the IEC 61853 P_{max} Fitting as function of irradiance and temperature as explained in section 3.4.4 of chapter 3. Based on the above measurement uncertainties of irradiance and temperature, the uncertainty of annual energy yield for c-Si and CIGS PV modules were determined through Monte Carlo simulation and are listed in Table 8. The monthly energy yield estimation uncertainties of the c-Si module, as an example, are shown in Figure 52.

Table 8: Uncertainty of annual energy yield of c-Si and CIGS PV module.

Module	P_{max} (Wp)	Uncertainty	Distribution
c-Si	10	2.78 %	Normal
CIGS	5	15.45%	Normal

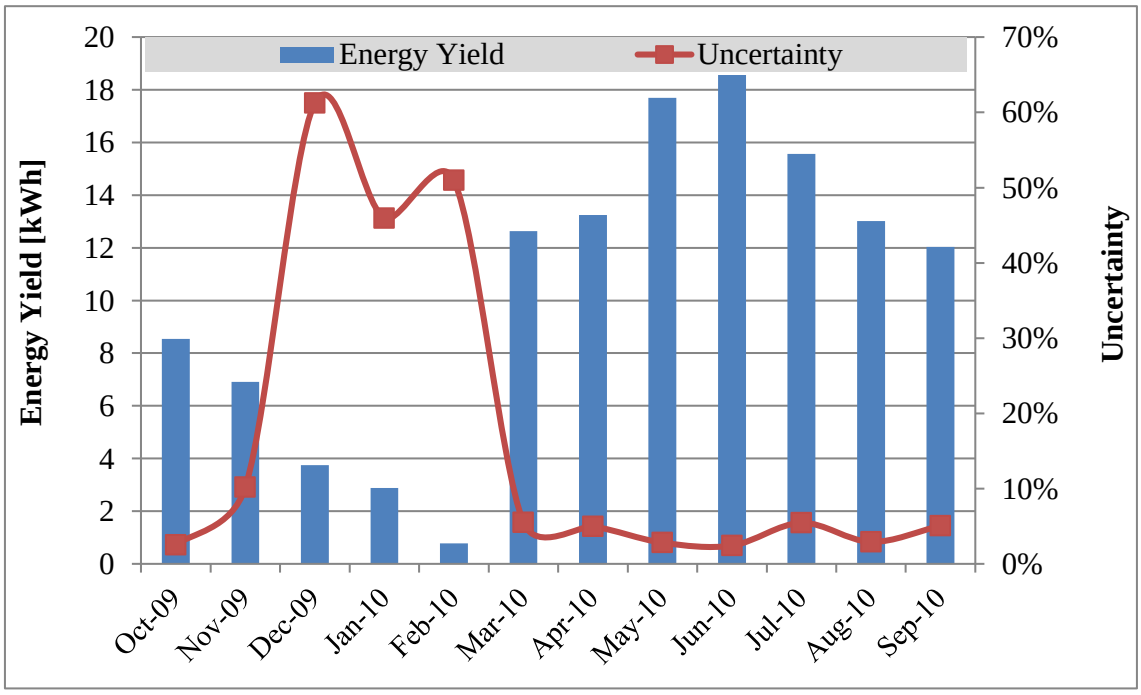

Figure 52: Monthly energy yield (kWh) and their uncertainties in the UK climate for a c-Si module.

Higher uncertainties in December to February occur due to not only the higher input uncertainties from irradiance and temperature measurements but quite significantly due to the reason that the linear regression of P_{max} does not match well at lower

irradiance levels. The linear regression method is suggested in the IEC 61853 to estimate the P_{max} at target irradiances and temperatures.

4.4 Validation of Energy Yield Prediction Method

This section analyses the prediction method, which involves

- modelling to translate the available solar irradiance data to the system specific geometry.
  Different irradiance component separator methods and in-plane irradiance translation methods are analysed and validated against their respective measured values.
- a translation method to estimate the module temperature as a function of ambient temperature and irradiance.

The above methods are applied to study the annual energy yield prediction of three different device technologies.

All the necessary data are measured at the CREST outdoor monitoring system (COMS). The annual time period of the measurements is used from October 2009 to September 2010. For the irradiance model validation study, beam and diffuse irradiance is measured in the horizontal plan and also in the plan of array . Measured global horizontal irradiance (G_{Hor}) and ambient temperature (T_{amb}) are taken from COMS as environmental input parameters into the yield estimation method. A matrix of maximum power (P_{max}) of PV modules over a wide range of irradiance and temperature are used as module descriptor.

This matrix was measured at Arsenal Research, Austria. Power matrices of three device technologies are used in this study: c-Si, a-Si and CIGS. The same modules are also measured during this study on the CREST outdoor system to log their annual energy output. The P_{max} at target irradiance and temperature are estimated by linear regression method at each timestamp of the annual time period. The procedure of the prediction method is illustrated in Figure 53.

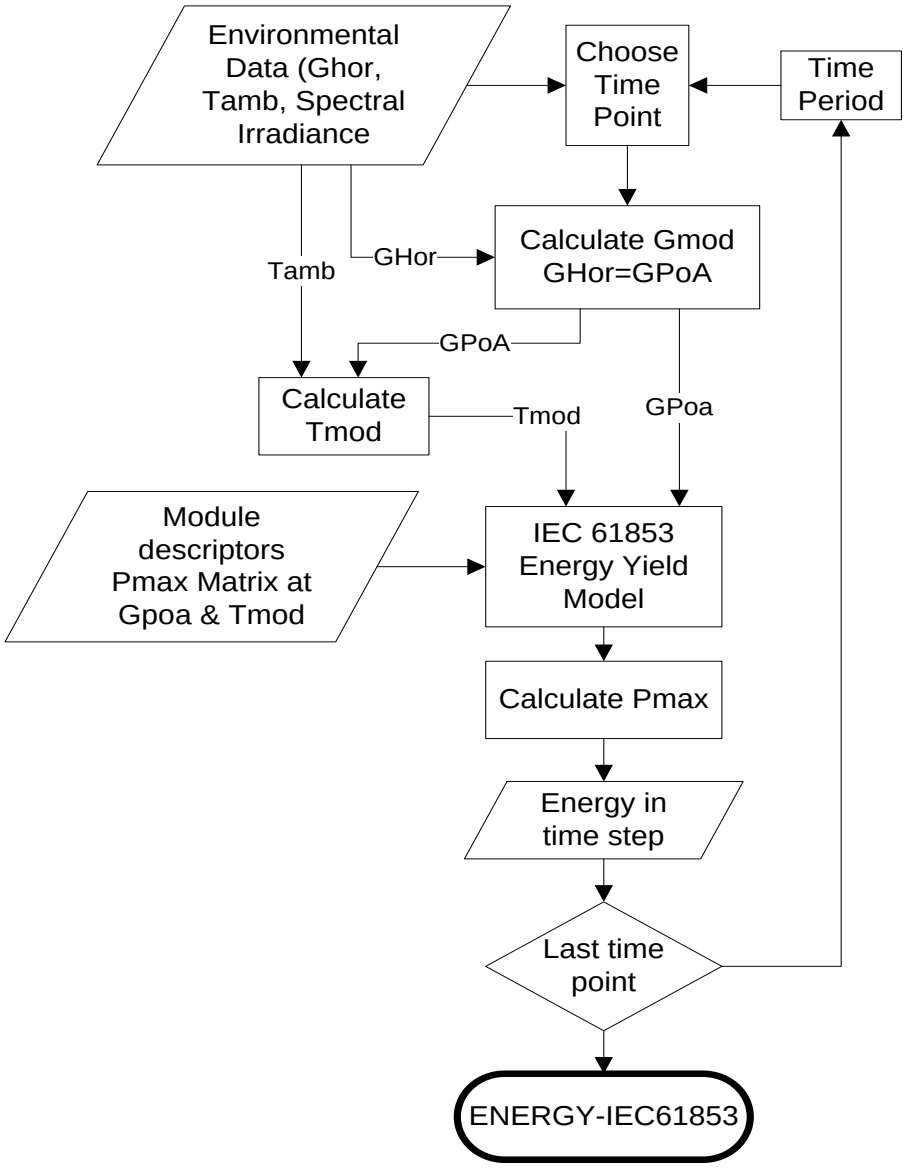

Figure 53: Procedure of the energy yield prediction methodology with IEC 61853 power calculation method

4.4.1 Irradiance Modelling

Irradiance is linearly correlated with the output of the device. So the accurate assessment of the availability of the different components of irradiance (beam and diffuse) influences the accuracy of the final yield estimation of the system.

Typically, the measured irradiance data available for various locations are global horizontal irradiance (G_{Hor}). A translation is required to convert the horizontal irradiance to the tilted surface of the PV system (G_{Poa}). This translation method

needs to be followed in two consecutive manners. First the global horizontal irradiance needs to be separated into horizontal beam and horizontal diffuse irradiance. Then horizontal beam and horizontal diffuse irradiance components have to be translated onto the tilted surface of the PV modules.

This thesis analyses four different horizontal irradiance separator models and three horizontal to in-plane translation models. Analysis of different methods helps to identify the best matched methods for the UK climate, where the estimated models are validated. A flow chart is given in Figure 54 explaining the irradiance modelling steps followed to translate G_{Hor} to G_{Poa}.

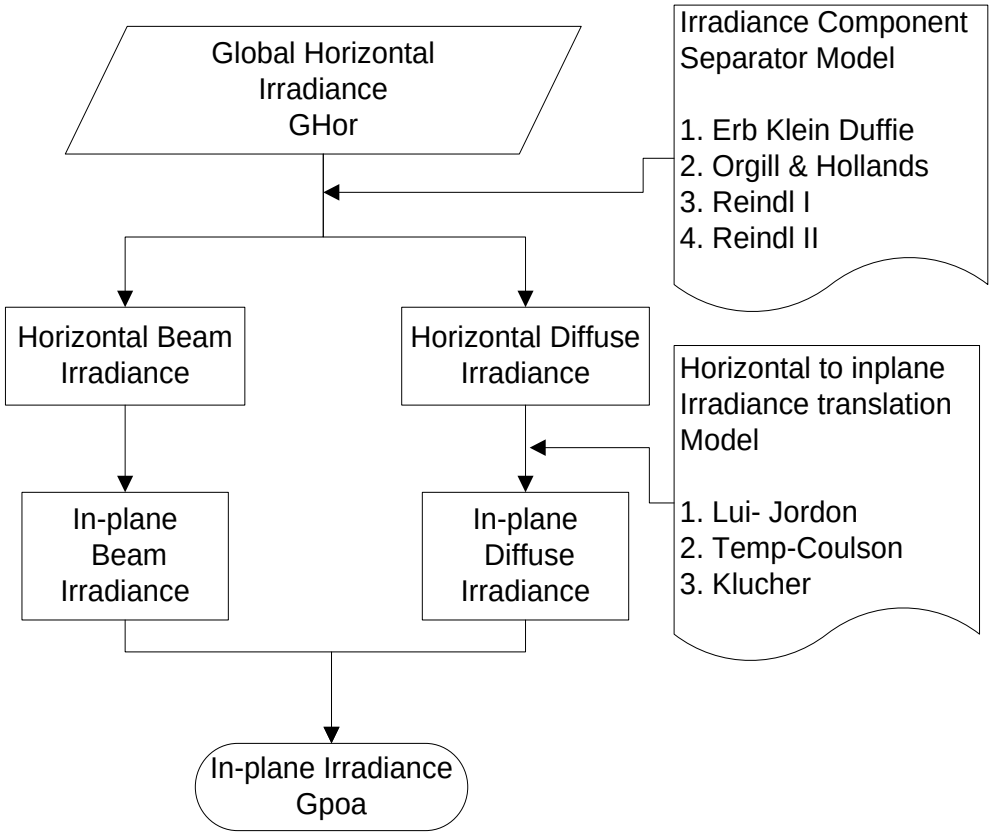

Figure 54: Flow chart of horizontal to in-plane irradiance translation.

Knowledge of direct irradiance density is important especially in applications where the solar radiation is concentrated. Direct irradiance can be estimated with two different kinds of models,

- Parametric or atmospheric transmittance models and

- models that calculate the decomposition of global irradiance in its components.

Atmospheric transmittance models require detailed information of atmospheric parameters such as distribution of clouds, the fractional sunshine, atmospheric turbidity, precipitable water content and cloud cover [77, 78]. On the other hand, decomposition models try to estimate direct and diffuse irradiance from global irradiance data [79-84].

Due to the relative simplicity of the model, decomposition models are widely used within the research communities, are also analysed here. These models are based on the correlation between the clearness index, k_t (global irradiance/horizontal extra-terrestrial irradiance) and the diffuse fraction, Ψ (diffuse irradiance/global irradiance).

Four different component separator models of global horizontal irradiance are analysed proposed by

- Orgill and Hollands [79],
- Erbs et al. [80],
- Reindl et al 1. [82].
- Reindl et al 2. [82].

All the above models estimate direct irradiance from the diffuse fraction. The results provided by these models depend on the clearness index, k_t, and the solar elevation. Each of these models represents a correlation between the hourly clearness index, k_t, and the corresponding diffuse fraction, Ψ of the irradiance. The model developed by Reindl introduces the solar elevation angle as a new variable in the model. The direct irradiance is obtained from the following equation (22) when diffuse fraction is estimated from Ψ -k_t correlations.

$$G_{beam\_hor} = G_{hor}(1 - \Psi)\sin \propto \tag{22}$$

Where *G* is the global radiation, α is the solar elevation angle, and Ψ is the hourly diffuse fraction.

Orgill and Hollands model:

$$\Psi = 1.0 - 0.249k_t \quad k_t < 0.35 \tag{23}$$

$$\Psi = 1.577 - 1.84k_t \quad 0.35 \leq k_t \leq 0.75 \tag{24}$$

$$\Psi = 0.177 \quad k_t > 0.75 \tag{25}$$

Erb Klein Duffie *model:*

$$\Psi = 1.0 - 0.09k_t \quad k_t \leq 0.22 \tag{26}$$

$$\Psi = 0.9511 - 0.1604k_t + 4.388k_t^2 - 16.638k_t^3 + 12.366k_t^4 \quad 0.22 < k_t \leq 0.8 \tag{27}$$

$$\Psi = 0.165 \quad k_t > 0.8 \tag{28}$$

Reindl-I model:

$$\Psi = 1.020 - 0.248k_t \quad k_t \leq 0.30 \tag{29}$$

$$\Psi = 1.450 - 1.670k_t \quad 0.30 < k_t < 0.78 \tag{30}$$

$$\Psi = 0.147 \quad k_t \geq 0.78 \tag{31}$$

Reindl-II model:

$$\Psi = 1.020 - 0.254k_t + 0.0123 \sin \propto \quad k_t \leq 0.30 \tag{32}$$

$$\Psi = 1.400 - 1.749k_t + 0.177 \sin \propto \quad 0.30 < k_t < 0.78 \tag{33}$$

$$\Psi = 0.147 - 0.182 \sin \propto \quad k_t \geq 0.78 \tag{34}$$

All the above models are implemented in Delphi and validated against the measured values of respective parameters taken from CREST outdoor monitoring system.

4.4.1.1 Horizontal Diffuse Irradiance:

Estimated values using the four (equation (23) - (34)) horizontal diffuse irradiance methods above are validated with actual measured values (Figure 55 - Figure 62), that includes the histograms of the deviation between measured and estimated values at an irradiance bin width of 50 W/m^2. The agreements between the models are similar against the measured values and the best matched model is Reindl-II method which shows better agreement in the UK climatic conditions (Figure 61).

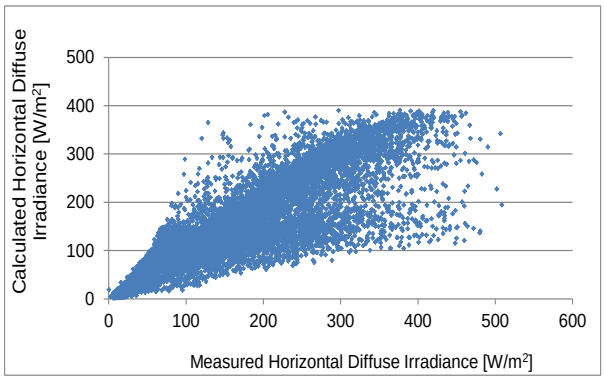

Figure 55: Measured vs estimated horizontal diffuse irradiance using the Erb Klein Duffy model.

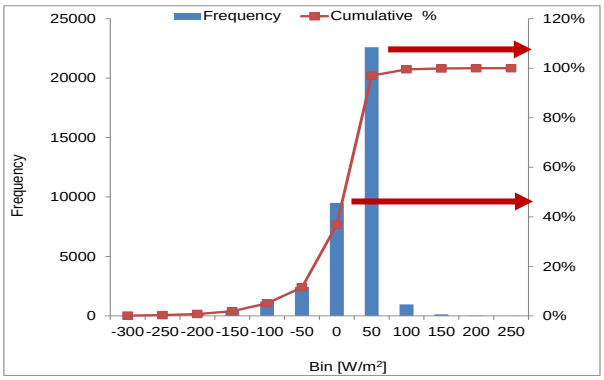

Figure 56: Histogram of the deviation between estimated (by Erb-Klein-Duffy) and measured horizontal diffuse irradiance.

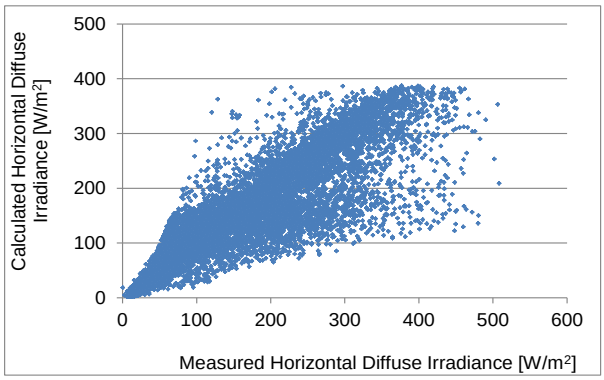

Figure 57: Measured vs estimated horizontal diffuse irradiance using Origill Hollands model.

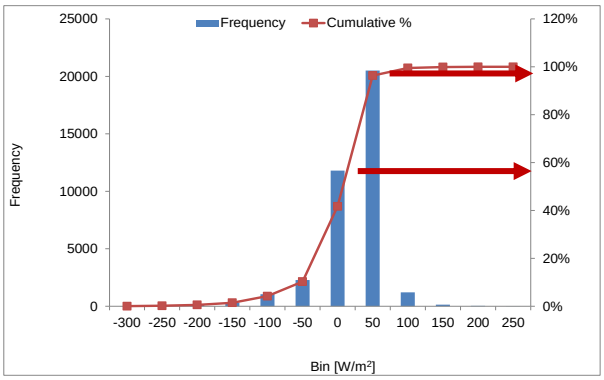

Figure 58: Histogram of the deviation between estimated (by Origill Hollands) and measured horizontal diffuse irradiance

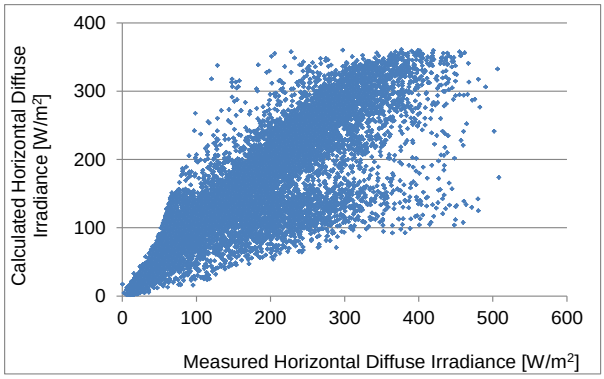

Figure 59: Measured vs estimated horizontal diffuse irradiance using Reindl-I model.

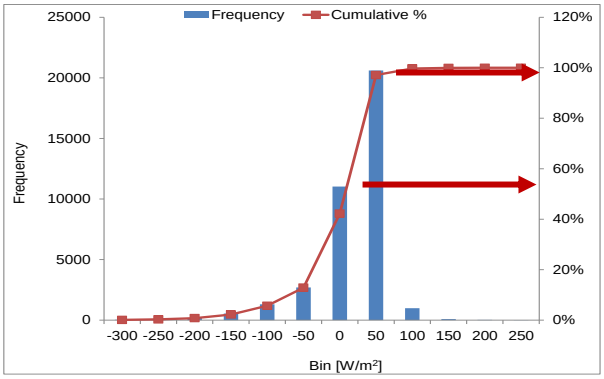

Figure 60: Histogram of deviation between estimated (by Reindl-I) and measured horizontal diffuse irradiance

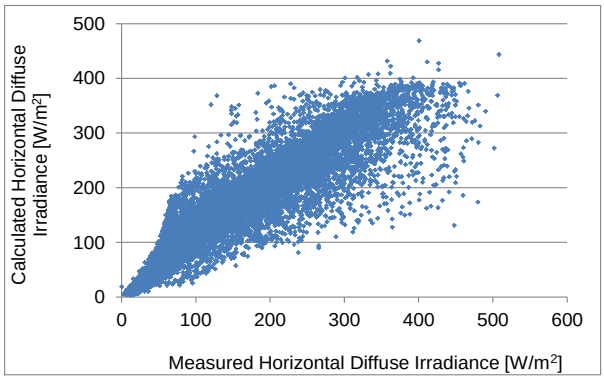

Figure 61: Measured vs estimated horizontal diffuse irradiance using Reindl-II model.

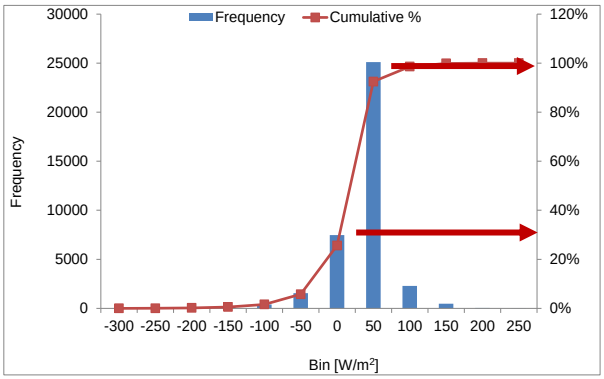

Figure 62: Histogram of deviation between estimated (by Reindl-II) and measured horizontal diffuse irradiance

Arrows in the histograms (Figure 56, Figure 58, Figure 60 Figure 62) show the percentage contribution of the deviation between measured and modelled value at bin width 50 W/m^2 and 100 W/m^2. This indicates the lower percentage contribution of error by Reindl-II method at bin width 50 W/m^2 compared to other models, whereas the error contributions at bin width 100 W/m^2 of all four models shown similar results.

4.4.1.2 Horizontal Beam Irradiance:

Again, the histograms (Figure 64, Figure 66, Figure 68 and Figure 70) for horizontal beam irradiance modelling shows lower percentage contribution of error against measured values by Reindl-II method.

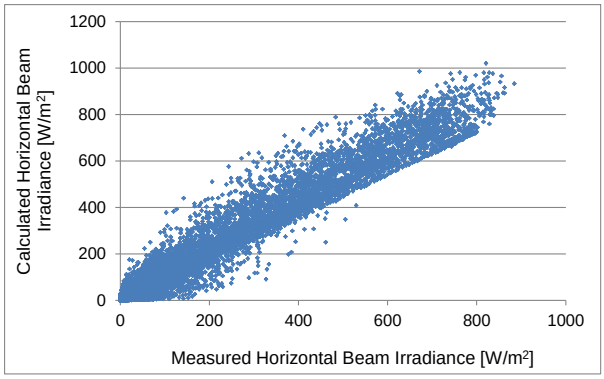

Figure 63**:** Measured vs estimated horizontal beam irradiance using the Erb Klein Duffy model.

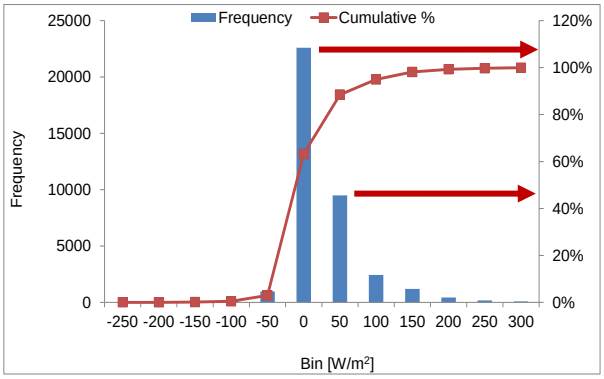

Figure 64: Histogram of deviation between estimated (by Erb Klein Duffy) and measured horizontal beam irradiance.

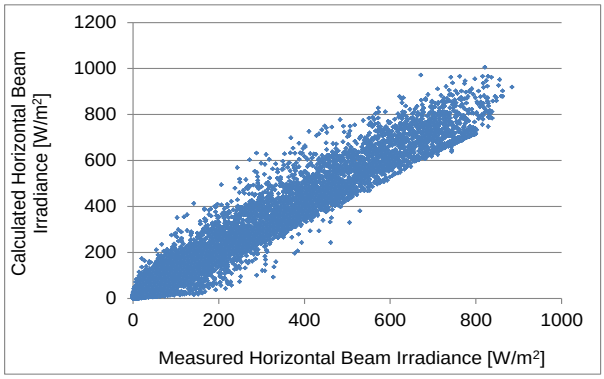

Figure 65: Measured vs estimated horizontal beam irradiance using Origill Hollands model.

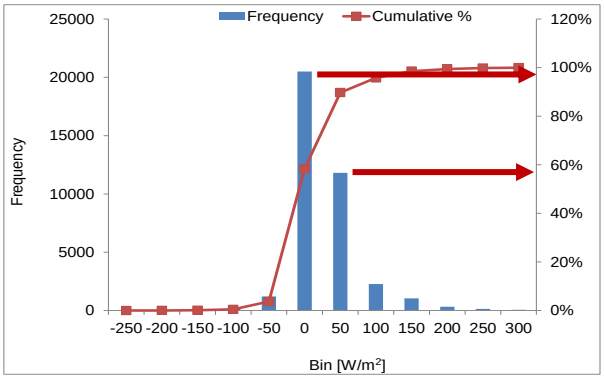

Figure 66: Histogram of deviation between estimated (by Origill Hollands) and measured horizontal beam irradiance

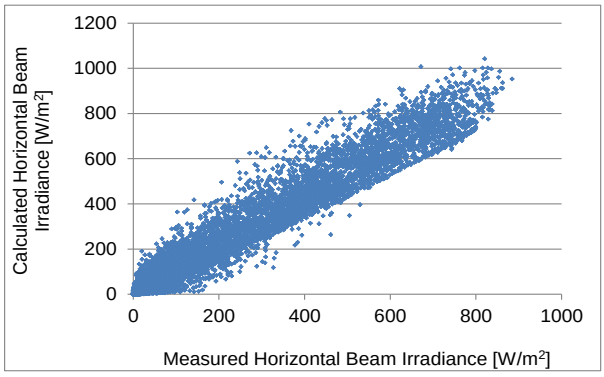

Figure 67: Measured vs estimated horizontal beam irradiance using Reindl-I model.

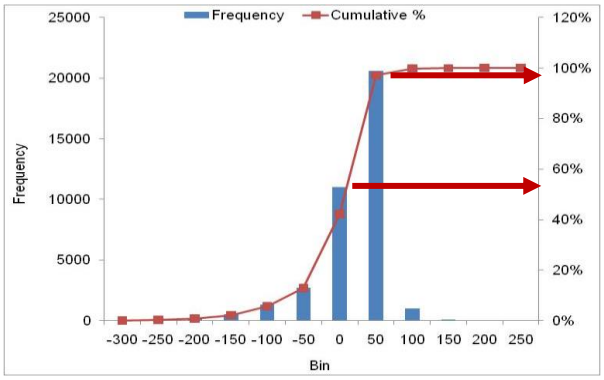

Figure 68: Histogram of deviation between estimated (by Reindl-I) and measured horizontal beam irradiance.

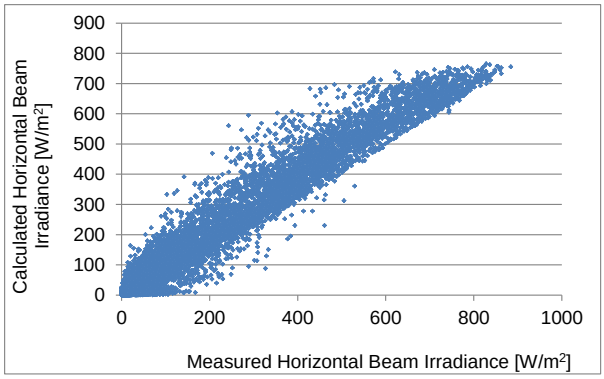

Figure 69: Measured vs estimated horizontal beam irradiance using Reindl-II model.

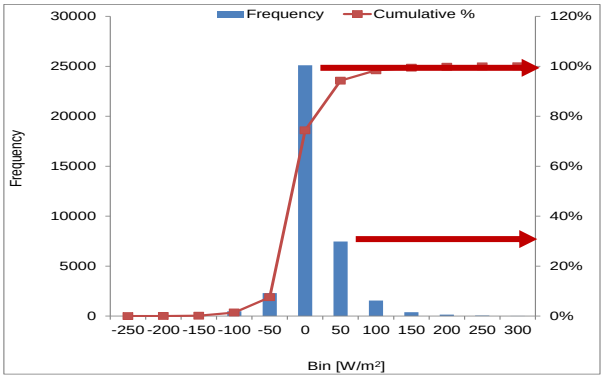

Figure 70: Histogram of deviation between estimated (by Reindl-II) and measured horizontal beam irradiance

The root mean square error (RMSE) and mean bias error (MBE) for all four methods compared with their respective measured values of horizontal beam and horizontal diffuse irradiance are shown in Table 9.

$$\mathrm{RMSE} = \left\{\left[\sum(\mathrm{Cal}-\mathrm{Meas})^2\right]/\mathrm{n}\right\}^{1/2} \quad (35)$$

$$\mathrm{MBE} = \left[\sum(\mathrm{Cal}-\mathrm{Meas})\right]/\mathrm{n} \quad (36)$$

Model	RMSE (W/m^2)	MBE (W/m^2)	RMSE %	MBE %
Erb Klein Duffie	49.0	8.0	34.0	5.8
Orgill & Hollands	46.0	6.0	32.0	5.8
Reindl I	51.0	11.0	35.4	8.0
Reindl II	41.0	-7.0	28.5	-5.2

Table 9: Comparison of statistical errors of the global horizontal irradiance component (beam & diffuse) separator models.

Table 9 represents the close agreement between the models with the best results achieved by the Reindl II model. Comparison between measured and estimated horizontal beam and diffuse irradiance using the Reildl-II model are shown in Figure 61 and Figure 69. Due to the better agreement of the Reindl–II model with measured values (Table 9) this method is used in this study as the irradiance component separator model. Based on the Reindl–II model, three in-plane irradiance estimation methods [85] are analysed for the UK climate as illustrated in Table 10.

Compared to all three G_{Hor} to G_{Poa} translation methods analysed in this thesis (Figure 54), the Klucher model shows the best agreement with measured values in the UK climate. It should also be noted that translation models are site dependent considering the sky conditions of the specific site. Comparison of measured and estimated in-plane irradiance by the Klucher model is shown in Figure 73.

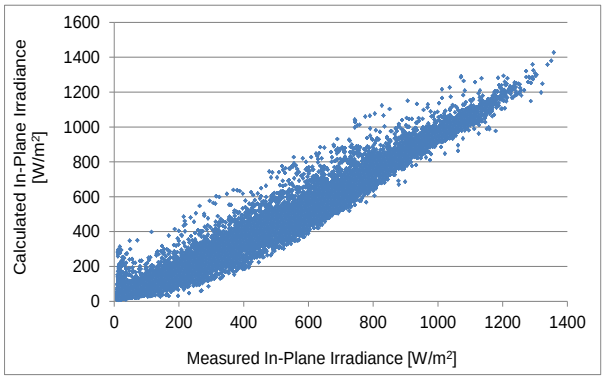

Figure 71**:** Measured vs estimated in-plane irradiance using the Lui Jordon model.

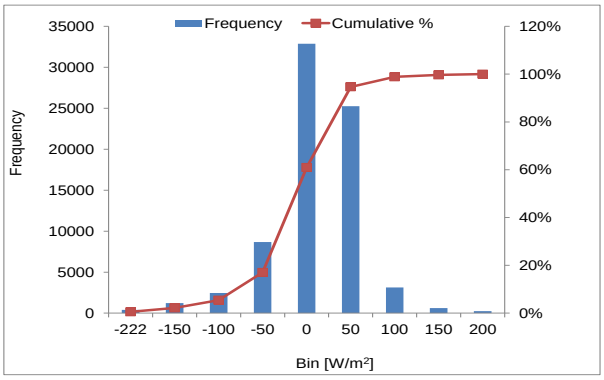

Figure 72: Histogram of the deviation between estimated (by Lui-Jordon model) and measured in-plane irradiance

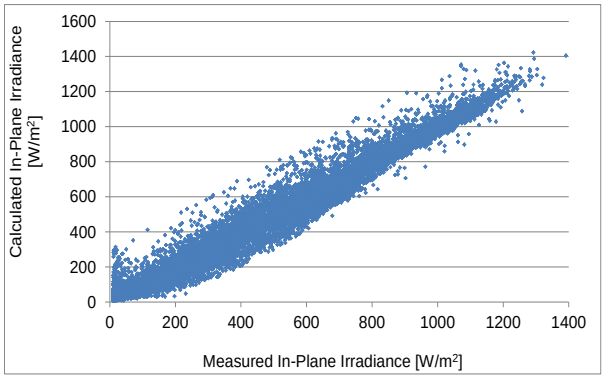

Figure 73: Measured vs estimated in-plane irradiance using the Klucher model.

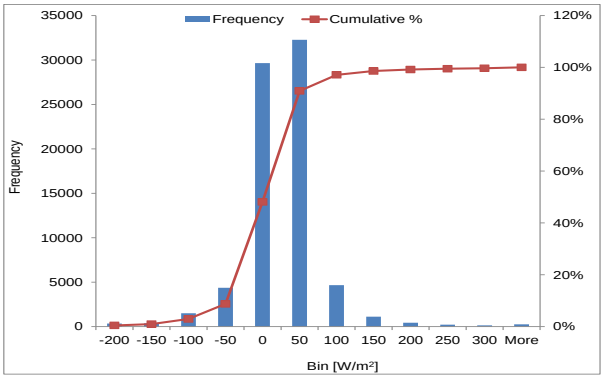

Figure 74: Histogram of the deviation between estimated (by Klucher model) and measured in-plane irradiance.

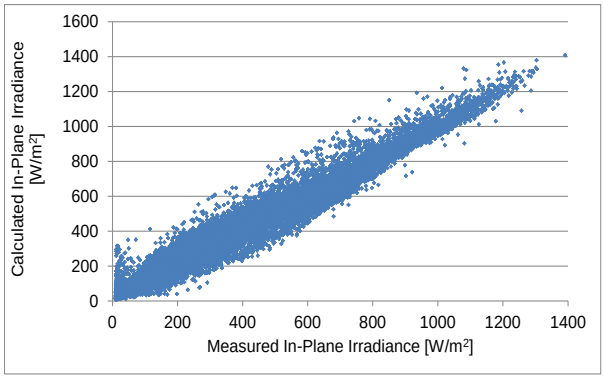

Figure 75: Measured vs estimated in-plane irradiance using the Temps-Coulson model.

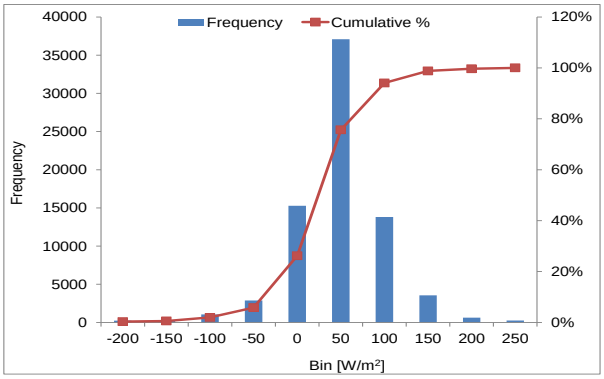

Figure 76: Histogram of the deviation between estimated (by Temps-Coulson model) and measured in-plane irradiance.

The RMSE and MBE for all three methods compared with the measured values of in-plane irradiance are shown in Table 10.

Model	RMSE (W/m^2)	MBE (W/m^2)	RMSE %	MBE %
Lui- Jordon	61.0	-13.0	21.3	-4.6
Temp-Coulson	64.0	22.0	22.4	8.0
Klucher	57.0	0.47	19.9	0.1

Table 10: Validation results of the horizontal to in-plane irradiance translation models.

All the above models are relatively old models but still representative. Compared to all three G_{Hor} to G_{Poa} translation methods analysed in this section, the Klucher model shows the best agreement with measured values (Figure 73 and Figure 74). Selection of irradiance translation model largely influence the modelling related uncertainty introduced by the two irradiance sub-models studied in this section. Also, the level of uncertainty varies as a function of irradiance intensity and it's higher at lower intensity of irradiance. So, the selection of irradiance sub-models should be a site dependent component in the energy yield prediction method considering the sky conditions of the specific site.

4.4.2 Temperature Modelling

Accurate estimation of module temperature (T_{mod}) should improve the accuracy of the energy yield estimation. In this study, T_{mod} is estimated as a function of ambient temperature (T_{amb}) and irradiance (G_{Poa}) using the equation (37) [86].

$$T_{\mathrm{mod}} = T_{amb} + k * G_{poa} \tag{37}$$

Where k is the irradiance factor. 'k' is estimated based on the data measured in the CREST outdoor monitoring system for different module technologies and those values are 0.016, 0.03 and 0.026 for c-Si, a-Si and CIGS, respectively. The estimated T_{mod} (using equation (37)) is then compared with the measured T_{mod} for c-Si, a-Si and CIGS modules. The RMSE and MBE between the estimated and measured T_{mod} is shown in Table 11 for all three modules.

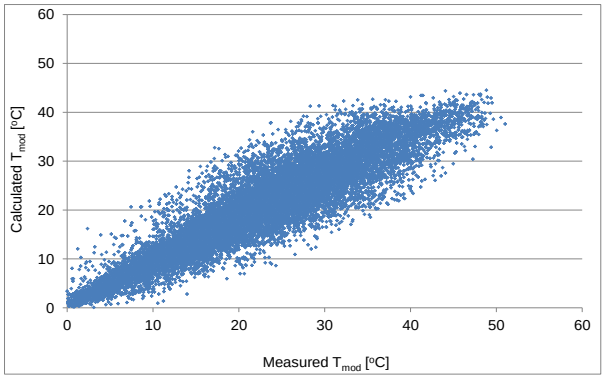

Figure 77: Measured vs estimated T_{mod} for c-Si module.

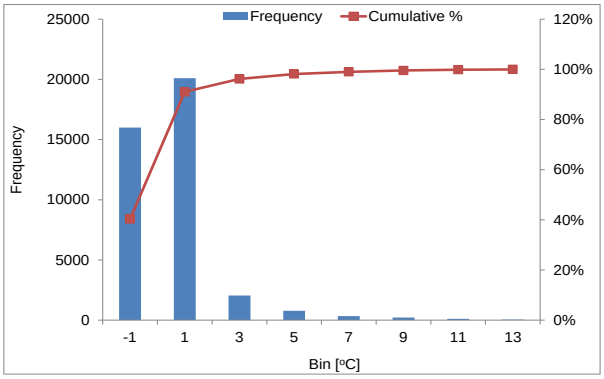

Figure 78: Histogram of the difference between estimated and measured module temperature for c-Si module.

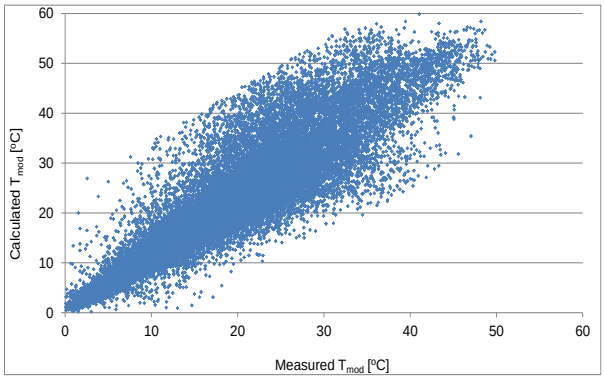

Figure 79: Measured vs estimated T_{mod} for a-Si module.

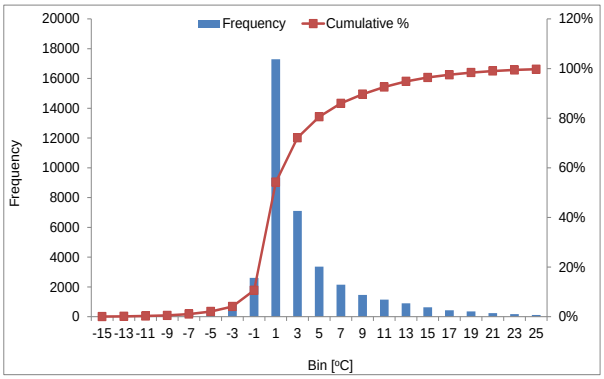

Figure 80: Histogram of the difference between estimated and measured module temperature for a-Si module.

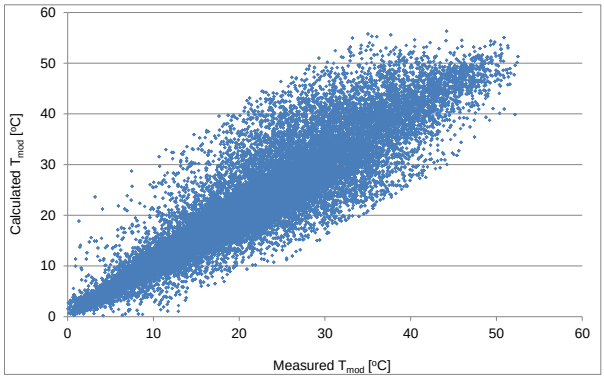

Figure 81: Measured vs estimated T_{mod} for CIGS module.

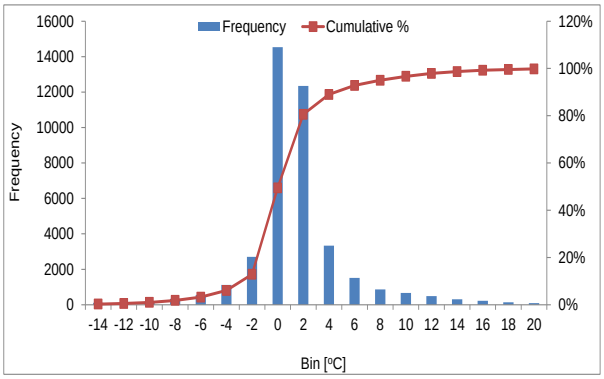

Figure 82: Histogram of the difference between estimated and measured module temperature for CIGS module.

Figure 77, Figure 79 and Figure 81 shows the measured vs estimated T_{mod} for c-Si, a-Si and CIGS module.

Module	RMSE (^{o}C)	MBE (^{o}C)	RMSE (%)	MBE (%)
c-Si	3	-1	17.3	-6.8
a-Si	5	2	31.5	13.4
CIGS	3	0.5	21.1	2.9

Table 11: Error analysis to estimate module temperature of different devices.

Calculation of module temperature largely depends on the type of module, module mounting system, thermal effect due to wind speed and these factors directly linked with the module temperature modelling uncertainty. Also, the level of uncertainty varies as a function of temperature intensity and the above factors. The uncertainty level varies as the similar pattern as irradiance but at lower scale and it's higher at lower temperature.

4.4.3 P_{max} Modelling

Matrices of measured P_{max} over a wide range of G_{mod} and T_{mod} are used as the module descriptor for all three different modules. Maximum power at target

irradiance (G_{Poa}) and module temperature (T_{mod}) of the environmental data at all timestamps are estimated by linear regression from the input P_{max} matrix plot. This method is suggested in the draft energy rating standard [87]. Three modules of the different technologies are also measured for the same period of time on the CREST outdoor monitoring system and the maximum power (P_{max}) for each module is recorded at the same timestamp. The estimated P_{max} values are compared with the measured values at real operation. The errors between estimated and measured values of all three modules are validated, shown in Table 12. Measured and estimated P_{max} for c-Si, a-Si and CIGS modules are shown in Figure 83, Figure 85 and Figure 87 respectively.

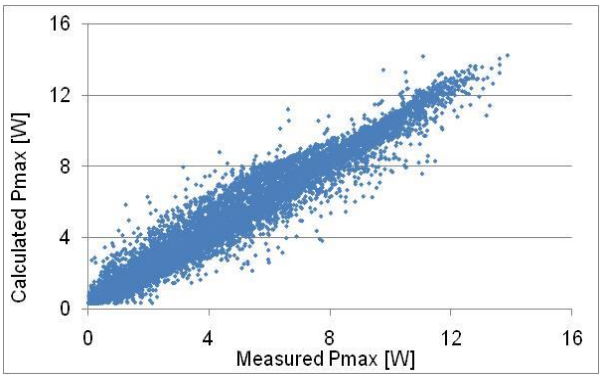

Figure 83: Measured vs. estimated P_{max} for c-Si module.

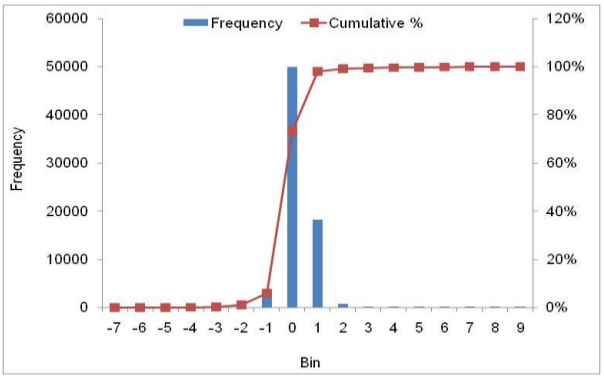

Figure 84: Histogram of the difference between estimated and P_{max} for c-Si module.

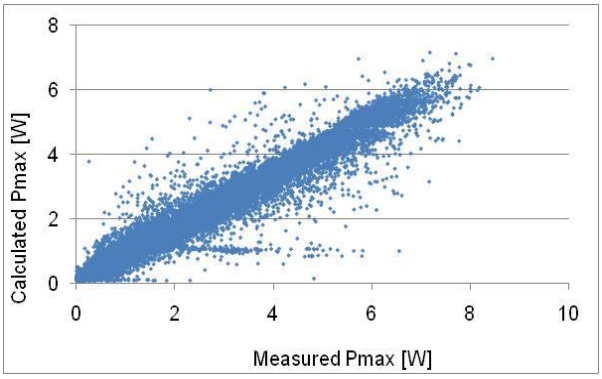

Figure 85: Measured vs. estimated P_{max} for a-Si module.

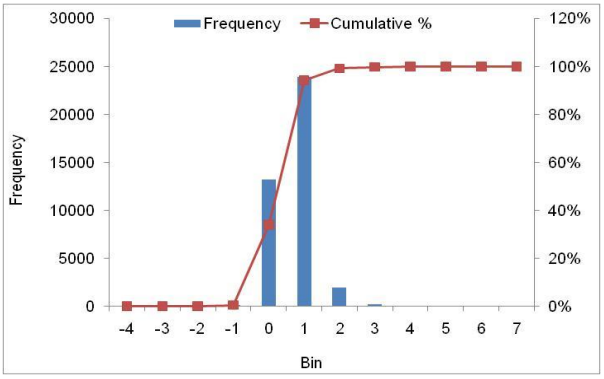

Figure 86: Histogram of the difference between estimated and P_{max} for a-Si module.

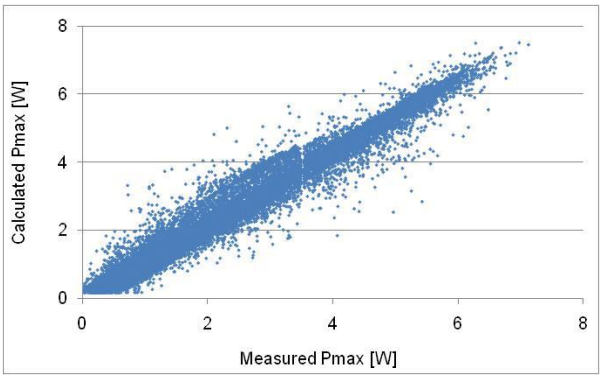

Figure 87: Measured vs. estimated P_{max} for CIGS module.

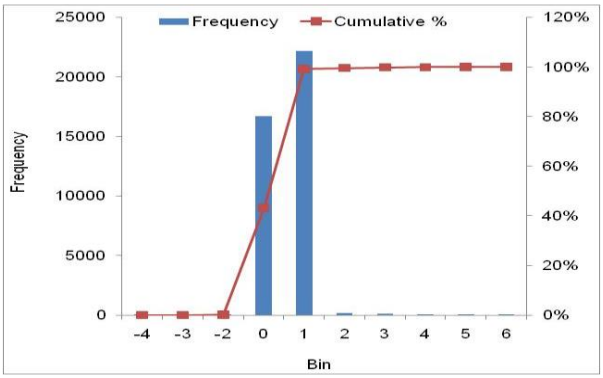

Figure 88: Histogram of the difference between estimated and P_{max} for CIGS module.

Module	RMSE (W_p)	MBE (W_p)	RMSE (%)	MBE (%)
c-Si	0.73	-0.17	25.6	-5.9
a-Si	0.51	0.22	36.5	15.6
CIGS	0.35	-0.06	23.7	-3.8

Table 12: Variation of errors of the estimated and measured P_{max} of three PV modules.

The uncertainty of the measured in-plane irradiance and module temperature contributes towards the error in the above table (Table 12). Additional uncertainty contributors are comes from the P_{max} measurement, irradiance and temperature translation models including P_{max} calculation method.

4.5 Conclusions

The level of accuracy in the IEC energy rating method is analysed by evaluating the uncertainty of the environmental parameters and validating the estimation method against real measurements.

In this chapter a robust analytical procedure for propagating the measurement uncertainties of irradiance and temperature for energy yield prediction was established. A Monte Carlo simulation approach was employed which is applicable to any location. For the evaluation of this procedure, the method has been validated at Loughborough, UK. The irradiance sensor used in this thesis is a CM 11 pyranometer which gives ±1.56% annual irradiation uncertainty in the UK climate. The temperature sensor studied is a HMP45C Pt1000 sensor which resulted ±0.08°C annual average temperature uncertainty. It should also be noted that the level of uncertainty depends on the site dependent weather conditions and also the type of measurement equipment.

The best-performing horizontal irradiance component separator model for the UK climate was identified as the Reindl-II model. Similarly the Klucher model to translate the horizontal to in-plane irradiance was identified as the best for UK climatic conditions amongst the models studied.

The agreement between estimated and measured module temperature for three modules was found to be in the range of ± 3-5°C. This number may be improved by considering the thermal effects due to wind speed, but already is of similar scale of observed temperature variation within a single module [88].

Estimation of P_{max} for c-Si and CIGS modules was underestimated by 5.9% and 3.8%, respectively, whereas that of the a-Si module was overestimated by over 15%. Possible reasons for this over estimation are the high spectral sensitivity of the a-Si module and seasonal material changes. Considering the spectral irradiance effects would potentially improve the predicted energy yield values close to the real measurement.

The range of realistic operating conditions including spectral irradiance is analysed in chapter 5 in relation to the performance of the PV module. This helps to identify the measurement points for the module descriptor at a range irradiance, temperature and spectral irradiance conditions.

5 Fast Energy Yield Calculations (FEnYCs) Methodology

5.1 Introduction

To establish a reliable performance predictor for PV modules, efforts on energy yield prediction methodologies and energy rating standard are underway as demonstrated in the previous chapter. In order to achieve a realistic and accurate energy prediction method, the importance of good quality environmental data and module characterisation measurements were also explained in chapter four. This chapter explains in detail the requirements of a customized module characterisation methodology that will test the module over all relevant environmental conditions. The main objectives of this chapter are

- To establish a new module characterisation methodology replicating the full range of realistic operational environmental conditions.
- To establish the full procedure of FEnYCs methodology
- To establish the modelling approach of FEnYCs power calculation from a multi-dimensional power matrix at irradiance, temperature and spectral irradiance

The matrix based energy yield calculation, explained before, requires either indoor or outdoor based PV module characterisation in order to obtain a performance matrix over the wide range of relevant environmental conditions. There are advantages with both indoor and outdoor based measurement campaigns. Indoor measurements are performed in a solar simulator by generating variable irradiance at constant air mass 1.5 spectrum and over a controllable range of temperatures. Outdoor characterisation performs the measurement campaign in real conditions at different, uncontrolled, irradiance, spectral and temperature conditions.

In an indoor test campaign, a wide ranging performance matrix of any PV module can be generated within very short period of time (a few hours) using solar simulator. This is the major advantage of indoor based measurement campaign which allows a fast characterisation of any PV module. But solar simulators have a particular limitation: current simulators are generally not able to generate the variable

irradiance spectra that are experienced in real operation. It is only possible to measure different irradiance at AM 1.5 spectrum. Due to this restriction, a spectral mismatch appears in the energy yield prediction method compared to the actual generation in real operation. The influence of spectral mismatch effects can be significant for strongly spectrally sensitive PV technologies, e.g. a-Si, as demonstrated in Chapter 4.

Module characterisation in an outdoor measurement campaign can generate different irradiance conditions at different (and realistic) spectra and also at different temperatures. This method can offer accurate energy yield prediction as the module encounters all relevant environmental conditions. However, in order to achieve the full performance matrix over the required wide range of irradiance-temperature-spectrum (G-T-E) conditions, it is required to expose that PV module for a long period of time, generally a full calendar year. So with outdoor based module characterisation, energy yield estimation can present an accurate method but with the penalty that it is time consuming (more than industry would tolerate). Also the range of weather conditions depends on location, so outdoor based characterisation may not be possible at all locations - as a result the implementation of this method as a standard would be an issue for some established test institutes.

In the ideal case, a fast and accurate energy yield estimation method requires indoor equipment which can better replicate the outdoor weather conditions. To achieve this, a custom-built LED (Light Emitting Diode) based solar simulator is available at CREST which can generate variable irradiance, temperature and at the same time variable spectrum also.

This chapter establishes the range of different operating conditions (irradiance, temperature and spectral irradiance) and the required measurement setup in the LED simulator to generate the module characterisation data for a robust energy yield prediction. This includes the characteristic analysis of the environmental data, which aims to specify the range of different parameters under which a PV module operates in real operation and identify the conditions of major energy generation contribution over the year. A correlation between irradiance-temperature and spectral irradiance in relation to the PV module performance outdoors is also analysed. The measurement settings of different influencing parameters are then established for

characterisation of the PV module indoors at compatible realistic outdoor operational conditions. This chapter helps to achieve the ultimate aim of this thesis to establish the fast energy yield prediction (FEnYCs) method for PV module of any technology with better accuracy.

5.2 FEnYCs Methodology Development

5.2.1 **Overview of the proposed model**

The requirements of the proposed method are explained in this section. Similar to other energy yield prediction methods, this proposed method also requires two basic input measurement data sets i.e. PV module characterisation data and meteorological data of the operating location(s).

Modules require characterisation indoors under variable irradiance, temperature and spectral irradiance to form a multidimensional performance matrix. Required measured meteorological data are irradiance, ambient temperature, spectral irradiance and wind speed. A matrix of meteorological data of the same parameters (as the indoor measurement matrix) is then required from any arbitrary site in order to estimate the energy yield (Figure 89) of the PV module.

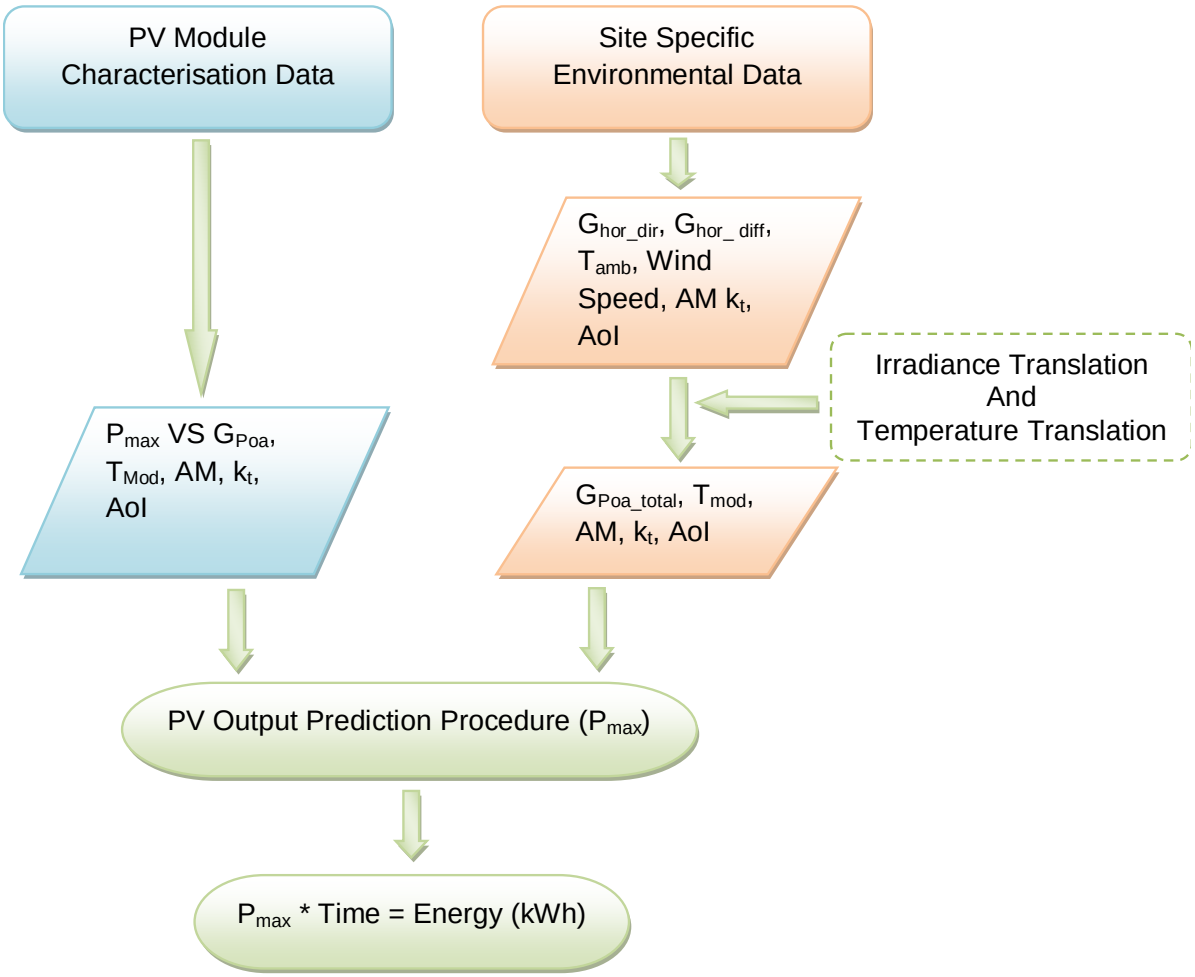

Figure 89: Flow chart of Fast Energy Yield Prediction (FEnYCs) of PV modules.

To develop the proposed method, all the meteorological data are taken from the CREST outdoor measuring systems. Total irradiance is estimated from the direct and diffuse components and translated from the horizontal to the plane of module array. The module temperature is calculated as a function of total irradiance, ambient air temperature and wind speed.

5.2.2 Analysis of Meteorological Data and Identification of Suitable Test Conditions

This section analyses the environmental data in Loughborough to represent the UK climate for this study. The objectives of this study are to:

1. Specify the extents of the different dimensions (parameter range) in the matrix, to successfully characterise the device.
2. Define the modelling procedure, to show how to combine the module characteristics determined in step 1) with the meteorological data from anywhere to give the annual energy yield.
3. Evaluate the uncertainty overall and from each contribution.

This information is used to define the measurement settings for the indoor measurement system by reproducing the outdoor conditions. This method enables module characterisation within short period of time (a few hours) under artificially generated realistic climatic conditions that PV devices can experience in real operation.

5.2.2.1 Range of Operating Environmental Conditions

The parameters considered in this study are irradiance, temperature and spectral irradiance and the selected time period of the measured dataset is from January 2009 to December 2009.

A three dimensional binning method is applied to analyse the above mentioned parametric annual dataset. Annual incoming energy (solar irradiation) has been binned by the above three parameters, with bin widths of 100W/m^2, 10°C and 0.5AM for irradiance, temperature and spectrum, respectively. The results are shown in

Figure 90.

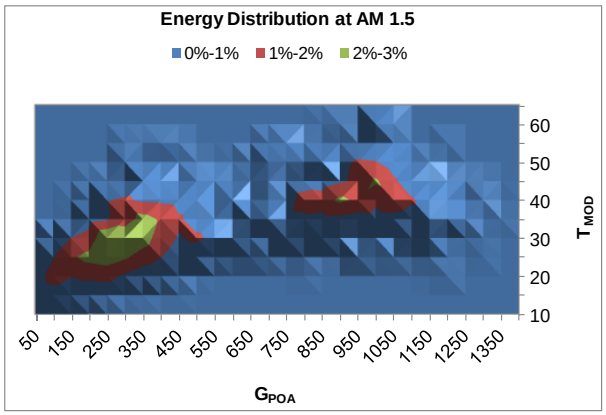

Figure 90-a: Energy distribution from sum at AM 1.5 as a function of irradiance and temperature

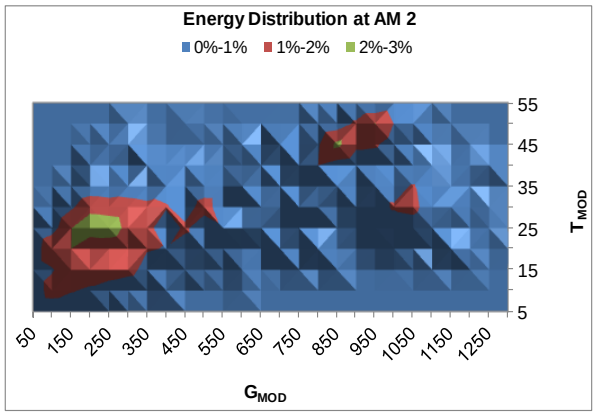

Figure 90-b: Energy distribution from sum at AM 2 as a function of irradiance and temperature

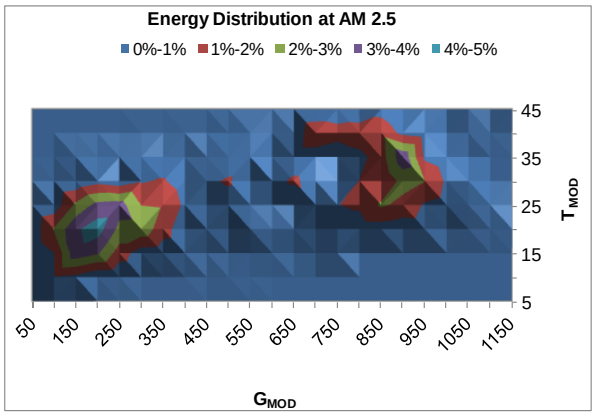

Figure 90-c: Energy distribution from sum at AM 2.5 as a function of irradiance and temperature

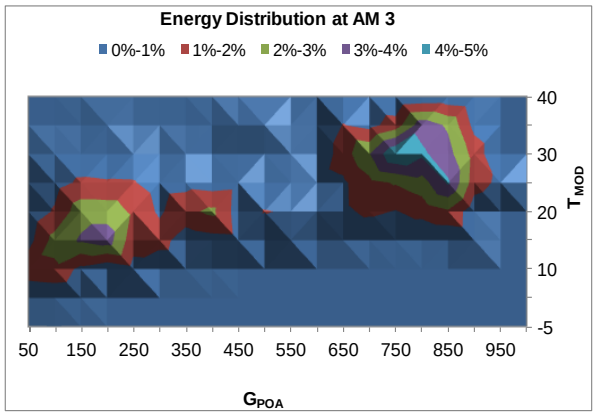

Figure 90-d: Energy distribution from sum at AM 3 as a function of irradiance and temperature

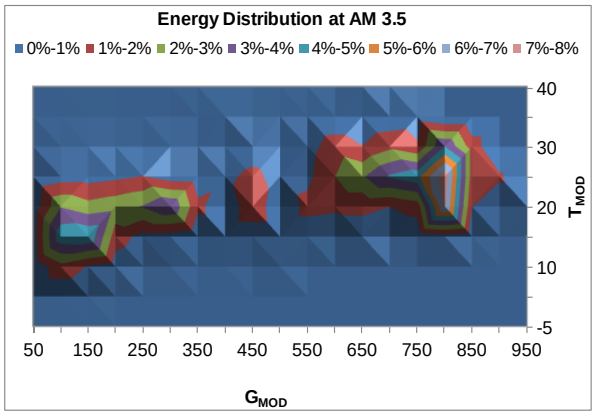

Figure 90-e: Energy distribution from sum at AM 3.5 as a function of irradiance and temperature

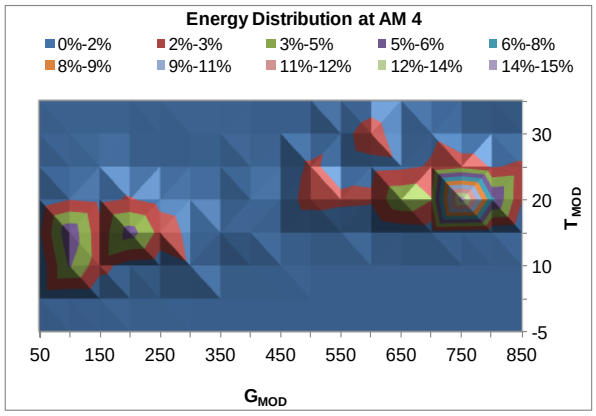

Figure 90-f: Energy distribution from sum at AM 4 as a function of irradiance and temperature

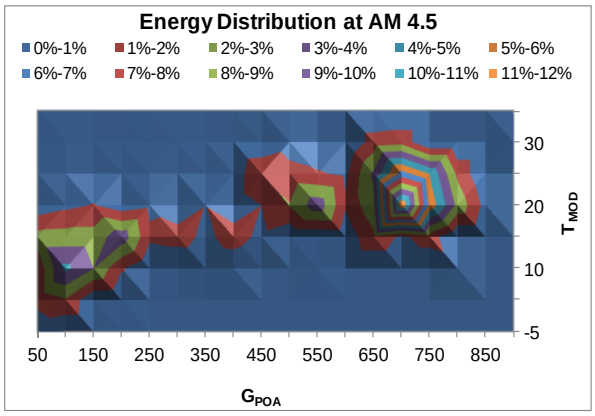

Figure 90-g: Energy distribution from sum at AM 4.5 as a function of irradiance and temperature

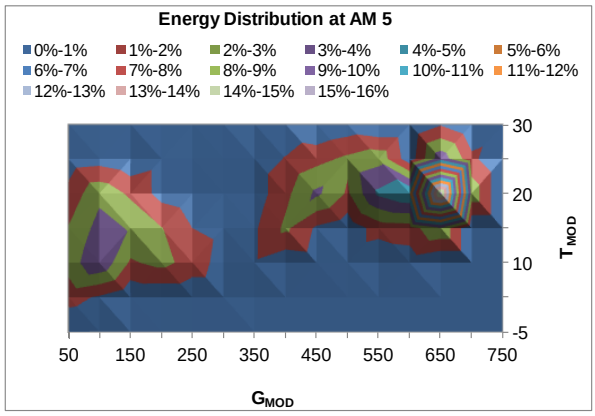

Figure 90-h: Energy distribution from sum at AM 5 as a function of irradiance and temperature

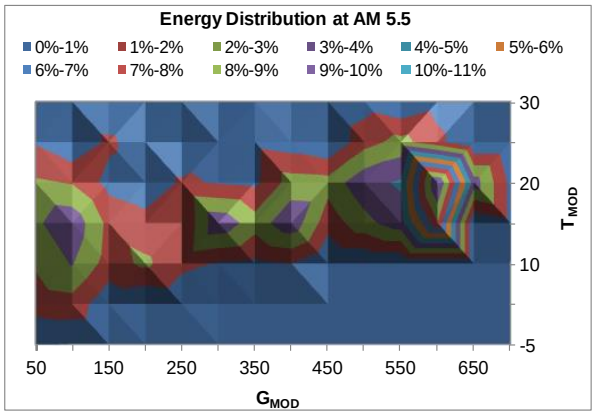

Figure 90-i: Energy distribution from sum at AM 5.5 as a function of irradiance and temperature

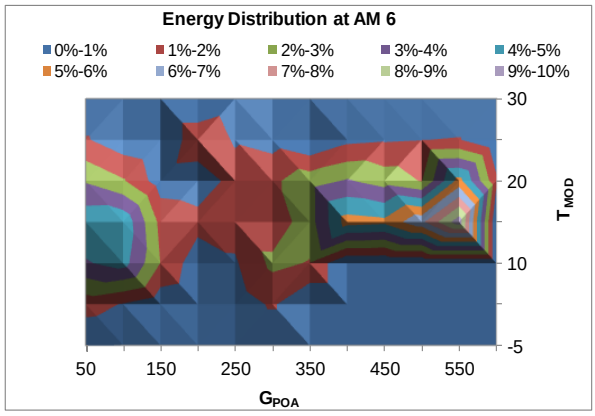

Figure 90-j: Energy distribution from sum at AM 6 as a function of irradiance and temperature

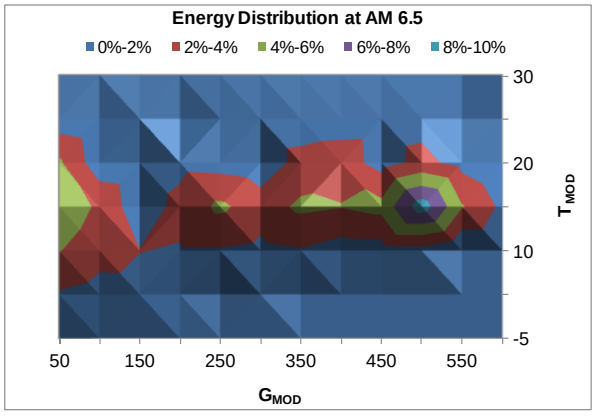

Figure 90-k: Energy distribution from sum at AM 6.5 as a function of irradiance and temperature

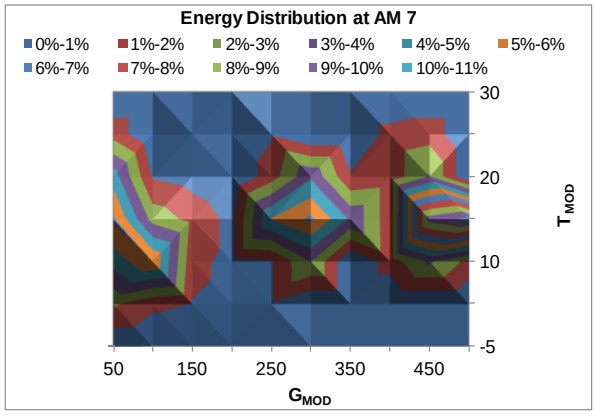

Figure 90-l: Energy distribution from sum at AM 7 as a function of irradiance and temperature

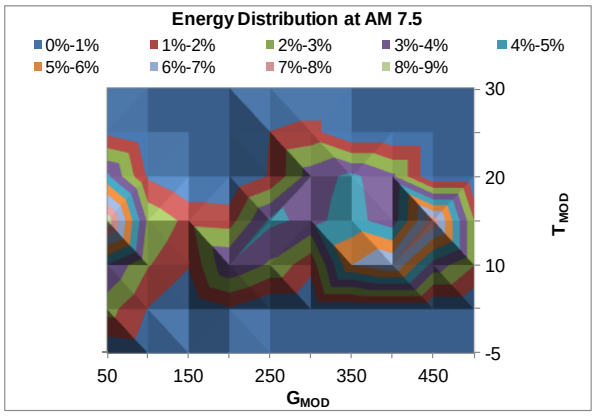

Figure 90-m: Energy distribution from sum at AM 7.5 as a function of irradiance and temperature

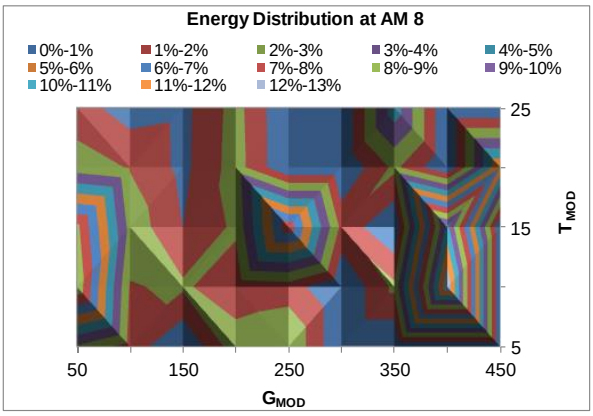

Figure 90-n: Energy distribution from sum at AM 8 as a function of irradiance and temperature

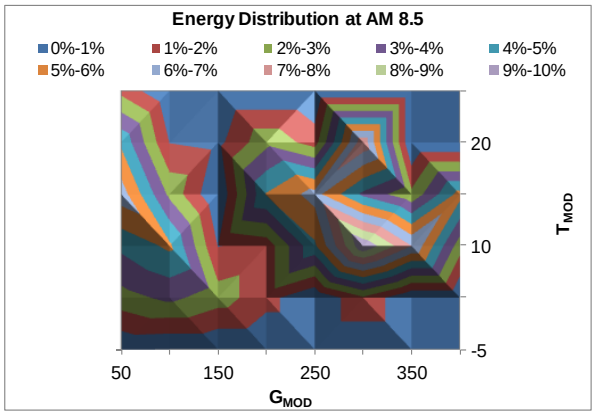

Figure 90-o: Energy distribution from sum at AM 8.5 as a function of irradiance and temperature

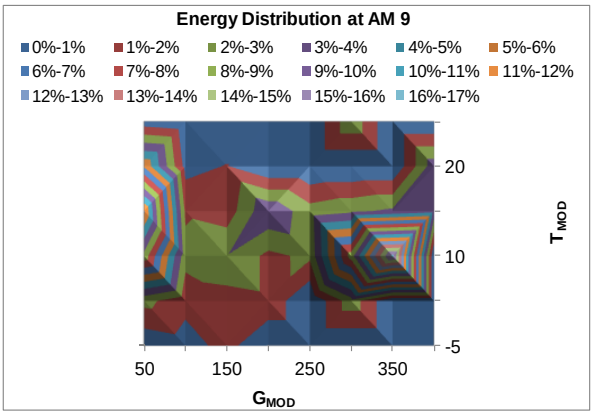

Figure 90-p: Energy distribution from sum at AM 9 as a function of irradiance and temperature

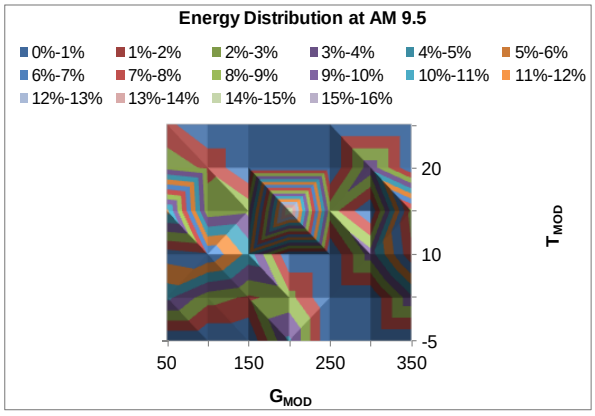

Figure 90-q: Energy distribution from sum at AM 9.5 as a function of irradiance and temperature

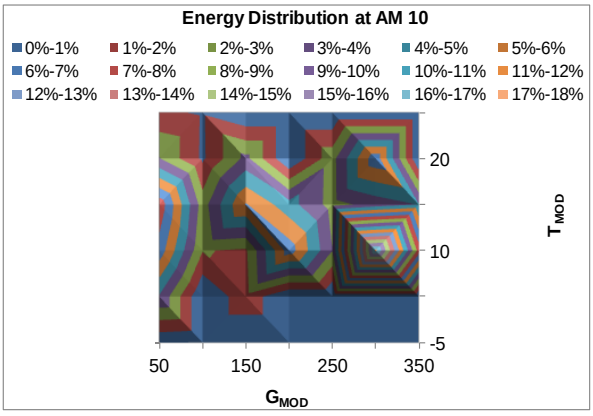

Figure 90-r: Energy distribution from sum at AM 10 as a function of irradiance and temperature

Figure 90: Incoming energy distribution from sum at AM 1.5 to AM 10 as a function of irradiance and temperature.

The energy distribution surface plots above reveal at which levels of irradiance and temperature and at which AM spectum, the largest contributions of solar resource are available for a PV system in the UK climate.The ranges of operating conditions of irradiance and temperature at different AM spectra are listed in Table 13.

Table 13: Range of climatic conditions in the UK covering major annual incoming energy density.

AM Range	Irradiance Range (W/m^2)	Temperature Range ($^{\circ}C$)	Incoming energy contribution (%)	Annual Energy contribution cumulative (%)
1.5 – 2	50 – 1050	10 – 55	38.7	
2.5 – 3	50 – 950	10 – 45	20.4	
3.5 – 4	50 – 350 550 – 900	10 – 35	13.1	81.5
4.5 – 5	50 – 250 500 – 850	5 – 30	9.3	
5.5 – 6	50 – 150 300 – 700	5 – 30	4.8	
6.5 – 7	50 – 600	5 – 25	3.2	
7.5 – 8	50 – 500	5 – 25	2.2	
8.5 – 9	50 – 400	5 – 25	1.7	
9.5 – 10	50 – 400	5 – 25	1.2	94.6

Table 13 shows the correlation of the ranges of irradiance and temperature at different air mass bands in relation to the annual solar energy contributions at Loughborough, UK. The bins of AM selected for the purposes of module characterisation have been primarily based on the level of their energy contrbutions. It is noticed that over 80% of annual energy is incident at spectra up to AM 5 and close to 95% up to AM 10 for the UK climate.

SPECTRAL IRRADIANCE DEFINITION

Integration of spectral irradiance at a range of wavelength is called irradiance. Different climatic region and cloudiness strongly influences the spectral irradiance and the intensity of the solar irradiance [89]. The spectral response of different module technology is different; hence the production of energy is different of different PV modules in different locations. Spectral mismatch effects are presented by other research groups [90-94].

So far, in this study, the spectral irradiance has been defined only by the air mass. However, there are other parameters that potentially can also influence the spectral irradiance such as the cloud condition (k_t) and angle of incidence (AOI). Also, there is an on-going research in the research community for a unique number descriptor for spectral irradiance [93, 95]. Characterisation of spectral data, Average Photon Energy (APE) as a unique number descriptor for spectral irradiance is studied. APE of each spectrum of different Air Mass (AM) is then estimated using the equation (38). The unit of APE is the electron volt (eV).

$$APE = \frac{\int_{300}^{1700} E(\lambda) d\lambda}{q \int_{300}^{1700} \frac{E(\lambda)}{Ephoton(\lambda)} d\lambda} \quad (38)$$

Where E is the spectral irradiance, λ is the wavelength within the range 300nm to 1700nm; q is the charge of electron.

Total incoming energy from the sun (H_{POA}) is binned as a function of irradiance at plane of array, ambient temperature and APE with a bin size of 50 W/m^2, 5°C and 0.05eV, respectively. The annual irradiation distribution over different APE at

Loughborough are shown in Figure 91 with the APE of the standard AM1.5G spectrum in the range between 350 and 1700 nm is approximately 1.59 eV.

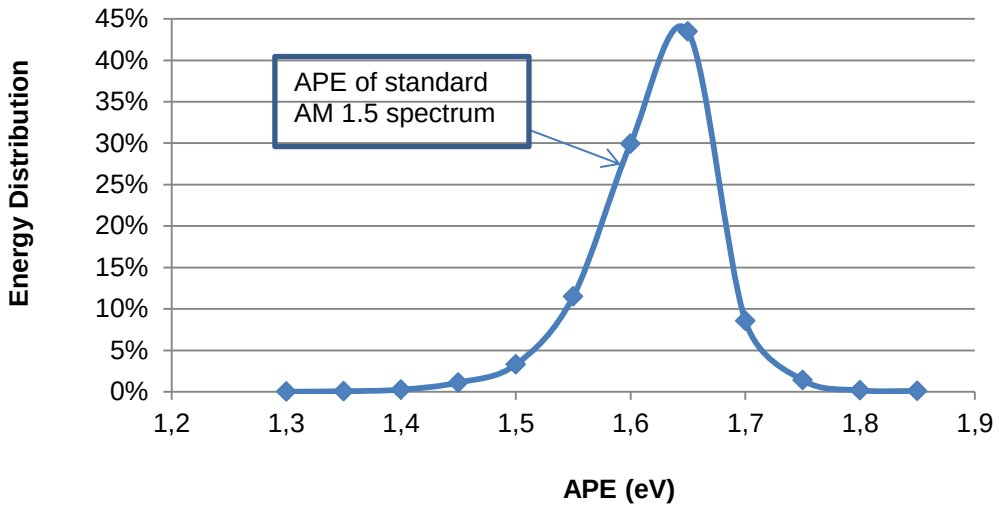

Figure 91: Distribution of energy from sun as a function of APE.

Other studies have already aimed to assess APE as a unique spectral irradiance descriptor [89, 93, 95].

The annual energy distribution in the module plane (mounting frame at azimuth 0° and tilt angle at 45°) of array over different AM is shown in Figure 92.

Clearness index (k_t) is another environmental parameter considered to affect spectral irradiance. Clearness index distinguishes the sky conditions and indicates the level of cloudiness. Inclusion of the clearness index in the energy yield prediction method helps to define spectral irradiance characterisation points more realistically than assuming solely AM dependence.

Spectral irradiance is also influenced by the solar angle of incidence (AoI). The energy distribution profile over different AoI is shown in Figure 93 and it's largely influenced by the cosine effect, then reflection, then spectrum probably last. It is been found that major energy contribution takes place at near 35° AoI in Loughborough.

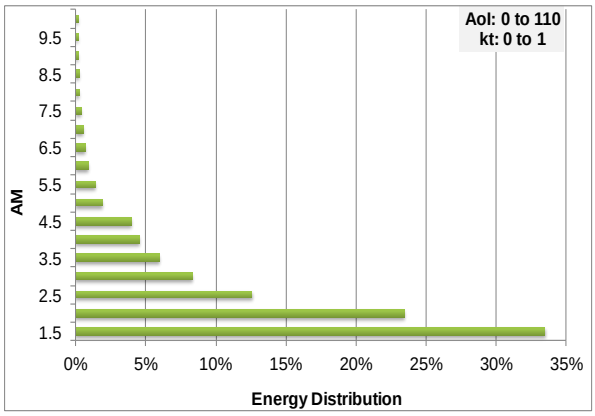

Figure 92: Incoming in-plane irradiation distribution at different AM.

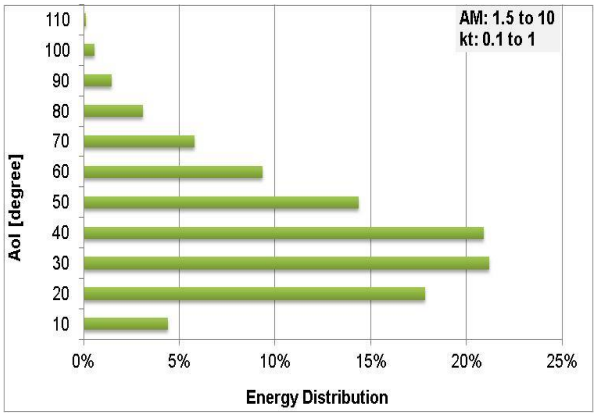

Figure 93: Incoming in-plane irradiation distribution at different AoI.

Analysing all the above parameters, finally, spectral irradiance is defined as a function of AM, AoI, clearness index (k_t). To classify the spectral irradiance, G_{POA} (incoming energy from sun) is binned as a function of AM, k_t and AoI with their bin width of 0.5, 0.1 and 10° respectively and the energy distributions of each bin is shown in Figure 94.

It is noted that at AoI upto 20°, the major contribution of energy from sun comes at lower AM spectrum (up to AM 2.5) in all sky conditions (k_t: 0.2-1). Previously, Figure 93 shows that major energy comes at AoI between 30° – 40° in the UK climate, which match the results shown below where the significant quantity of energy comes at clear sky condition (k_t: 0.7 – 0.9) at higher irradiance level.

An energy contribution at AoI above 50° mostly occurs in combination of partial cloud conditions and overcast condition at AM spectrum of 1.5 to 4.

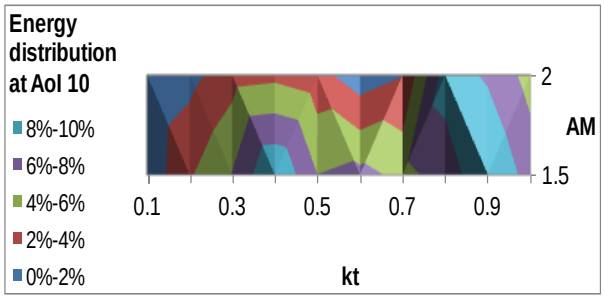

Figure 94-a: Incoming energy distribution as a function of different AM and Kt and AoI at 10°

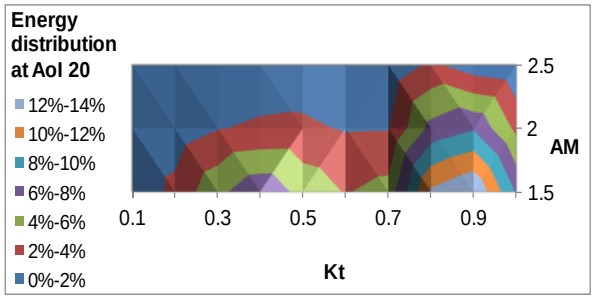

Figure 94-b: Incoming energy distribution as a function of different AM and Kt and AoI at 20°

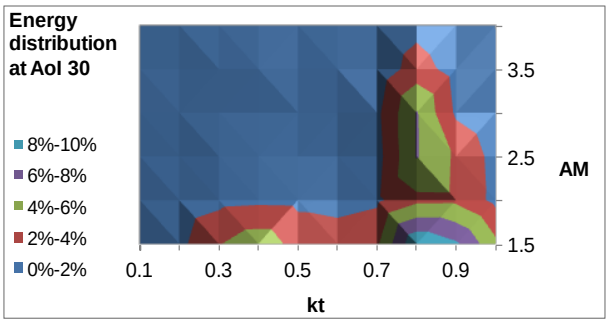

Figure 94-c: Incoming energy distribution as a function of different AM and Kt and AoI at 30°

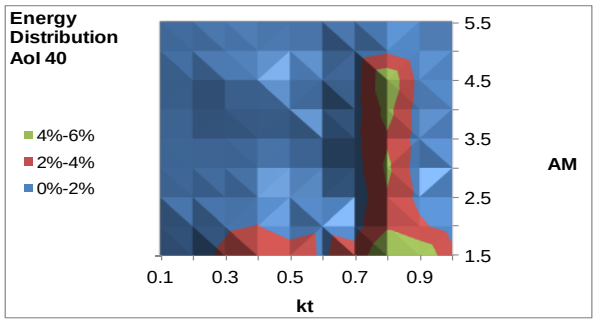

Figure 94-d: Incoming energy distribution as a function of different AM and Kt and AoI at 40°

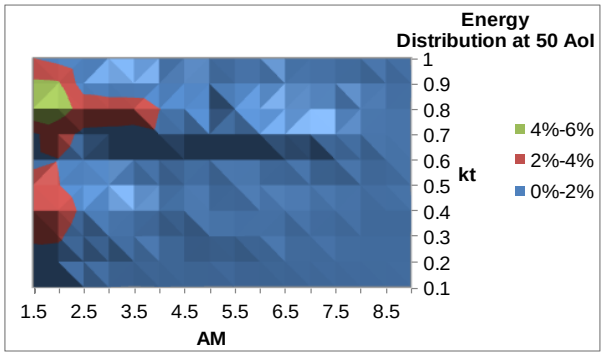

Figure 94-e: Incoming energy distribution as a function of different AM and Kt and AoI at 50°

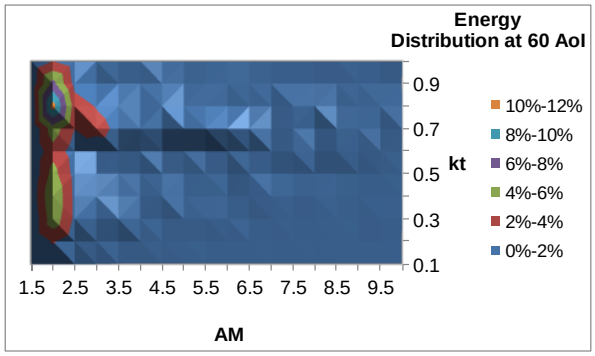

Figure 94-f: Incoming energy distribution as a function of different AM and Kt and AoI at 60°

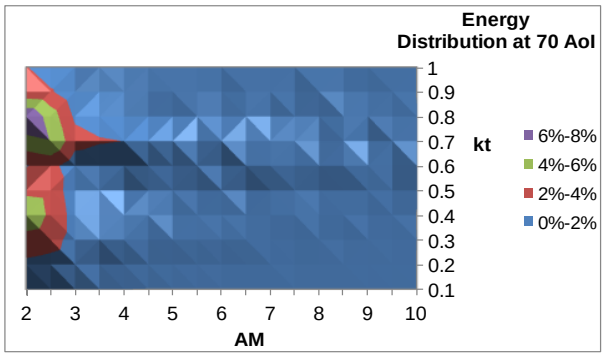

Figure 94-g: Incoming energy distribution as a function of different AM and Kt and AoI at 70°

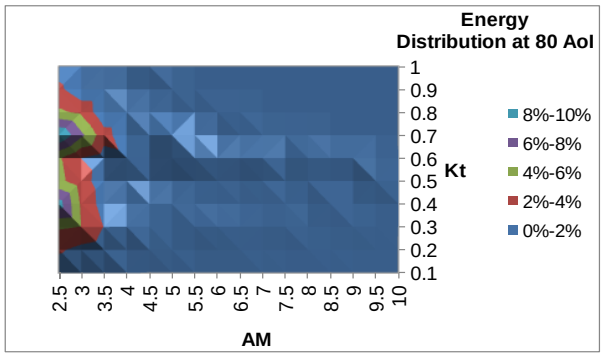

Figure 94-h: Incoming energy distribution as a function of different AM and Kt and AoI at 80°

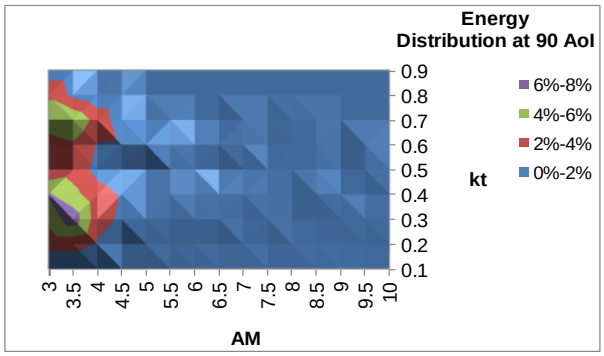

Figure 94-i: Incoming energy distribution as a function of different AM and Kt and AoI at 90°

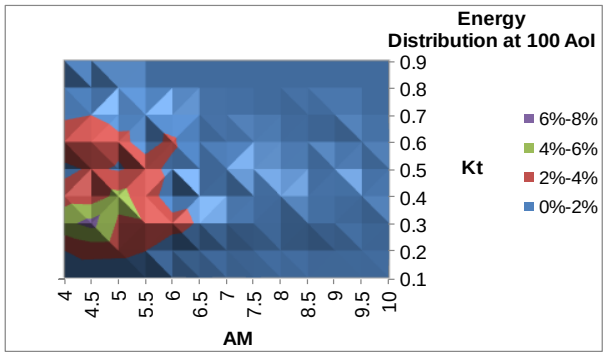

Figure 94-j: Incoming energy distribution as a function of different AM and Kt and AoI at 100°

Figure 94: Incoming energy distribution as a function of different AM and Kt and AoI from 0° to 100°.

So far, the above meteorological data has been analysed to identify the range of operating conditions of each climatic parameter in the UK climate. This indicates the operating range of relevant environmental conditions for a PV system in outdoor operation at this location. The following section presents the correlation of the above environmental parameters in relation to PV performance for use in a generalised way.

5.2.2.2 Correlations of Irradiance-Temperature-Spectral Irradiance (G-T-E) in Relation to PV Performance

The aim of this section is to identify the measurement setup required for PV module characterisation indoors for the proposed energy yield prediction method of this thesis. The idea is to minimise the complexity of and time taken for the module characterisation, while maintaining the lowest possible uncertainties.

Three different mini modules of different technologies (c-Si, a-Si and CIGS) were installed on the CREST outdoor testing facilities under the scope of this thesis, as shown in Figure 95. The electrical parameters of each module are measured and logged alongside the above environmental parameters.

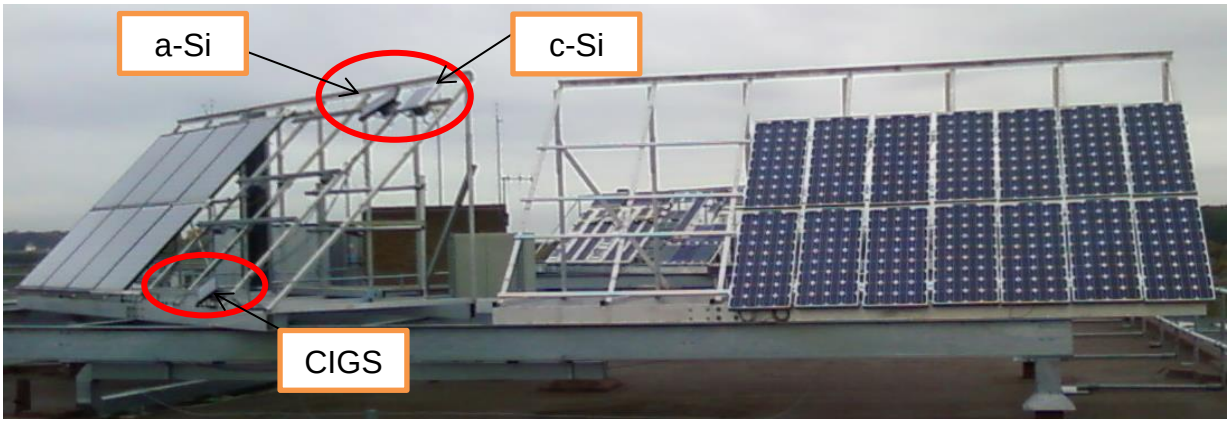

Figure 95: Three mini modules under test at CREST Outdoor Test System.

To establish the correlations between the PV module performance and the irradiance, temperature and spectral irradiance, a five way binning method is applied. The dataset of this analysis is from January to December 2009.

Maximum power (P_{max}) generation of each PV module are binned as a function of irradiance at PV module plane (G_{poa}), module temperature (T_{mod}), air mass (AM), clearness index (k_t) and angle of incidence (AoI). Integration of the P_{max} values of each bin gives the annual energy yield contribution from different combinations of all the above environmental parameters. The selected bin widths are 50 W/m^2, 5°C, 0.5 AM, 0.25 and 10° respectively for G_{poa}, T_{mod}, AM, k_t and AoI.

Selective surface plot of the annual energy contributions from the c-Si module are shown in Figure 96 at a combination of the above bin classes up to AM 10 and kt up to 1. Due to the limitation of the measurement system (LED simulation), AoI variation is not taken into account and the outdoor data is considered with no restriction (the full range of operation within 0 – 120 degree is used).

From this analysis, a four dimensional power matrix is formed as a function of G_{poa}, T_{mod}, AM, k_t (Energy $_{\text{Sum of Pmax}}$ = f {G_{poa}, T_{mod}, AM, k_t}).

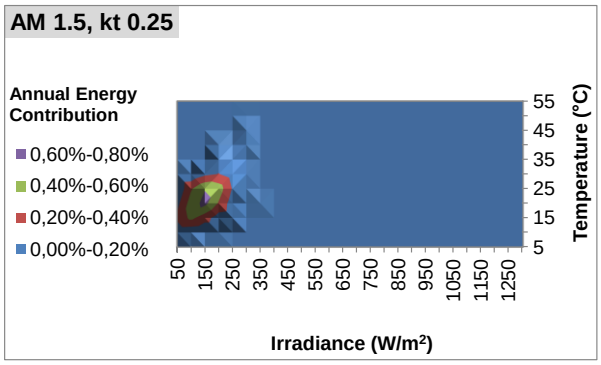

Figure 96-a: Annual energy distribution as a function of irradiance, temperature, AM1.5, k_t 0.25 at the AoI range 0 - 120°

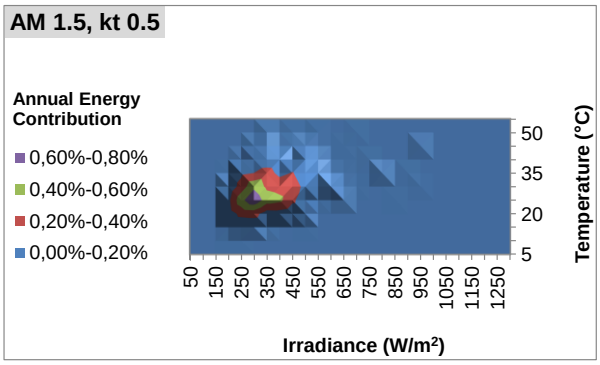

Figure 96-b: Annual energy distribution as a function of irradiance, temperature, AM1.5, k_t 0.5 at the AoI range 0 - 120°

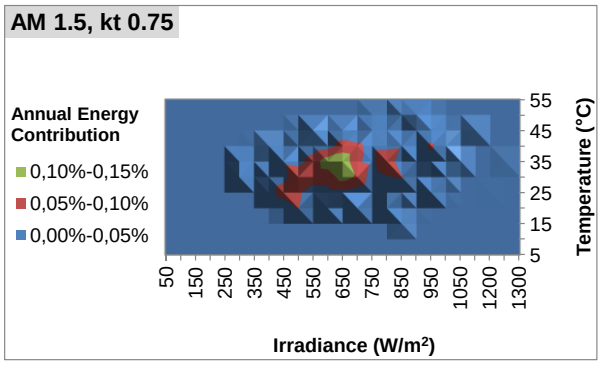

Figure 96-c: Annual energy distribution as a function of irradiance, temperature, AM1.5, k_t 0.75 at the AoI range 0 - 120°

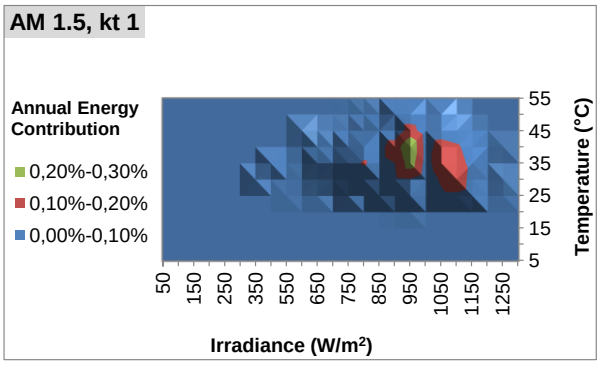

Figure 96-d: Annual energy distribution as a function of irradiance, temperature, AM1.5, k_t 1 at the AoI range 0 - 120°

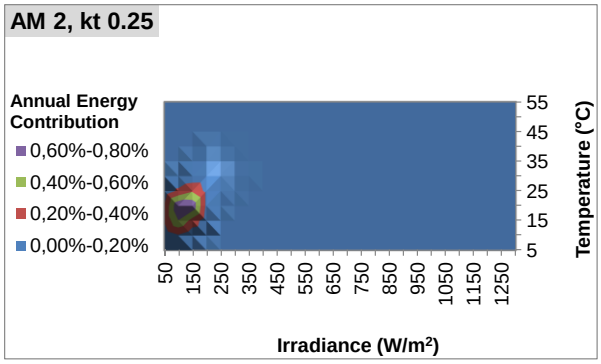

Figure 96-e: Annual energy distribution as a function of irradiance, temperature, AM2, k_t 0.25 at the AoI range 0 - 120°

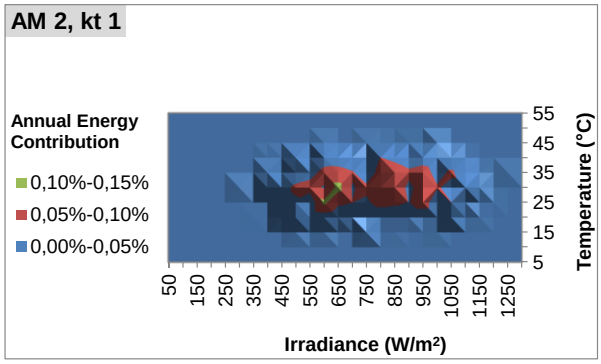

Figure 96-f: Annual energy distribution as a function of irradiance, temperature, AM2, k_t 1 at the AoI range 0 - 120°

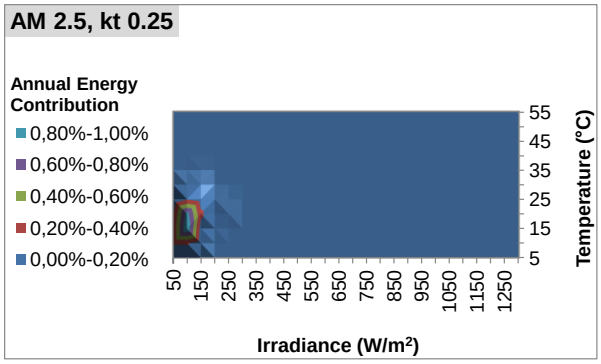

Figure 96-g: Annual energy distribution as a function of irradiance, temperature, AM2.5, k_t 0.25 at the AoI range 0 - 120°

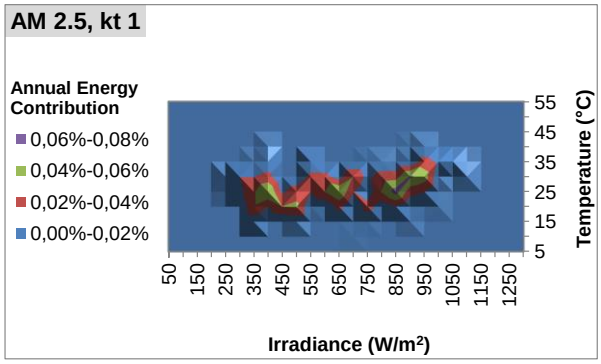

Figure 96-h: Annual energy distribution as a function of irradiance, temperature, AM2.5, k_t 1 at the AoI range 0 - 120°

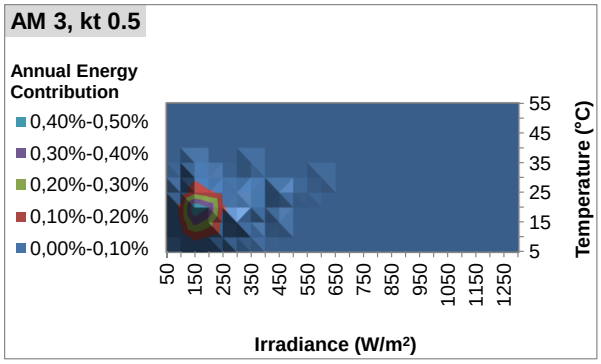

Figure 96-i: Annual energy distribution as a function of irradiance, temperature, AM3, k_t 0.5 at the AoI range 0 - 120°

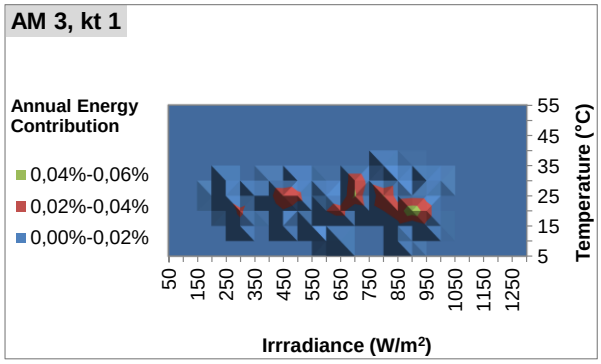

Figure 96-j: Annual energy distribution as a function of irradiance, temperature, AM3, k_t 1 at the AoI range 0 - 120°

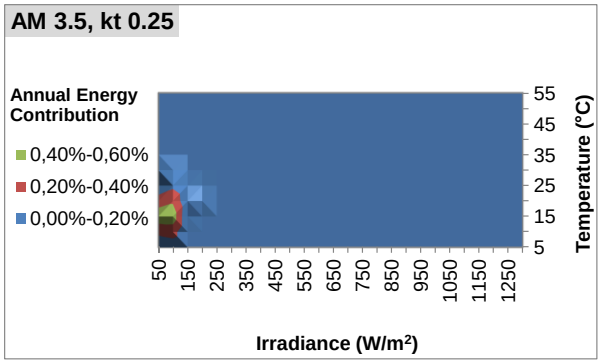

Figure 96-k: Annual energy distribution as a function of irradiance, temperature, AM3.5, k_t 0.25 at the AoI range 0 - 120°

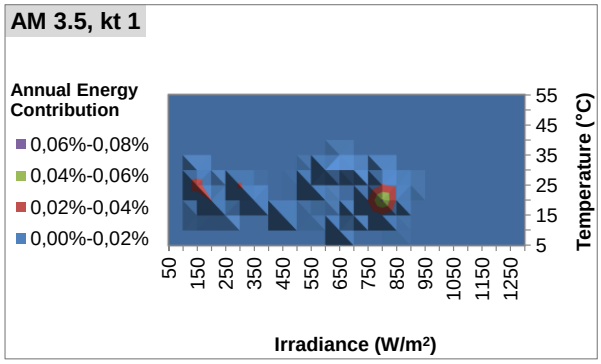

Figure 96-l: Annual energy distribution as a function of irradiance, temperature, AM3.5, k_t 1 at the AoI range 0 - 120°

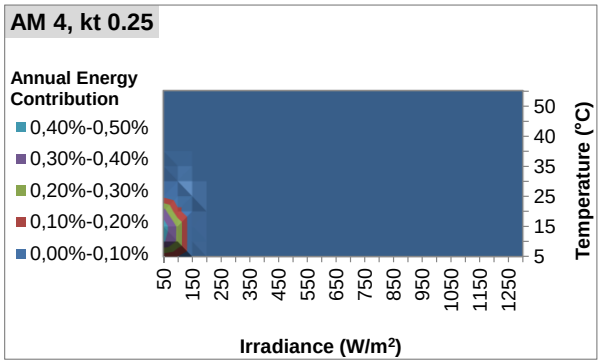

Figure 96-m: Annual energy distribution as a function of irradiance, temperature, AM4, k_t 0.25 at the AoI range 0 - 120°

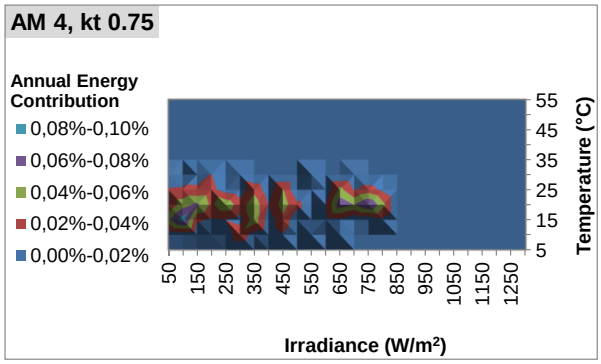

Figure 96-n: Annual energy distribution as a function of irradiance, temperature, AM4, k_t 0.75 at the AoI range 0 - 120°

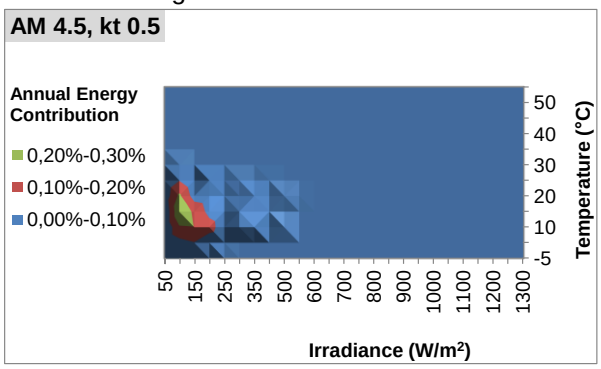

Figure 96-o: Annual energy distribution as a function of irradiance, temperature, AM4.5, k_t 0.5 at the AoI range 0 - 120°

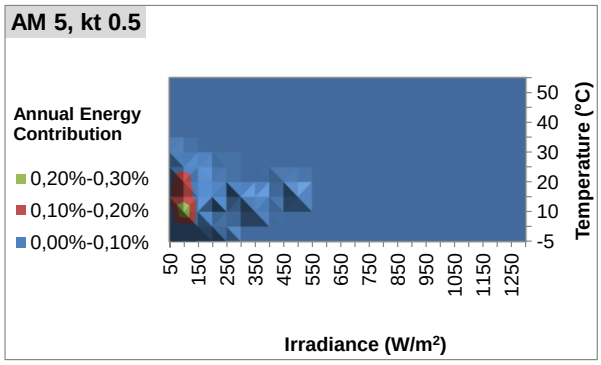

Figure 96-p: Annual energy distribution as a function of irradiance, temperature, AM5, k_t 0.5 at the AoI range 0 - 120°

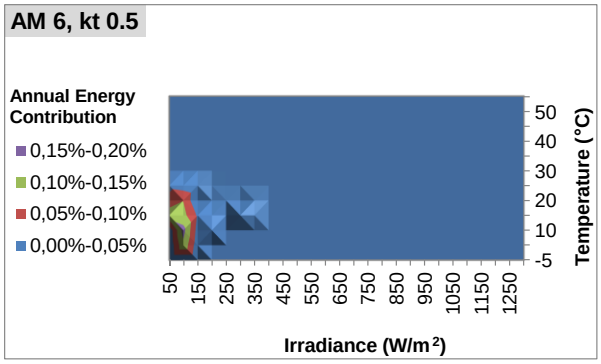

Figure 96-q: Annual energy distribution as a function of irradiance, temperature, AM6, k_t 0.5 at the AoI range 0 - 120°

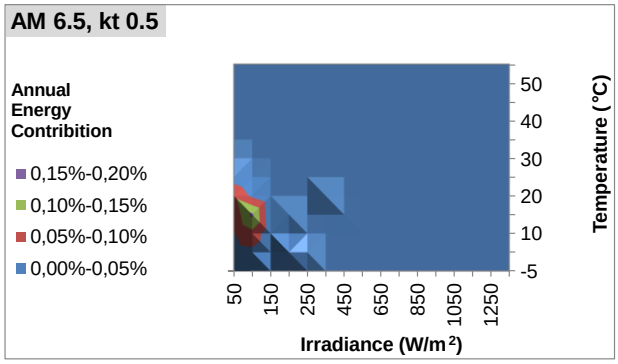

Figure 96-r: Annual energy distribution as a function of irradiance, temperature, AM6.5, k_t 0.5 at the AoI range 0 - 120°

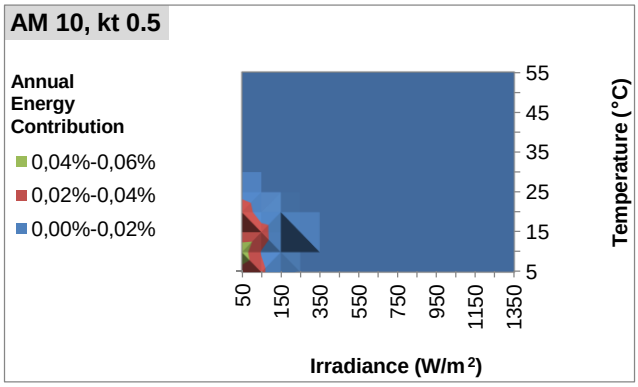

Figure 96: Annual energy distribution of c-Si module as a function of irradiance, temperature, AM, k_t at the AoI range 0 - 120°.

Measurement Set Up for Indoor Module Characterisation

Based on the correlation of irradiance, temperature, air mass and clearness index with maximum power generation, measurement settings of a c-Si module in the UK climate is illustrated in Table 14. An extended set of measurement target points across all conditions are listed below. It should also be noted that this measurement settings might vary in different location with different climatic profile. In that case, similar annual energy distribution of a module as a function of irradiance, temperature, AM, k_t needed to be carryied out for more accurate module charactirisation measurement settings.

To identify the suitable modelling method for power calculation - with the module characterised data using above measurement settings and local weather data – different current-voltage translation approach are analysed in the next section.

Suitable modelling method help optimisation of the measurement points by minimising the required measurement settings, hence minimises the time and cost for manufacturers to testing a module.

Table 14: Extended measurement setting for module characterisation.

AM	K_t	AoI	Irradiance (W/m^2)	Module Temperature (°C)
1.5	0.25	0-120	50, 100	15, 25, 40
	0.5		200, 300, 400	15, 25, 40
	0.75		550, 700	20, 40
	1		900, 1150	25, 35, 50
2	0.25	0-120	50, 100	15, 25
	0.5		200, 300	15, 35
	0.75		450, 650	20, 40
	1		800,1000	25, 40
2.5	0.25	0-120	50, 100	15, 25
	0.5		200, 300	15, 25
	0.75		400, 600	15, 35
	1		850-1000	15, 35
3	0.25	0-120	50, 100	5, 15,30
	0.5		200, 300	5, 15, 30
	0.75		400	15, 35
	1		650, 1000	15, 30
3.5	0.25	0-120	50, 100	5, 15, 30

	0.5		200	5, 15, 30
	0.75		300, 400	15, 30
	1		600, 800, 900	15, 30
4	0.25	0-120	50, 100	5, 15, 25
	0.5		200	5, 15, 30
	0.75		350, 450, 650, 800	15, 25
4.5	0.5	0-120	50, 100, 200	0, 15, 25
	0.75		450, 600, 750	15, 25
5	0.5	0-120	50, 100, 200	0, 15, 30
	0.75		350, 450,600, 700	15, 25
5.5	0.5	0-120	50, 100	0, 15, 30
	0.75		200, 300,450, 650	15, 25
6	0.5	0-120	50, 100, 200	0, 15, 25
	0.75		300,450,600	0, 15, 25
6.5	0.5	0-120	50, 100, 200	0, 15, 30
	0.75		300, 400, 550	5, 20
7	0.5	0-120	50, 100	5, 15, 25
	0.75		200, 300, 400, 500	5, 15, 25
7.5	0.5	0-120	50,100, 150	0, 15, 25
8	0.5	0-120	50,100, 150	0, 15, 25
8.5	0.5	0-120	50,100, 150	5, 15, 30

9	0.5	0-120	50, 100, 250	0, 15, 25
9.5	0.5	0-120	50, 100, 250	0, 15, 25
10	0.5	0-120	50, 100, 250	5, 15, 25

5.2.2.3 Optimisation of Required Number of Irradiance and Temperature Measurement Points: I-V Translation Methodologies

So far in this thesis, a linear fitting of irradiance and temperature is applied. In order to optimise the required number of measurement points for module characterisation for fast energy yield calculation and for better understanding the characteristics of PV module performance over the range of irradiance and temperature, different current-voltage (I-V) correction methods are analysed in this section.

5.2.2.3.1 I-V Translation Methodologies:

There are number of current –voltage (I-V) translation methods available [96-100] to estimate the I-V points and ultimately P_{max} at a target irradiance and temperature. These translation models are illustrated elsewhere: Marion et al [97], explains an indoor characterisation method to determine a PV module's temperature and irradiance correction factors in order to translate a reference I-V curve to outdoor conditions of PV module temperature and irradiance for energy yield calculation. This is based on the translation equations of ASTM E 1036–96 96]. Anderson et al [98] demonstrated an I-V translation approached using dimensionless temperature coefficients for current and voltage, which is based on Procedure 2 of the IEC 60891 standard [100].

Procedure 1 is based on the measured current-voltage characteristic which can be corrected to Standard Test Conditions or other selected temperature and irradiance values. Procedure 2 is based on the simplified one-diode model. Both procedure 1 and 2 require I-V correction parameter extraction from two I-V curve measurements

at different temperature and irradiance conditions. Those extracted parameters are temperature coefficient of I_{sc} and V_{oc}, internal series resistance (Rs') temperature coefficient of internal series resistance (k').

Procedure 3 of IEC 60891 [100] standard is based on the procedure developed by Hishikawa et al [101]. This procedure is based on linear interpolation with respect to two measured I-V characteristics to estimate the target I-V characteristics at a target irradiance and temperature.

Analysis of the different I-V translation methods also helped to identify the suitable modelling approach for the proposed energy yield estimation. To study the characteristics of module performance at a range of irradiance and temperature, a c-Si PV module has been tested indoors under variable irradiance and temperature using the LED-based solar simulator. The deviation of actual measured P_{max} and estimated P_{max} of different approaches of I-V translation is then compared using Procedures 2 and 3. These modelling approaches indicate the expected level of accuracy of each translation method and ultimately an indication of the scale of modelling errors in the energy yield prediction of PV modules.

I-V Translations: The measured current-voltage characteristics are translated according to procedure 2 of IEC 60891 to the target irradiance and temperature conditions using equation (39) and (40**)**.

$$I_T = I_1 * (1 + \alpha_{rel} * (T_T - T_1)) * \frac{G_T}{G_1} \tag{39}$$

$$V_T = V_1 + V_{oc1} * \left(\beta_{rel} * (T_T - T_1) + a * \ln\left({G_T}/{G_1} \right) \right) - k * I_T * (T_T - T_1) \tag{40}$$

Where (I_1, V_1) are coordinates and V_{oc1} is the open circuit voltage at measured irradiance G_1 and temperature T_1. (I_T, V_T) are targeted coordinates at target irradiance G_T and target temperature T_T. α and β are the relative current and voltage temperature coefficients at G_1. 'a' is the irradiance correction factor for open circuit

voltage with a typical value of 0.06 [100]. “k” is the curve correction factor of the test sample. Estimation of curve correction factor is outlined in Figure 97.

Temperature coefficients for current and voltage are determined from measured I-V curves at AM1.5 spectrum and irradiance at 765 W/m^2 (the maximum irradiance the LED solar simulator can measure at AM1.5 spectrum) and temperatures in the range of 15-55 °C. To calculate the curve corrector factor (k), the I-V characteristics at lowest temperature and at constant irradiance are used. All other I-V curves at different temperatures within the range of interest and at higher irradiances are translated to the I-V curve at temperature of 15°C using equation (39) and (40**)** also temperature coefficients as described in Figure 97.

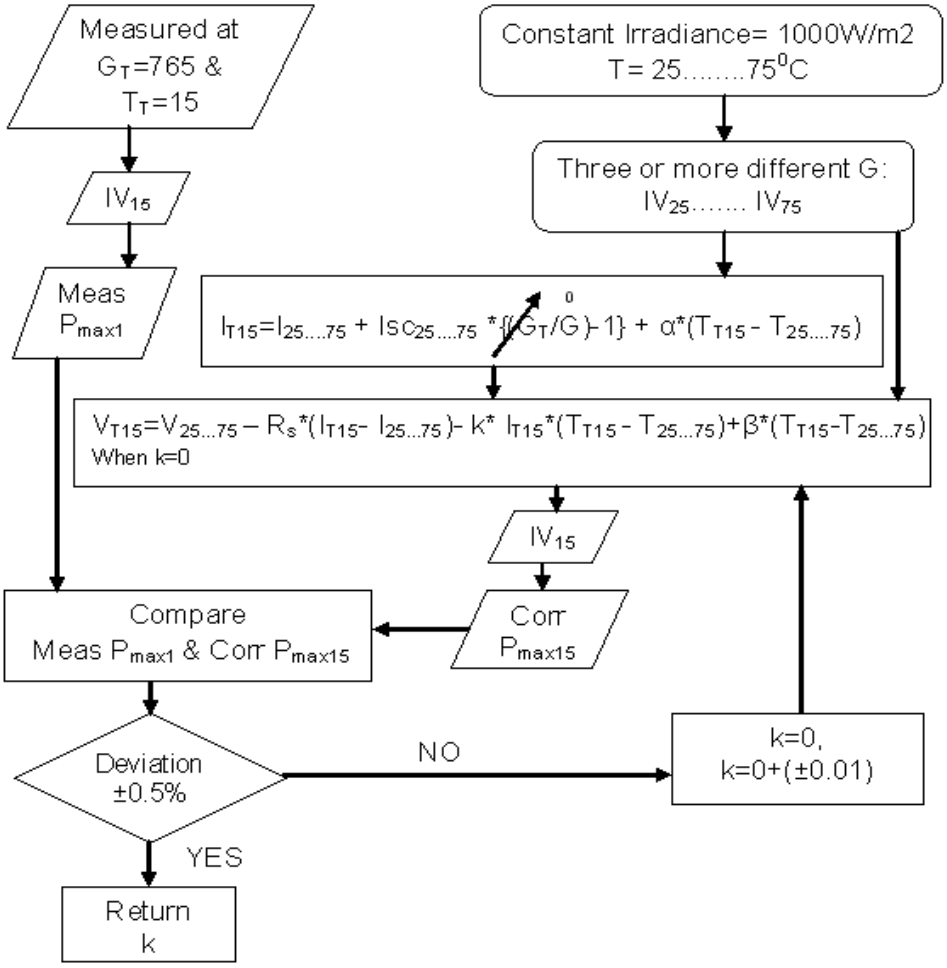

Figure 97: Flow diagram to estimate curve correction factor (k).

Maximum Power Interpolation: Linear interpolation is applied using equation (41) and (42) to estimate the maximum power (P_{max}) at the intermediate points of the power matrix of the c-Si PV module as a function of irradiance and temperature at AM1.5 spectrum.

$$P_T = P_1 + a * (P_2 - P_1) \tag{41}$$

$$a_G = \frac{(G_T - G_1)}{(G_2 - G_1)} \; OR \; a_T = \frac{(T_T - T_1)}{(T_2 - T_1)} \tag{42}$$

Where P_T is the maximum power of the I-V curve at target irradiance and temperature (G_T,T_T). P_1 and P_2 are the measured maximum power of the I-V curves at irradiance and temperature at (G_1,T_1) and (G_2,T_2) respectively. a_G and a_T are the interpolation coefficients for power interpolation against irradiance and temperature respectively.

P_{max} is corrected to its intermediate values from the four measured various irradiances and temperatures. A surface of power matrix as a function of irradiance and temperature is shown in Figure 98, where the blue squares represent the measured maximum power points of a c-Si module. All the other points of maximum power at different irradiance and temperature points (white squares) are estimated by bilinear interpolation method. Deviation of estimated P_{max} by linear interpolation against the measured P_{max} are analysed and shown in Figure 100 and Figure 101.

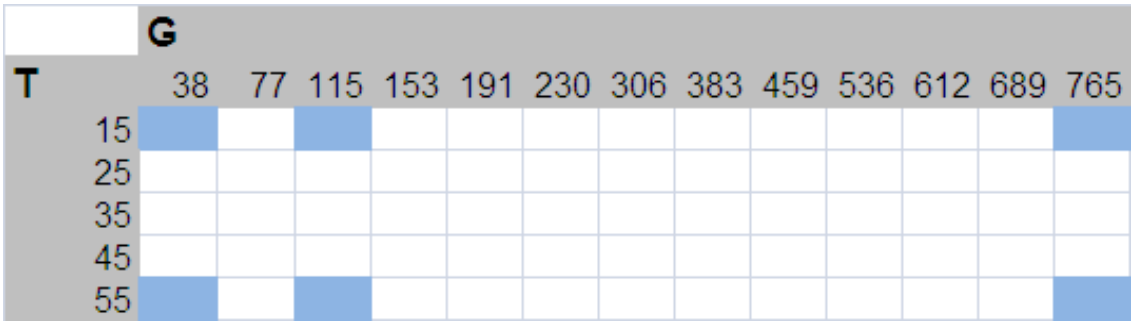

Figure 98: Different sets of data points in the power matrix as a function of irradiance and temperature.

I-V Correction Results: The maximum measured irradiance of the LED simulator, developed by other researchers at CREST, is 765 W/m^2. For Procedure 2 of IEC 60891 (equation (39) and (40)), the reference measured irradiance and temperature for I-V characteristics are 765 W/m^2 and 25°C respectively. All the other I-V curves are translated to other irradiance and temperature points of interest as shown in Figure 99. The estimated and measured maximum power points of each curve are then compared. Deviations between the estimated P_{max} and the actual measured P_{max} are shown in Figure 99.

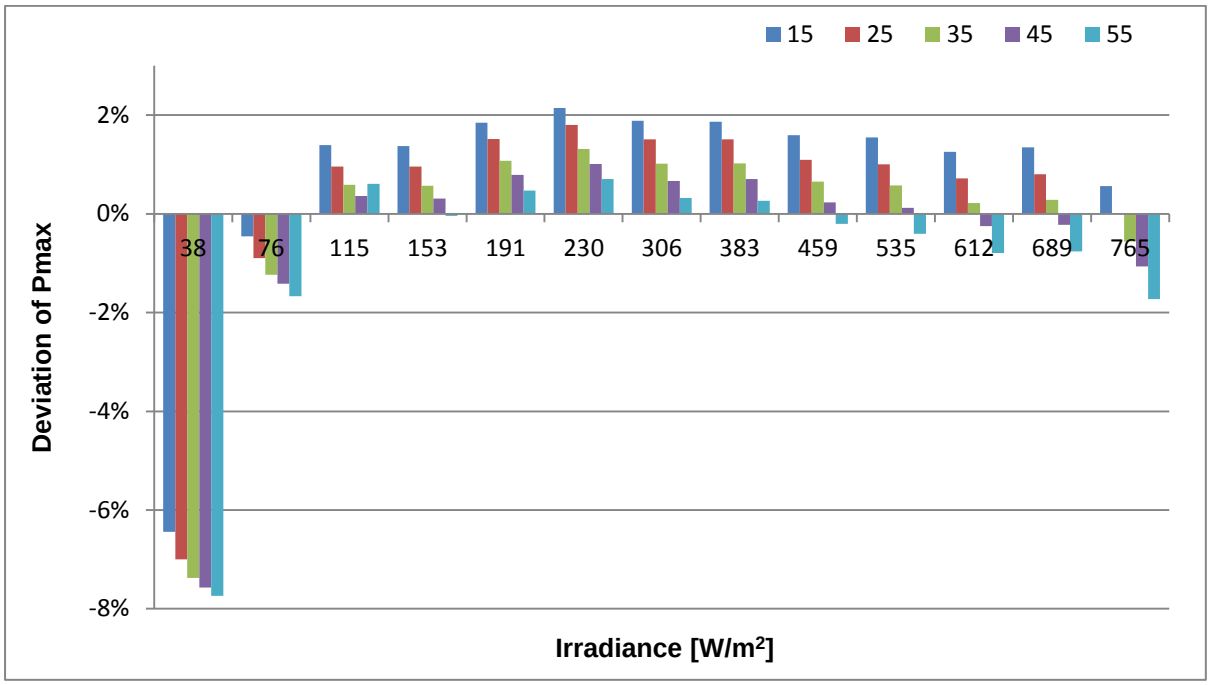

Figure 99: Deviation of measured and translated P_{max} based on procedure 2 of IEC 60891 standard.

It is clearly noticeable that the agreement between measured and estimated P_{max} by I-V translation procedure 2 of IEC 60891 standard is within ±2% at higher irradiance level with over ±6% at low light condition. Hence using this I-V translation method for targeted power calculation in lower irradiance zones can lead to a higher error in the prediction e.g. in the UK climatic zone.

For better accuracy at lower intensity levels Hishikawa et al [99], demonstrated a linear interpolation/extrapolation between the four measured I-V curves within the range of irradiance and temperature conditions. A similar approach based on equation (41) and (42) in the power matrix is carried out in this study. With this

method the agreement between the estimated and measured P_{max} is up to ±6%, as shown in Figure 100. The reason for this high deviation is the non-linearity effect of power at low intensity level of irradiance against the linear interpolation modelling approach between four extreme irradiance and temperature points.

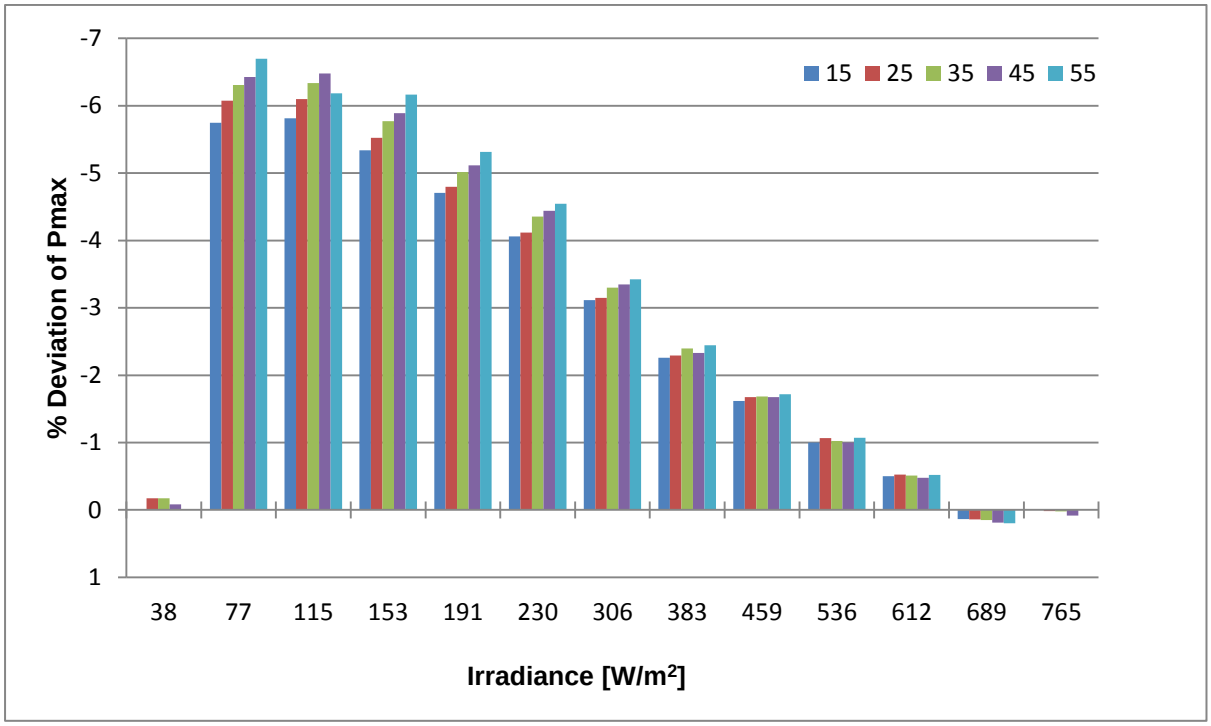

Figure 100: Deviation of measured and interpolated P_{max} with four extreme points of irradiance and temperature in the power matrix.

To minimise the modelling uncertainty in order to achieve an accurate energy yield prediction method, the number of measurement points at other irradiances and temperatures is increased. The bilinear interpolation method is executed again by selecting different sets of data points (Figure 98) within the operational range of irradiance and temperature.

Selecting two sets of data points (blue squares blocks in Figure 98), the deviation of P_{max} is minimised to within 2.5% as shown in Figure 101.

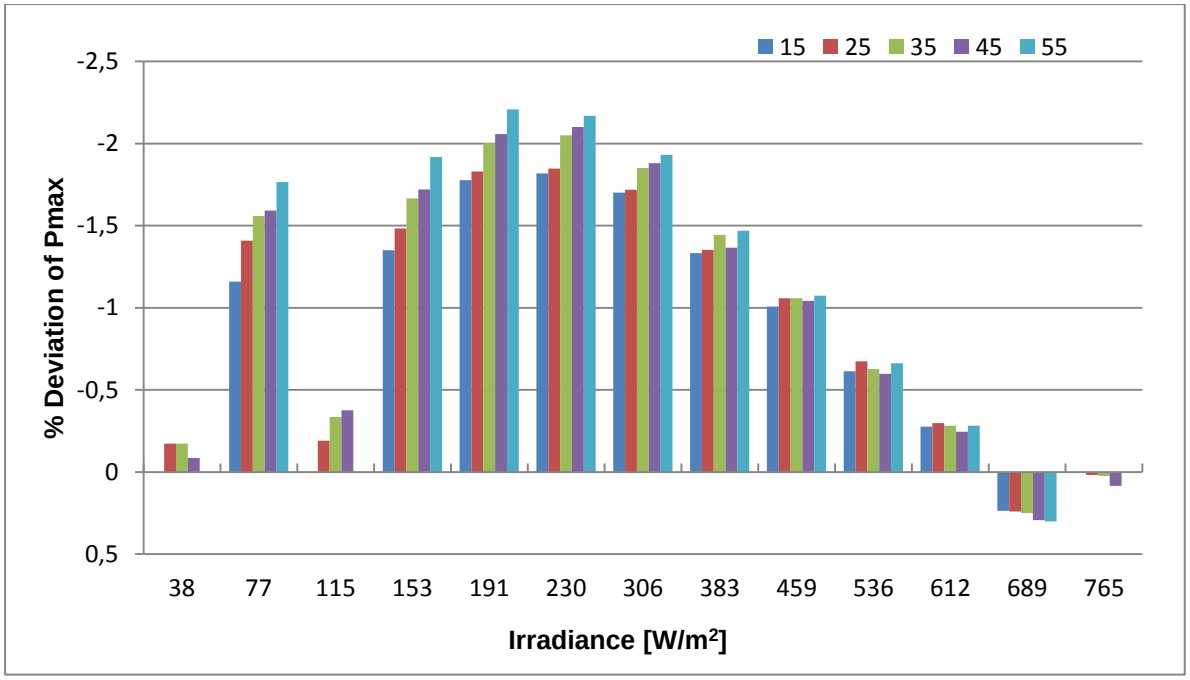

Figure 101: Deviation of measured and interpolated P_{max} with two sets of four points of irradiance and temperature in the power matrix.

This deviation implies that the power output of c-Si is non-linear at lower irradiance level but it is linear against temperature. Measurement of other module technologies and their I-V modelling show similar characteristics to the c-Si module for the number of irradiance and temperature points studied. The number of irradiance and temperature measurement points are optimised by realising the linear characteristics of PV modules at the range of irradiance and temperature, shown in Table 15.

Table 15: Optimised measurement set up for module characterisation.

AM	K_t	Irradiance (W/m^2)	Module Temperature (°C)
1.5	0.25	50, 100	15, 25, 50
	0.5	200, 400	15, 25, 50
	0.75	600	15, 25, 50
	1	800, 1100	15, 25, 50

2	0.25	50, 100	15, 25
	0.5	200, 400	15, 35
	0.75	600	20, 40
	1	800, 1100	25, 40
2.5	0.25	50, 100	15, 25
	0.5	200, 400	15, 25
	0.75	600	15, 35
	1	800, 1100	15, 35
3	0.25	50, 100	5, 15,30
	0.5	200, 300	5, 15, 30
	0.75	400	15, 35
	1	650, 1000	15, 30
3.5	0.25	50, 100	5, 15, 30
	0.5	200	5, 15, 30
	0.75	300, 400	15, 30
	1	600, 800, 1000	15, 30
4	0.25	50, 100	5, 15, 25
	0.5	200	5, 15, 30
	0.75	400, 600, 800	15, 25
4.5	0.5	50, 100, 200	0, 15, 25
	0.75	400, 600, 800	15, 25
5.5	0.5	50, 100	0, 15, 30
	0.75	200, 300,450, 650	15, 25
7	0.5	50, 100	5, 15, 25

	0.75	200, 300, 400, 500	5, 15, 25
7.5	0.5	50,100, 150	0, 15, 25
10	0.5	50, 100, 250	5, 15, 25

5.3 Evaluation of The FEnYCs Method

In this section the Fast Energy Yield Calculations (FEnYCs) method is evaluated. The procedure of the calculation methodology is illustrated comprising the measurement and modelling elements. Meteorological data are taken from the CREST outdoor test facility. The energy output of PV devices of three different technologies are modelled with the FEnYCs method and compared with measured values. The required module characterisation data based on the measurement settings described in chapter 5 are extracted from the annual outdoor measurement dataset.

A tri-linear interpolation method is utilised to calculate the maximum power of each device at target irradiance, temperature and AM spectrum, as dictated by the time series of weather data. Validation of the FEnYCs method is then presented for each device over a range of environmental conditions available throughout a year.

5.3.1 **FEnYCs Procedure**

The procedure of the FEnYCs method comprises a combination of different measurements and modelling approaches.

1. Measurement
    i. The measurement of the environmental data
        a. Global horizontal irradiance, clearness index (kt), ambient temperature.
        b. Module power matrix as a function of G_{mod}, T_{mod} and AM spectrum.
2. Modelling
    ii. Global horizontal irradiance to global horizontal beam and diffuse and then to plane of array irradiance (G_{mod})

iii. Ambient temperature to module temperature considering irradiance factors

iv. FEnYCs energy yield calculation: tri-linear interpolation between power matrix points against target G_{mod}, T_{mod} and AM spectrum.

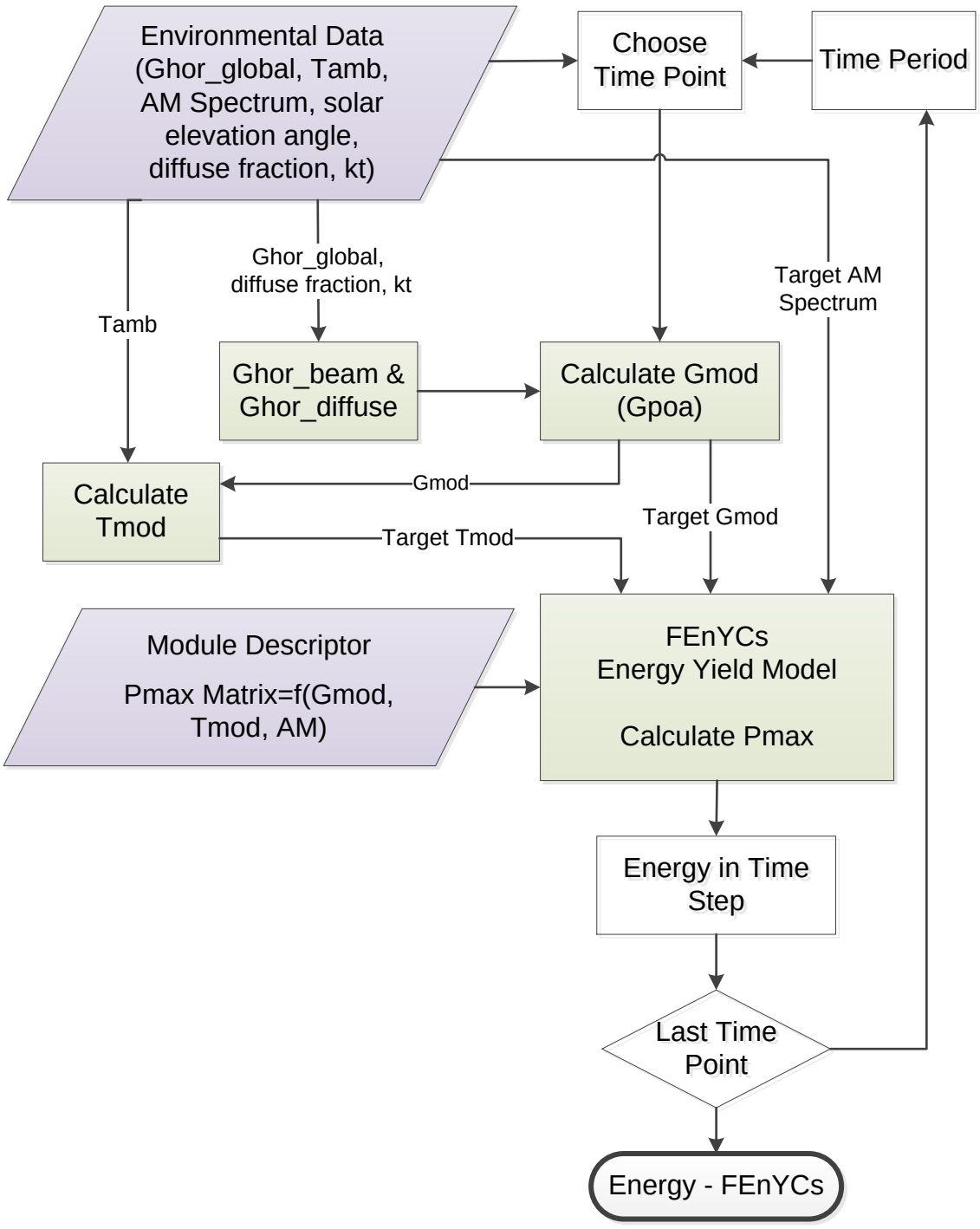

Figure 102: Procedure of the Fast Energy Yield Calculation (FEnYCs) Method

Blue colour blocks represent the measurement elements of the procedure and grey blocks represent the modelling elements. The above procedure is applied to calculate the annual energy yield of three different device technologies.

5.3.1.1 Outdoor Measurement

The measured environmental data are taken from the CREST outdoor monitoring system (COMS) at Loughborough. The duration of the measurement period is from October 2009 to November 2010.

The same three PV modules are investigated as shown in Table 4: small crystalline silicon (c-Si), amorphous silicon (a-Si) and copper indium gallium selenide (CIGS) modules. I-V curves of these modules are measured in the COMS system every 5 minutes and this provides their annual energy yields. The parameters extracted from the measured data are irradiance in module plane, module temperature and maximum power of each module from October 2009 to November 2010. In addition, solar geometry calculations provide corresponding AM values for each timestamp.

5.3.1.2 Irradiance modelling Approach

Irradiance modelling in the FEnYCs method follows the two steps translation modelling as presented in Chapter 4, where Reindl II method shows the best results between measured and estimated horizontal beam and diffuse irradiance values and the Klucher model shows the best agreement with measured values for horizontal to plane of array irradiance as presented in chapter 4 (section 4.4.1) of this thesis,

5.3.1.3 Temperature modelling Approach

Module temperature (T_{mod}) is estimated as a function of ambient temperature (T_{amb}) and irradiance (G_{Poa}) as shown in (37) (chapter 4). Irradiance factor of module temperature is calculated considering the type of module, module mounting system, thermal effect due to wind speed.

5.3.1.4 P_{max} modelling

Since the target G_{mod}, T_{mod} and AM points from the environment data time series will not generally coincide with the modules characterisation matrix points, a tri-linear interpolation method is applied within a cube of measured P_{max} at the vertices of the cube. The cube is formed, as shown in Figure 103 of a three dimensional matrix of measured P_{max} from the module characterisation over a wide range of G_{mod}, T_{mod} and AM (as the spectral representative). This multi-dimensional matrix is used as the module descriptor for all three different modules (each with its own characterisation dataset). Maximum power at target irradiance (G_{Poa}), module temperature (T_{mod}) and AM of the environmental data at all timestamps are estimated by a tri-linear interpolation from the input multi-dimensional P_{max} matrix plot.

The vertices of the cube of maximum The matrix of the maximum power of the module as a function of irradiance, temperature and AM is loaded. Then the length of the arrays of irradiance, temperature, AM and maximum power of each module are set. The tool then searches for the relevant bounding values of irradiance, temperature and AM and looks up the respective P_{max} values at the combination of these environmental parameters. A cube is then defined of its eight P_{max} values (Figure 103) of each device at eight different combinations of irradiance, temperature and AM spectrum. Cube selection criteria also includes the target irradiance, target temperature and target AM spectrum and two nearby points of each of these parameters for linear interpolation.

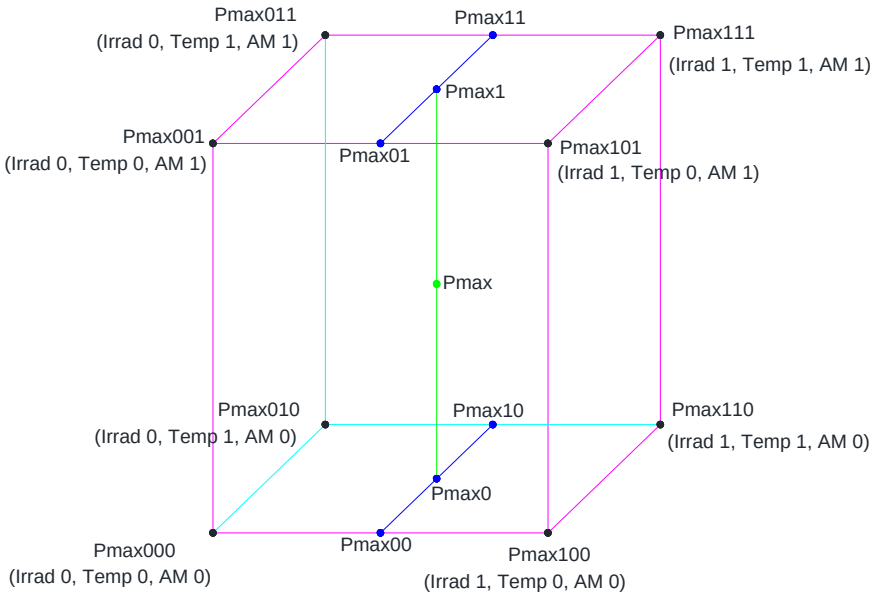

Figure 103: Tri-linear interpolation

Power coefficients of the four dimensional tri-linear interpolation method are calculated by using the following calculations:

$$c0 = P_{max}000 \quad (43)$$

$$c1 = (P_{max}100 - P_{max}000) \quad (44)$$

$$c2 = (P_{max}010 - P_{max}000) \quad (45)$$

$$c3 = (P_{max}001 - P_{max}000) \quad (46)$$

$$c4 = (P_{max}110 - P_{max}010 - P_{max}100 + P_{max}000) \quad (47)$$

$$c5 = (P_{max}011 - P_{max}001 - P_{max}010 + P_{max}000) \quad (48)$$

$$c6 = (P_{max}101 - P_{max}001 - P_{max}100 + P_{max}000) \quad (49)$$

$$c7 = (P_{max}111 - P_{max}011 - P_{max}101 - P_{max}110 + P_{max}100 + P_{max}001 + P_{max}010 - P_{max}000) \quad (50)$$

Using the selected cube of the power matrix and the above power coefficients, the power at target conditions is calculated by the following tri-linear formula. Tri-linear interpolation is derived by applying the bilinear interpolation seven times – three times each to determine the P_{max} 1 and P_{max} 0, then one more time to calculate the point P_{max}.

$$\text{Targeted } P_{max} = c0 + c1 * \Delta G_{mod} + c2 * \Delta T_{mod} + c3 * \Delta AM + c4 * \Delta G_{mod} * \Delta T_{mod} + c5 * \Delta T_{mod} * \Delta AM + c6 * \Delta G_{mod} * \Delta AM + c7 * \Delta G_{mod} * \Delta T_{mod} * \Delta AM; \quad (51)$$

Where:

ΔG_{mod}:= (Targeted G_{mod} - Irrad0) / (Irrad1 - Irrad0);

ΔT_{mod}:= (Targeted T_{mod} - Temp0) / (Temp1 - Temp0);

ΔAM:= (Targeted AM - AM0) / (AM1 - AM0);

Irrad0 and Irrad1 are the bracketing irradiances to the target irradiance. Temp0 and Temp1 are the bracketing module temperatures to the target temperature. AM0 and AM1 are the bracketing AM values of the target AM spectrum.

5.3.2 **Validation of FEnYCs Method**

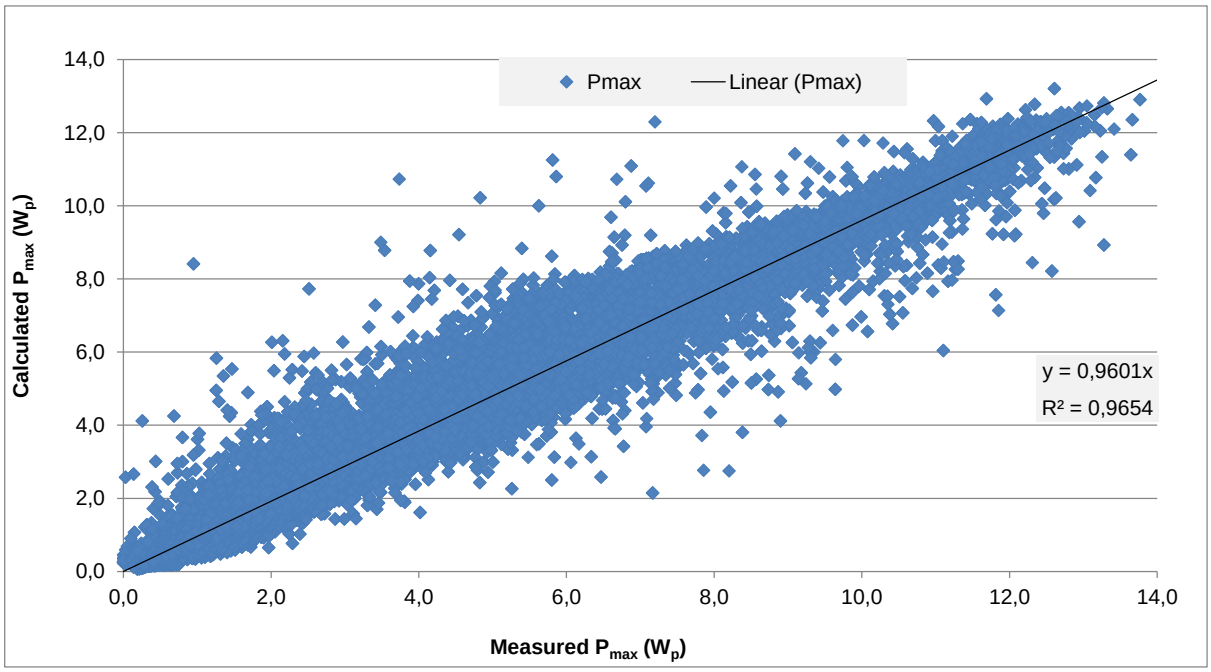

Figure 104: Validation of FEnYCs energy yield method for c-Si module in Loughborough, UK.

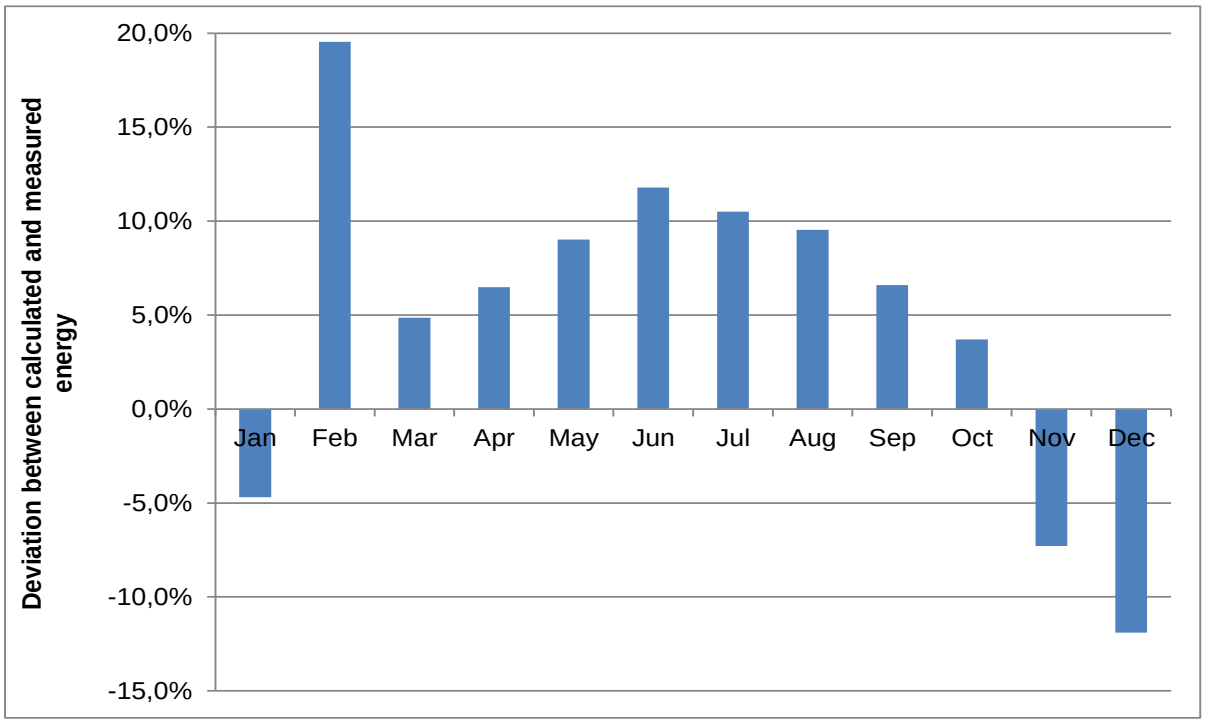

Figure 105: Deviation of monthly energy yield between calculated and measured values for c-Si module in Loughborough, UK.

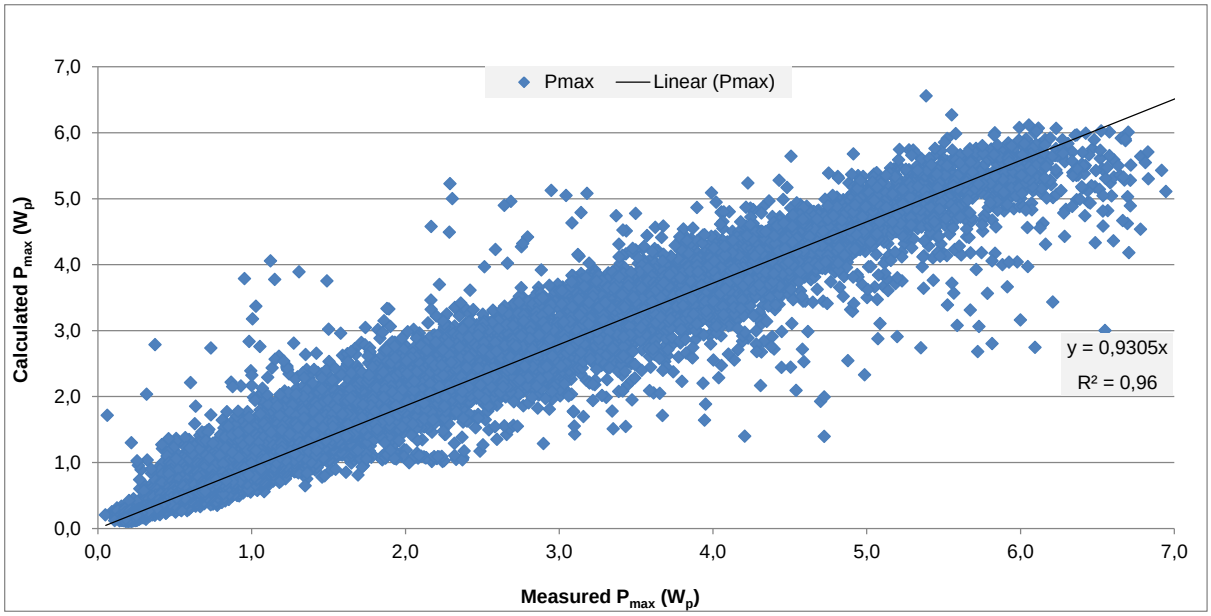

Figure 106: Validation of FEnYCs energy yield method for a-Si module in Loughborough, UK.

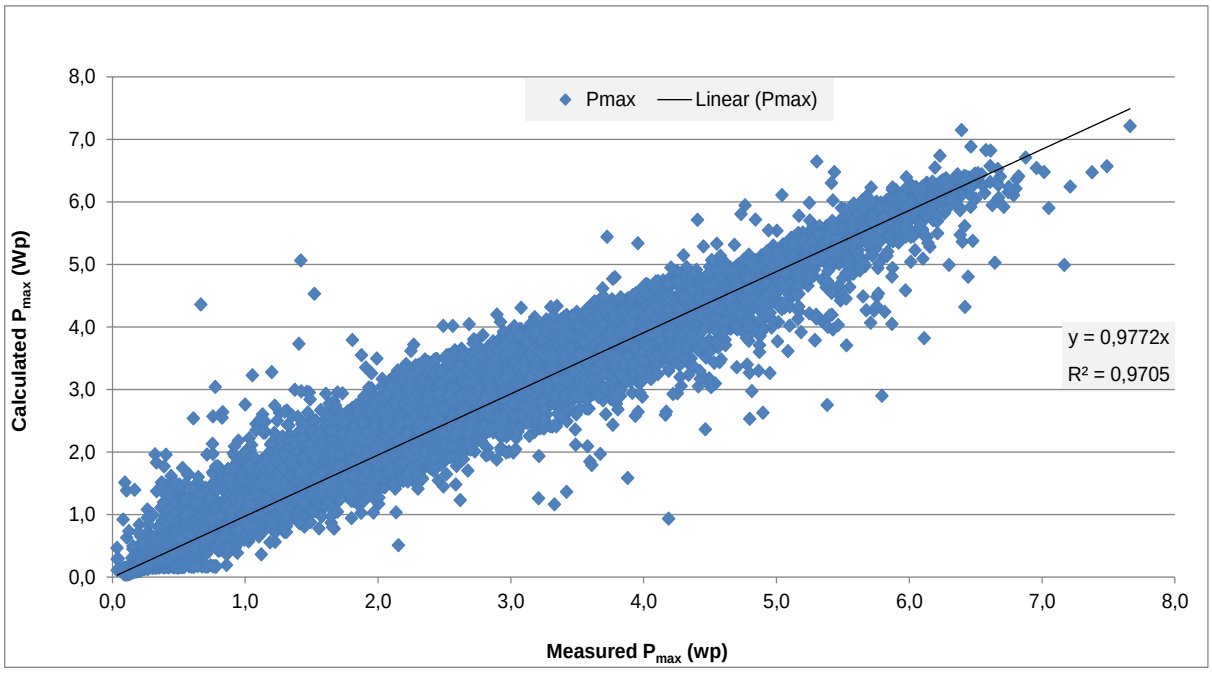

Figure 107: Validation of FEnYCs energy yield method for CIGS module in Loughborough, UK.

A good agreement between calculated and measured Pmax on an annual basis is shown in Figure 104, Figure 106 and Figure 107 for the c-Si, a-Si and CIGS modules, respectively. Figure 105 shows the Deviation of monthly energy yield between calculated and measured values for c-Si module and a similar pattern is

also observed for the a-Si and CIGS modules. It is seen that the FEnYCs method tends to overestimate the power at higher irradiance and temperature levels. This overestimation is expected potentially due to the sensitivity of introducing spectral influences in the power calculation. Due to the large number of outliers in the power calculation for February month, a larger deviation is noticed. This is due to the combination of the variability in the measurements and experimental error that occurs in the COMs system in February 2010. It should also be noted that the small number of measurements available in February leads to the higher deviation for this month.

5.3.2.1 Accuracy of the estimated energy yield against measured energy yield of the PV modules

The RMSE and MBE between the calculated and measured P_{max} of all three devices are shown in Table 16. Previously these values are estimated for IEC 61853 method shown in Table 12 (chapter 4). There is a minor improvement in the c-Si and CIGS modules are noticed, with a significant improvement for the a-Si module. This is largely due to AM influence consideration in the FEnYCs method.

Module	RMSE (W_p)	MBE (W_p)	RMSE (%)	MBE (%)
c-Si	0,57	0,16	19,46	5,48
a-Si	0,33	0,10	22,76	6,97
CIGS	0,27	0,05	16,54	3,10

Table 16: Error analysis of calculated P_{max} of different devices against measured values.

Sensitivity of power at different AM spectrum of all these module is shown in Figure 14. The best performance of a-Si module is appears in AM1.5 spectrum and the contribution of incoming energy from the sun in the range of AM1.5 – AM2 is 38.7% in the UK climate. The irradiance data used in the validation of IEC 61853 method

only contains AM1.5 spectrum data compare to up to AM10 spectral irradiance is used in the FEnYCs method, hence the improvement is observed in the yield calculation for the most spectrally sensitive PV module in this study.

The spectral response range of c-Si and CIGS module is similar and they are relatively less spectrally sensitive with best performance at the range of AM4 to AM5 spectrum, which covers over 81% of incoming energy (Table 13) in UK climate. A further minor improvement in the FEnYCs method for all three modules are highly expected by using a good full year data, as the February months outliers introduces larger deviation between estimated and measured energies of each technologies.

5.4 Conclusions

In this chapter the climatic parameters that influence the performance of PV devices were analysed. The range of operating irradiance, temperature, AM and kt are identified that needed for module characterisation, i.e. G_{poa} = 0 - 1400W/m^2, T_{mod} = -5 - 55°C, AM = 1.5 - 10, kt =0.25 – 1. The identified operating range would be 0 – 120°. These operating conditions contributed 94.6% of the annual energy yield of the c-Si module studied in this thesis. It should be noted that a site specific analysis is needed to identify the range of operating conditions, which gives an expected energy yield profile.

A correlation between irradiance, temperature and spectral irradiance in the UK climate is identified in relation to PV performance, which helps to identify the realistic module characterisation measurement points for Fast Energy Yield Calculation (FEnYCs) method covering all relevant environmental conditions.

Different I-V translation methods are evaluated to identify a suitable modelling method for FEnYCs. The variation of power against all relevant environmental conditions and their level of accuracy in the power calculation are evaluated. Analysing the accuracy in the power calculation, the linear interpolation method is identified for FEnYCs method and accordingly customised the number of measurement points.

The number of measurement points are 160 for module characterisation is identified. These numbers are identified based on the linearity of the power variation against irradiance and temperature – i.e. the frequency of measurement of irradiance and temperature is higher at non-linear regime of the power.

Higher the number of measurement points potentially increases the chance of better agreement of calculated power against real measurements. But it should also be noted that every measurement takes time and also the cost associated with it, plus potentially introduce the chance of additional measurement uncertainty.

Validation of the FEnYCs method is presented in chapter 5 to evaluate the level of accuracy of the proposed model and how the results compare with the validation results of IEC energy rating standard.

The evaluation of the Fast Energy Yield Calculations (FEnYCs) method is carried out introducing tri-linear interpolation of the power as a function of irradiance, temperature and AM spectrum. The validation result showed an improvement in the calculated power against the measured values for different device technologies, especially for spectrally sensitive a-Si module, where near 8% improvement is noticed.

The FEnYCs method assessment is carried out based on the outdoor module characterised data and the maritime climate weather data is used. Reindl II and Klucher models are applied as in-plane irradiance translation models and a simple but widely used module temperature translation model is used as presented in Chapter 4. It should be noted that the selection of irradiance sub-models should be a site dependent component in the energy yield prediction method considering the sky conditions of the specific site.

The tri-linear interpolation promised to be a better power calculation modelling approach in this study. With this promise, a full validation of FEnYCs method at different climatic conditions is needed in order to establish its robustness for energy yield calculation of all commercial modules. This includes the validation method based on the indoor module characterisation of the same measurement settings.

6 Thesis Conclusions and Future Work

6.1 Conclusions

A new energy yield calculation method – FEnYCs - is established with a novel multi-dimensional module characterisation method and a tri-linear interpolation method that is used first time in any PV yield estimation model. To develop the FEnYCs method and to identify the specific requirements of a robust energy yield method, a detail validation of the proposed energy rating algorithm is evaluated. A detail validation of different irradiance and temperature translation methods are analysed and identified the best suited irradiance translation model for the UK climate. Uncertainty analysis of the irradiance and temperature measurements as environmental input data are performed.

6.1.1 **Validation of Energy Rating Method**

Partial validation of this standard was performed elsewhere, but a full validation effort is made in this first time within the scope of this research. This is a 2D matrix based module characterisation method at AM1.5 spectrum with spectral irradiance correction. Part 1 and Part 2 is IEC 61853 standard is now commercially available. Overall, the IEC energy rating procedure is a complex one and it's not beneficial for an accurate energy prediction. Part 3 of this standard is the calculation part, which has lack of clarity in some of the modelling algorithm. This includes, the interpolations method of spectral correction algorithm and irregular resolution in the given spectral irradiance and spectral response of the modules. It also fails to give clarity on the modelling approach to estimate a power at targeted irradiance and temperature – it's rather open to select linear regression or linear interpolation.

The six reference days are not particularly mapping the global range of weather pattern and represents as a standard weather dataset, hence collaborative effort is ongoing within EU PV community to establish a standard dataset for this energy rating standard. Commercial success of this energy rating standard is not very promising with its current status but has a potential to be adoptable in the PV commercial community with some modification in the algorithm.

6.2 Performance Modelling of Photovoltaic Modules and Uncertainties

Irradiance is the most influencing environmental parameters that affect the performance of a PV module. The irradiance of all weather dataset is typically available at horizontal plane. Then a modelling approach is needed to convert this global horizontal irradiance to plane of module array. There are different translation models available. Evaluating different methods, first time ever for the UK climate, the best-performing horizontal irradiance component separator model was identified as the Reindl-II model. Similarly the Klucher model to translate the horizontal to in-plane irradiance was identified as the best model for UK climatic condition. Both of these two models are applied in the FEnYCs method.

Similarly, a temperature translation model is requiring converting the ambient temperature to module temperature. Calculation of module temperature largely depends on the type of module, module mounting system, and thermal effect due to wind speed. In this thesis a simplified module temperature calculation is applied as a function of ambient temperature and irradiance factor –k. 'k' is estimated based on the data measured in the CREST outdoor monitoring system for c-Si, a-Si and CIGS module technologies and those values are 0.016, 0.03 and 0.026 for, respectively. These 'k' values can be applied in the commercial application in the UK while designing a PV system string configuration and to get an indication of the maximum module temperature in a given ambient temperature.

A novel approach is applied for uncertainty analysis of irradiance and temperature measurement using Monte Carlo technique. A thermopile pyranometer – CM11 - is analysed considering its uncertainties that changes over the annual time period of measurement time and uncertainties that changes at each timestamp of the measurement. This procedure is validated in the UK climate, which gives ±1.56% annual irradiation uncertainty in the UK climate with monthly variation in the range of ±2% to ±6%. Lower the irradiance level higher the level of measurement uncertainties. All given uncertainties in the manufacture's manual are modelled at each timestamp of the measured irradiance level rather than just using the uncertainty values given in the manual. Using this method one can expect a robust uncertainty analysis of thermopile type pyranometer in any location.

A similar Monte Carlo approach is applied for temperature measurement uncertainty analysis. The measurement uncertainty is calculated in the range of ±0.18°C to ±0.46%°C in different months of the year with an annual average uncertainty as ±0.08^{O}C.

Based on the above measurement uncertainties of irradiance and temperature, the uncertainty of annual energy yield for c-Si and CIGS PV modules were determined through Monte Carlo simulation and they are ±2.78% and ±15.45.

This uncertainty results are useful for any commercial PV system these days in the financial risk analysis process.

6.3 Fast Energy Yield Calculations (FEnYCs)

A three-dimensional matrix is established as the module descriptor which is independent of module technologies. Maximum power at any given irradiance, temperature and AM in any location can be calculated by a tri-linear interpolation method from the input three-dimensional P_{max} matrix plot. The operational range of all relevant environmental parameters to be considered before applying FEnYCs algorithm for better accuracy achievement in the energy prediction.

The operational range of irradiance, temperature, AM and kt in the UK climate is studied and the identified values are: G_{poa} = 0 - 1400W/m^2, T_{mod} = -5 - 55°C, AM = 1.5 – 10 (upto 94.6% annual incoming energy), kt =0.25 – 1. A site specific environmental data analysis is require to identify the range of operating conditions and the expected energy generational profile of different technologies. This also helps to establish a correlation between different environmental parameters with respect to a PV device performance.

A novel approach, tri-linear interpolation of power against three parameters – irradiance, temperature and AM – is applied as the power calculation model of FEnYCs method with a customised number of measurement points in the module characterisation power matrix.

Considering the linear nature of the power variation against irradiance and temperature, a novel three-dimensional module characterisation power matrix with

160 measurement points are identified. In this measurement setting, the number of irradiance measurements are higher in lower intensity level (shorter interval within the full range), where the power is non-linear.

More measurement points of the matrix minimise the interval of the distribution, which ideally minimise the modelling error of the power calculation using linear interpolation between points. But increasing the number of measurement point not necessarily is the best solution in terms of the energy yield calculation accuracy, because more measurement means potentially increasing the measurement uncertainty. Also every measurement is associated with cost. Optimisation of the measurement points against the level of calculation accuracy is important.

FEnYCs algorithm also presented other two sub-models - irradiance and temperature translation models. Reindl II and Klucher models are applied as in-plane irradiance translation models and a simple but widely used module temperature translation model is used. Selection of irradiance sub-models should be site specific and to be identified as per the local environmental conditions in relation to the direct and diffuse fraction of irradiance, solar elevation angle, clearness index.

Validation results of the FEnYCs method showed a good agreement against real measured values of all three device technologies. Improvement is noticed in the modelling accuracy against the IEC energy rating standard and a comparison in shown in Table 17. A minor improvement is noticed for c-Si and CIGS module. But above 8% improvement is noticed for a-Si module.

Spectral corrections are not applied in the above results of IEC 61853 method (only used AM1.5 spectral irradiance). Whereas a-Si performs best in lower AM spectrum and the incoming energy from the sun in the range of AM1.5 – AM2 is 38.7% in the UK climate. Hence a significant improvement is achieved in the FEnYCs method. The best performance of c-Si and CIGS occurs at spectrum range of AM4 to AM5, which contains 81% of energy; hence a little improvement is noticed in the FEnYCs method. A further improvement is expected in the above results as there are some outliers in the February month weather data.

Table 17: Comparison of calculation error of FEnYCs method against IEC 61853 energy rating method

Module	IEC 61853 Method (without spectral correction)		FEnYCs Method	
	RMSE (%)	MBE (%)	RMSE (%)	MBE (%)
c-Si	25.6	-5.9	19.46	5.48
a-Si	36.5	15.6	22.76	6.97
CIGS	23.7	-3.8	16.54	3.10

FEnYCs method shown favourable results applicable to different device technologies with both its unit module characterisation approach and the tri-linear interpolation approach for power calculation. With this potential for more accurate and applicable to all technologies, FEnYCs energy yield prediction method requires a full validation at different climatic conditions in order to establish its robustness for energy yield calculation. This includes the validation method based on the indoor module characterisation of the same measurement settings.

6.4 Future Work

A full validation of this method based on the indoor module characterisation data leads to the requirements of a solar simulator which should be able to characterise the module at variable irradiance at different spectrum and temperature at the full operational range.

For application of the full FEnYCs methodology to be validated in different climate conditions. Measurement uncertainties of FEnYCs module characterisation (indoors & outdoors) would improve the robustness of prediction method.

For better representation of the of IEC 61853 energy rating method, the IEC Technical Committee 82 can adopt the FEnYCs module characterisation method and the tri-linear modelling approach for power calculation.

7 References:

[1] IEC 60904-1, Measurement of photovoltaic current-voltage characteristics.

[2] IEC 60904-3, Measurement principles for terrestrial photovoltaic solar devices with reference spectral irradiance data.

[3] William, S.R., et al., Evaluating the state of art of Photovoltaic performance modelling in Europe, in 20th European Photovoltaic Solar Energy Conference, Barcelona, 2005.

[4] William, S.R., et al., Accuracy of energy prediction methodologies, 4th IEEE, 2006

[5] Kenny et al., Energy rating of PV modules based on PVGIS irradiance and temperature database, in 21st European Photovoltaic Solar Energy Conference, Dresden, October 2006.

[6] Bucher et al., RRC Module Energy Rating: A module Survey, 26th PVSC, Sep 30 – Oct 3, 1997, Anheim, CA.

[7] Kenny et al., Energy rating of PV modules: comparison of methods and approach, Progress in Photovoltaics: Research and Applications, Vol. 3, 2002.

[8] Kenny et al., A practical method for energy rating of c-Si photovoltaic modules based on standard tests, Progress in Photovoltaics: Research and Applications, 14, 2006, pp155-166.

[9] Kroposki,B et al., Photovoltaic module energy rating methodology development, 1996, 14,, IEEE, New York, NY, USA Washington, DC, USA.

[10] Kroposki,B et al., A comparison of photovoltaic module performance evaluation methodologies for energy ratings, 1994, 62,, IEEE, New York, NY, USA Waikoloa, HI, USA.

[11] Gianoli-Rossi, E. et al., Energy rating of PV modules by outdoor response analysis, 1988, 14, Kluwer, Dordrecht, Netherlands Florence, Italy.

[12] Wohlgemuth, J. et al., Energy Ratings for PV Modules, EUROPEAN PHOTOVOLTAIC SOLAR ENERGY CONFERENCE, 1997, 313-316.

[13] Raicu, A. et al., Realistic Reporting Conditions (RRC) for Site-Dependent Energy Rating of PV Devices, Commission of the European Communities, 1992, 1323-1326.

[14] IEC 61853-1, “Photovoltaic (PV) Module Performance Testing and Energy Rating-Part 1: Irradiance and Temperature Performance Measurements and Power Rating, October 2007.

[15] IEC 61853-2, “Photovoltaic (PV) Module Performance Testing and Energy Rating-Part 2: Spectral Response, Incidence Angle and Module Operating Temperature Measurements, 2007.

[16] IEC 61853-3 Draft C Standard, “Photovoltaic (PV) Module Performance Testing and Energy Rating-Part 3: Energy Rating of PV Modules, 2007.

[17] IEC 61853-draft standard. Performance Testing and Energy Rating of Terrestrial Photovoltaic (PV) Modules., January 2001.

[18] Duffie, J. A. & Beckman, W. A. in Solar Engineering of Thermal Processes.

[19] Wenham, S. R. et al., Applied Photovoltaics.

[20] Gxasheka, et al., Evaluation of performance parameters of PV modules deployed outdoors. 30, 611–620 (2005).

[21] CREST MSc Study note. Solar Power 1.

[22] H. Kawamura et al. Simulation of I–V characteristics of a PV module with shaded PV cells, 613–621 (2003).

[23] David L. K, Jay A. Kratochvil, and William E. Boyson. Temperature Coefficients for PV Modules and Arrays: Measurement Methods, Difficulties, and Results, IEEE, (1997).

[24] Cereghetti el at. Behaviour of Triple Junction a-Si Modules (16th European Photovoltaic Solar Energy Conference, 2000).

[25] Gottschalg el at. Experimental Investigation of Spectral Effects on Amorphous Silicon Solar Cell in Outdoor Operation (29th IEEE PVSC, 2002).

[26] Wohlgemuth el at. Performance of BP Solar Tanden Junction Amorphous Silicon Module, IEEE, 2002).

[27] Arya el at. Amorphous Silicon PV Module Manufacturing at BP Solar, Process in Photovoltaics: Research and Applications.

[28] King et al. Field experience with a new performance characterisation procedure for photovoltaic arrays (2nd world conference and exhibition on photovoltaic solar energy conversion, 1998).

[29] IEC 60891: Procedures for temperature and irradiance corrections to measured I-V characteristics of crystalline silicon photovoltaic devices. (1987).

[30] K. Nishioka el at. Field test analysis of PV system output characteristics focusing on module temperature. , 665-671 (2003).

[31] Riordan, C., el at. What is an Air Mass 1.5 Spectrum, IEEE, 1990.

[32] King et al. Measuring solar spectrum and angle of incidence on photovoltaic modules and solar irradiance sensors (26th PVSC, 1997).

[33] Minemoto et al. Effect of spectral irradiance distribution on the outdoor performance of amorphous Si//thin-film crystalline Si stacked photovoltaic modules. 91, 120-122 (2007).

[34] Roy J. Development of System Design and Controlling Program to Analysis the Effect of Angle of Incidence on the Performance of PV modules, MEng Thesis (2006).

[35] IEC 60904-1, Measurement of photovoltaic current-voltage characteristics.

[36] IEC 60904-3, Measurement principles for terrestrial photovoltaic solar devices with reference spectral irradiance data.

[37] William, S.R., et al., Evaluating the state of art of Photovoltaic performance modelling in Europe, in 20th European Photovoltaic Solar Energy Conference, Barcelona, 2005.

[38] Friesen, G., et al., Intercomparison of Different Energy Prediction Methods within the European Project “Performance”-Results of the 1st Round Robin, in 22th European Photovoltaic Solar Energy Conference, Milan, 2007.

[39] William, S.R., et al., Accuracy of energy prediction methodologies, 4th IEEE, 2006.

[40] Kenny et al., Energy rating of PV modules based on PVGIS irradiance and temperature database, in 21st European Photovoltaic Solar Energy Conference, Dresden, October 2006.

[41] Bucher et al., RRC Module Energy Rating: A module Survey, 26th PVSC, Sep 30 – Oct 3, 1997, Anheim, CA.

[42] Kenny et al., Energy rating of PV modules: comparison of methods and approach, Progress in Photovoltaics: Research and Applications, Vol. 3, 2002.

[43] Kenny et al., A practical method for energy rating of c-Si photovoltaic modules based on standard tests, Progress in Photovoltaics: Research and Applications, 14, 2006, pp155-166.

[44] Kroposki,B et al., Photovoltaic module energy rating methodology development, 1996, 14,, IEEE, New York, NY, USA Washington, DC, USA.

[45] Kroposki,B et al., A comparison of photovoltaic module performance evaluation methodologies for energy ratings, 1994, 62,, IEEE, New York, NY, USA Waikoloa, HI, USA.

[46] Gianoli-Rossi, E. et al., Energy rating of PV modules by outdoor response analysis, 1988, 14, Kluwer, Dordrecht, Netherlands Florence, Italy.

[47] Wohlgemuth,J. et al., Energy Ratings for PV Modules, EUROPEAN PHOTOVOLTAIC SOLAR ENERGY CONFERENCE, 1997, 313-316.

[48] Raicu,A. et al., Realistic Reporting Conditions (RRC) for Site-Dependent Energy Rating of PV Devices, Commission of the European Communities, 1992, 1323-1326.

[49] Friesen. G, et al., Energy rating measurements and predictions at ISAAC, Proceedings of the 22nd European Photovoltaic Solar Energy Conference, Fiera Milano, September 2007.

[50] Poissant et al, Simple test methods for evaluating the energy rating of |PV modules under various environmental conditions.

[51] IEC 61853-1, “Photovoltaic (PV) Module Performance Testing and Energy Rating-Part 1: Irradiance and Temperature Performance Measurements and Power Rating, October 2007

[52] IEC 61853-2, “Photovoltaic (PV) Module Performance Testing and Energy Rating-Part 2: Spectral Response, Incidence Angle and Module Operating Temperature Measurements, 2007

[53] IEC 61853-3 Draft C Standard, “Photovoltaic (PV) Module Performance Testing and Energy Rating-Part 3: Energy Rating of PV Modules, 2007

[54] IEC 61853-draft standard. Performance Testing and Energy Rating of Terrestrial Photovoltaic (PV) Modules., January 2001.

[55] Mau et al Quantifying environmental effects for different device technologies based on proposed energy rating standard, 22nd EUPVSEC, Sept 2007, Fiera Milano, Italy.

[56] Marion et al, Validation of a Photovoltaic Module Energy Ratings Procedure at NREL, NREL/TP-520-26909, August 1999, USA.

[57] IEC 61853-1, “Photovoltaic (PV) Module Performance Testing and Energy Rating-Part 1: Irradiance and Temperature Performance Measurements and Power Rating, October 2007

[58] IEC 61853-2, “Photovoltaic (PV) Module Performance Testing and Energy Rating-Part 2: Spectral Response, Incidence Angle and Module Operating Temperature Measurements, 2007

[59] IEC 61853-3 Draft C Standard, “Photovoltaic (PV) Module Performance Testing and Energy Rating-Part 3: Energy Rating of PV Modules, 2007

[60] K. Whitfield et al, Procedure for Determining the Uncertainty of Photovoltaic Module Outdoor Electrical Performance, Progress in Photovoltaics: Research and Applications, 2001.

[61] Myers et al, Estimates of Uncertainty for Measured Spectra in the SERI Spectral Solar Radiation Data Base, Solar Energy Vol. 43. No. 6, pp. 347-353. 1989.

[62] Atmaram et al, Uncertainty Estimate of Photovoltaic Module Power Rating for Outdoor Testing, IEEE, 2006.

[63] K. Emery et al, Uncertainty Analysis of Certified Photovoltaic Measurements at the National Renewable Energy Laboratory, Technical Report-NREL/TP-520-45299, August 2009, USA.

[64] K. Emery et al, Uncertainty Analysis of Photovoltaic Efficiency Measurements, IEEE, 1987.

[65] Mullejans et al, Analysis and mitigation of measurement uncertainties in the traceability chain for the calibration of photovoltaic devices, Measurement Science and Technology, 2009.

[66] Ossenbrink et al, PV Module Power Output: Sensitivity and Uncertainty in Non-STC Measurements, IEEE, 1991.

[67] Abernethy et al, The History and Statistical Development of the New ASME-SAE-AIAA-ISO Measurement Uncertainty Methodology,

[68] Abernethy et al, ASAM Measurement Uncertainty.

[69] General metrology — Part 3: Guide to the expression of uncertainty in measurement (GUM), PD 6461-3:1995.

[70] Kirkup. Les, An introduction to uncertainty in measurement using the GUM (guide to the expression of uncertainty).

[71] Kipp & Zonen CM11 Instrument manual.

[72] Kipp & Zonen CM22 Instrument manual.

[73] Kratzenberg et al, Uncertainty Calculation in Pyranometer measurements and Application, Proceedings of the ASME, 2006.

[74] Strobel et al, Uncertainty in Photovoltaic performance parameters–dependence on location and material, Solar Energy Materials & Solar Cells 93 (2009) 1124–1128.

[75] HMP45C Temperature and relative humidity probe, Instrument manual.

[76] Hubbard et al, Air Temperature Errors Caused by Air Filter and Construction Effects on HMP45C Temperature Sensors in Weather Stations, Structures & Environnent Division of ASAE, 2003.

[77] Gueymard et al, Mathematically integrable parameterization of clear-sky beam and global irradiance and its use in daily irradiation applications. Solar Energy 1993;50:385–97.

[78] Gueymard C. Critical Analysis and performance assessment of clear sky solar irradiance models using theoretical and measured data. Solar Energy 1993;51:121–38.

[79] Orgill et al, Correlation equation for hourly diffuse radiation on a horizontal surface. Solar Energy 1977;19:357–9.

[80] Erbs DG et al., Estimation of the diffuse radiation fraction for hourly, daily and monthly-average global radiation. Solar Energy 1982;28:293–302.

[81] Skartveit A et al., A model for the diffuse fraction of hourly global radiation. Solar Energy 1987;38:271–4.

[82] Reindl DT et al., Diffuse fraction correlations. Solar Energy 1990;45:1–7.

[83] Maxwell AL. A quasi-physical model for converting hourly global horizontal to direct normal insolation. Report SERI/TR-215-3087, Solar Energy Research Institute, Golden, CO, 1987.

[84] Louche A et al., Correlations for direct normal and global horizontal irradiation on French Mediterranean site. Solar Energy 1991;46:261–6.

[85] R. Posadillo et al., Evaluation of the performance of three diffuse hourly irradiation models on tilted surfaces according to the utilizability concept, Energy Conversion and Management 50 (2009) 2324–2330.

[86] S. Dittmann et al, Results of the 3rd Modelling Round Robin within the European Project “Performance” – Comparison of Module Energy Rating Methods, 23rd EUPVSEC Fiera Valencia, Spain, September 2008.

[87] Roy et al, ”Validation of Proposed Photovoltaic Energy Rating standard and sensitivity to environmental parameters” Proceedings of the 23rd European Photovoltaic Solar Energy Conference, Fiera Valencia, Spain, September 2008.

[88] D. Faiman, Assessing the Outdoor Operating Temperature of Photovoltaic Modules, Progress in Photovoltaics: Research and Applications 16 (2008) 307–315.

[89] T. R. Betts, “Investigation of Photovoltaic Device Operation under Varying Spectral Conditions” PhD Thesis, 2004.

[90] Gottschalg el at., “On the importance of considering the incident spectrum when measuring the outdoor performance of amorphous silicon photovoltaic devices”, Measurement science & technology. 15, Part 2 (2004): 460-466.

[91] S. Nagae el at., “Evaluation of the impact of solar spectrum and temperature variations on output power of silicon-based photovoltaic modules”, Solar Energy Materials & Solar Cells 90 (2006) 3568–3575.

[92] T Minemoto et al, “Effect of spectral irradiance distribution on the outdoor performance of amorphous Si//thin-film crystalline Si stacked photovoltaic modules”, Solar Energy Materials & Solar Cells 91 (2007) 120–122.

[93] T. R. Betts et al, “ Spectral Irradiance Correction for PV system Yield Calculation” Proceeding of the European Photovoltaic Solar Energy Conference, Paris.

[94] T Minemoto et al, “Evaluation of Outdoor Performance of Photovoltaic Modules using Solar Spectrum Index of Average Photon Energy”, World Renewable Energy Congress, 2008.

[95] T Minemoto et al, Uniqueness verification of solar spectrum index of average photon energy for evaluating outdoor performance of photovoltaic modules", Solar Energy 83 (2009) 1294–1299.

[96] ASTM E 1036-96, Standard Test Methods for Electrical Performance of Non-concentrator Terrestrial Photovoltaic Modules and Arrays Using Reference Cells, West Conshohocken, PA: American Society for Testing and Materials.

[97] B. Marion et al, A Method for Modelling the Current–Voltage Curve of a PV Module for Outdoor Conditions Progress in Photovoltaics: Research and Applications. 2002; 10:205–214.

[98] Anderson et al, Photovoltaic Translation Equations: A New Approach, NREL/TP-411-20279, January 1996.

[98]-11 Y. Tsuno et al, Translation Equation for Temperature and Irradiance of the I-V Curves of Various PV Cells and Modules". 1-4244-0016 IEEE 2006.

[99]-12 Y. Hishikawa et al, "Irradiance-dependence and translation of the I-V characteristics of crystalline silicon solar cells." 28th IEEE PV Specialist Conference, Anchorage, AK, 2000, pp.1464–1467.

[100]-13 IEC 60891 (Working Draft): Procedure for Temperature and Irradiance Corrections to Measured I-V Characteristics of Photovoltaic Devices.

[101]-14 Y. Hishikawa et al, Translation of the I-V Curves of Various Solar Cells by Improved Linear Interpolation, 21 UPPVSEC, 2006